DESIGN OF THE DIGITAL CONTROL ELECTRONICS FOR A GROUND-BASED RADIOMETER SYSTEM AND ESTIMATION OF RAIN ATTENUATION LOSSES IN THE SIGNAL TRANSMISSION LINK

Thesis submitted to the Andhra University, Visakhapatnam
in partial fulfillment of the requirement for the award of
Master of Technology in Remote Sensing and GIS

ANDHRA UNIVERSITY

Submitted by –
Ms. SHRADHA MOHANTY

Supervised by –

Shri Sanjay M. Trivedi
Scientist/Engineer 'SG'
Head, MSDPD/MSDG/MRSA
Space Applications Centre (ISRO)
Ahmedabad, India

Ms. Charu Singh
Scientist/Engineer 'SD'
Marine and Atmospheric Science Division
Indian Institute of Remote Sensing (ISRO)
Dehradun, India

Indian Institute of Remote Sensing, ISRO
Department of Space, Govt. of India
Dehradun – 248001
Uttrakhand, India
(August, 2015)

CERTIFICATE

This is to certify that this thesis work entitled ***"DESIGN OF THE DIGITAL CONTROL ELECTRONICS FOR A GROUND-BASED RADIOMETER SYSTEM AND ESTIMATION OF RAIN ATTENUATION LOSSES IN THE SIGNAL TRANSMISSION LINK"*** is submitted by Ms. Shradha Mohanty in partial fulfillment of the requirement for the award of ***Master of Technology in Remote Sensing and GIS (Marine and Atmospheric Sciences Division)*** by the Andhra University. The research work presented here in this thesis is an original work of the candidate and has been carried out in Microwave Sensor Data Acquisition and Processing Division (MSDPD/MSDG/MRSA), Space Applications Centre (ISRO), Ahmedabad, India under the guidance of Shri Sanjay M. Trivedi, Scientist/Engineer 'SG', Head/MSDPD/MRSA/SAC and Ms. Charu Singh, Scientist/Engineer 'SD' from Indian Institute of Remote Sensing (ISRO), Dehradun, India.

Shri Sanjay M. Trivedi
Scientist/Engineer 'SG'
Head, MSDPD/MSDG/MRSA
Space Applications Centre (ISRO)
Ahmedabad, India

Ms. Charu Singh
Scientist/Engineer 'SD'
Marine and Atmospheric Science Division
Indian Institute of Remote Sensing(ISRO)
Dehradun, India

Dr. Debashish Mitra
Scientist/Engineer 'SF'
Head, Marine and Atmospheric Science Division
Indian Institute of Remote Sensing (ISRO)
Dehradun, India

Dr. S.P.S. Kushwaha
Dean (Academics)
Indian Institute of Remote Sensing (ISRO)
Dehradun, India

Dr. A. Senthil Kumar
Director
Indian Institute of Remote Sensing (ISRO)
Dehradun, India

ACKNOWLEDGEMENT:

I would first and foremost like to express my deepest sense of obligation and gratitude to my co-guide Ms. Charu Singh, Scientist/Engineer 'SD'/MASD/IIRS, for being the source of continuous encouragement. She is the one behind making me pursue my dissertation at Space Applications Centre (ISRO), Ahmedabad. Her suggestions and support prior and during the course of dissertation has pushed me forward throughout this entire course period. Time and again she has led me to rethink and establish my goals and objectives in a defined way. I would extend my sincere thanks to Dr. Debashish Mitra, Head/MASD/IIRS, for making things easier for me during the initial days of project and those prior to that. In the same tone I would also like to thank Dr. Y. V. N. Krishnamurthy, ex-Director/IIRS, for giving me permission to explore this new field of research away from IIRS.

I would like to thank J. Ravisankar, Head/HRDD/Space Applications Centre, Ahmedabad, for his kind consideration to my application for undertaking the M.Tech final year dissertation at SAC, Ahmedabad. I acknowledge my very heartfelt thanks to my supervisor, Shri Sanjay M. Trivedi, Head/MSDPD/MSDG/MRSA, Space Applications Centre (ISRO), Ahmedabad for being with me from the start of the project. His valuable suggestions and motivations during the project were always over whelming and his timely check on the progress of the project has definitely improved my complete project. My gratefulness to Mrs. Amita A. Shah, Scientist/Engineer 'SE', MSDPD/MRSA/SAC, for being the actual force behind the completion of the project. Her continuum guidance, encouragement, efficient supervision and all kind of help provided have resulted in successful completion of the project. Right from day one, she has been the one to look to. I would also like to thank Shri Nilesh M. Desai, Deputy Director/MRSA/SAC regarding his clinical guidance in every matter.

I would like to thank Andhra University for providing Master of Technology Degree in Remote Sensing and GIS. Along with this, I would also like to thank Dr. S.K. Saha, Ex-Dean (Academics)/IIRS and Ms. Shefali Agarwal, M.Tech Course Director/IIRS for providing me with this unique opportunity to do the dissertation.

I would like to thank Shokeen Phogat, Scientist/Engineer 'SC', MSDPD/MSDG/MRSA for his valuable help in PSoC programming. Again I would also acknowledge thanks to Prantik Chakraborty, Scientist/Engineer ''SE', MSSD/MSIG/MRSA for all his efforts and help in undertaking the small work on water vapor retrieval using forward model. All scientists and staff of MSDPD (Lab-5232 and 5234) also need a mention for their timely help and support during the project phase in all possible ways.

My heart-felt appreciation and thanks goes for two of my best buddies, my sources of smile and confidence, Abhipsa and Mridu. I would like to take this opportunity to specially thank all my friends, whom I have met in these two years, with special mention about Sakshi, Ankita, Garima and Tanya Di. Each and every moment spent with them will be there in my time line forever. The happy and bad times were completely supported by them making them great buddies. The project period would have been really tough, had it not been for friends at SAC like Dolly, Jayshree, Swati, Sweta and Jaishree. There constant supports, encouragement, help and among all, their most valuable friendship will be cherished. I would also thank all my M.Tech batchmates, and other PG Diploma friends.

Finally, I am heartiest thankful to Baba, Mummy and Sainy for their love and blessings. The encouragement, trust, care and most importantly their strong faith in my capabilities has allowed me to take up this daunting task and complete it. Again my thankfulness to Agnish, for always being there, in thick and thin. His support, care and love have made me strive upfront and this gesture means a lot. This work is definitely dedicated to all these special persons who have come into my life at different junctures and colored it with different hues, thus leaving a deep impact on me.

Last but not the least; I would like to be grateful to the Almighty for being the guiding light throughout. Thank you everyone who was important for the successful completion of the dissertation and I express my sincere apologies for not been able to mention all names one by one.

Shradha Mohanty

ABSTRACT:

With growing relevance in modern information society, passive microwave remote sensing (MWRs in particular) represents a key part in influencing everyday life and finds use in the climate applications of satellite data. The project described below deals with the design of the digital control electronics of a Ground-based Radiometer (GBR) sensor system. This GBR is proposed to be installed at the IRNSS reference stations (INRES), with Ahmedabad and NewDelhi centres being chosen in the first phase. Among the proposed design technologies to be used for the design of digital control electronics, *i.e.*, Microcontrollers, Field Programmable Gate Arrays (FPGAs), Application Specific Integrated Chip (ASICs) and Programmable System on Chip (PSoC), the FPGA has been considered in the first phase of research and development because of its ability to provide true system level solutions in meeting the cost, performance and power requirements. Along with it, the inbuilt ADC of Cypress PSoC5LP family is also characterized. But due to time constraints, this was not used for the R&D. Apart from the traditional method of data interfacing using RS232, wireless data transfer using ZigBee module has also been tried for the first time for this project and was found to be device compatible. Furthermore, printed circuit board (PCB) layout and development of the actual board (hardware) is also done in due course of the dissertation.

The project also includes the estimation of signal losses in the transmission links due to hydrometeors, *esp*. rain at centimeter and millimeter wavelengths. The recommended *ITU-R-P618.8 Model* is used for Ahmedabad and New Delhi INRES for rain attenuation predictions for JJAS months from 2010-2014. Strong agreement was found between literature and calculated values, with attenuation increasing with both frequency and rain rate. These results may be used in future for determining the attenuation caused in GSAT-14 signal links and study of how weather affects Ka-band satellite communication.

Keywords: Microwave Radiometer, FPGA, PSoC, data interface, PCB design, rain attenuation, ITU-R model.

TABLE OF CONTENTS:

LIST OF FIGURES:

LIST OF TABLES

LIST OF ACRONYMS:

Abbreviations	Description
MWR	MicroWave Radiometer
GSAT	Geostationary Satellite
ISRO	Indian Space Research Organization
CNES	Centre National d'Etudes Spatiales
ONERA	Office National d'Etudes et de Recherches Aérospatiales
SAC	Space Applications Centre
ITU	International Telecommunication Union
GBR	Ground-Based Radiometer
PSoC	Programmable System on Chip
FPGA	Field Programmable Gate Array
ASIC	Application Specific Integrated Chip
PCB	Printed Circuit Board
NEΔT	Noise Equivalent Temperature Difference
HPDAS	High Precision Digital Acquisition System
ADC	Analog to Digital Converter
ENOB	Effective Number of Bits
SRAM	Static Random Access Memory
CLB	Configurable Logic Block
LVDS	Low Voltage Differential Signal
LVTT	Low Voltage Transistor-Transistor
PLD	Programmable Logic Devices
NRE	Non-Recursive Expenses
PLD	Programmable Logic Device
MCU	Micro Controller Unit
FSL	Free Space Loss
SAM	Specific Attenuation Model
DAH	Dissanayake Allnut Haidara
TRMM	Tropical Rain Measurement Mission
GPCP	Global Precipitation Climatology Project
WCRP	World Climate Research Program
ETRI	Electronics and Telecommunication Research Institute
ORG	Optical Rain Gauge
PDF	Probability Density Function
CDF	Cumulative Density Function
LSB	Least Significant Bit
MATLAB	Matrix Laboratory
INL	Integral Non Linearity
DNL	Differential Non Linearity
SNR	Signal to Noise Ratio
SINAD	Signal to Noise and Distortion ratio

THD	Total Harmonic Distortion
SFDR	Spurious Free Dynamic Range
IMD	India Meteorological Department
AES	Ahmedabad Earth Station
DES	Delhi Earth Station
INRES	INRSS Reference Station
AWS	Automatic Weather Station
JJAS	June July August September
TEMPCo	Temperature Coefficient
LDO	Low Droop Out
UART	Universal Asynchronous Receiver Transmitter
RTE	Radiative Transfer Equation
MPM	Millimeter-wave Propagation Model
ECMWF	European Centre for Medium-range Weather Forecasts

CHAPTER 1: INTRODUCTION

1.1. GENERAL:

Remote Sensing has a growing relevance in the modern information society. It represents a key technology as part of the aerospace industry and bears increasing economic relevance. Furthermore, remote sensing exceedingly influences everyday life, ranging from weather forecasts to reports on climate change or natural disasters [1]. Remote sensors can be either passive or active. Passive sensors respond to external stimuli and which measure energy that is naturally available. They can only be used to detect energy when the naturally occurring energy is available. For all reflected energy, this can only take place during the time when the sun is illuminating the Earth. Passive microwave radiometers have been at the forefront of the emerging field of climate applications of satellite data. Even though the pool of researchers is considerably smaller in passive microwave remote sensing than it is in visible and infrared remote sensing, the characteristics of microwave radiometers in some ways lend themselves more readily to climate applications.

A microwave radiometer (MWR) is a passive sensor that measures energy emitted at sub-millimeter-to-centimeter wavelengths (at frequencies of 1-500 GHz). Their primary application onboard spacecraft is measurement of atmospheric and terrestrial radiation, and hence, these are mostly used for meteorological or oceanographic remote-sensing [2]. Microwave Radiometers for ground-based, suborbital, and space flight observations have a long history of development. Development of the Radiometers, as well as the Imagers and Spectrometers, requires a multi-faceted team with expertise that includes instrument system design and system engineering, algorithm development, microwave, RF, analog and digital circuit design, fabrication, packaging design, instrument integration and test, field operations and data analysis.

1.2. BACKGROUND OF WORK:

Sometimes back, on January 5, 2014, ISRO launched GSAT-14, its 23rd geostationary Indian communication satellite under its GSAT series of satellites. The main objectives of GSAT-14 mission are:

- To augment the In-orbit capacity of Extended C and Ku-band transponders

- To provide a platform for new experiments.

Constructed by ISRO, the GSAT-14 spacecraft has a design life of 12 years. The satellite carries six Ku-band and six Extended C-band transponders to provide coverage of the whole of India. GSAT-14 also carries two Ka-band beacons which will be used to conduct attenuation studies and research into how weather affects Ka-band satellite communications. The extent of signal coverage of the GSAT-14 Ka band beacon signal is shown in Figure 1.2-1.

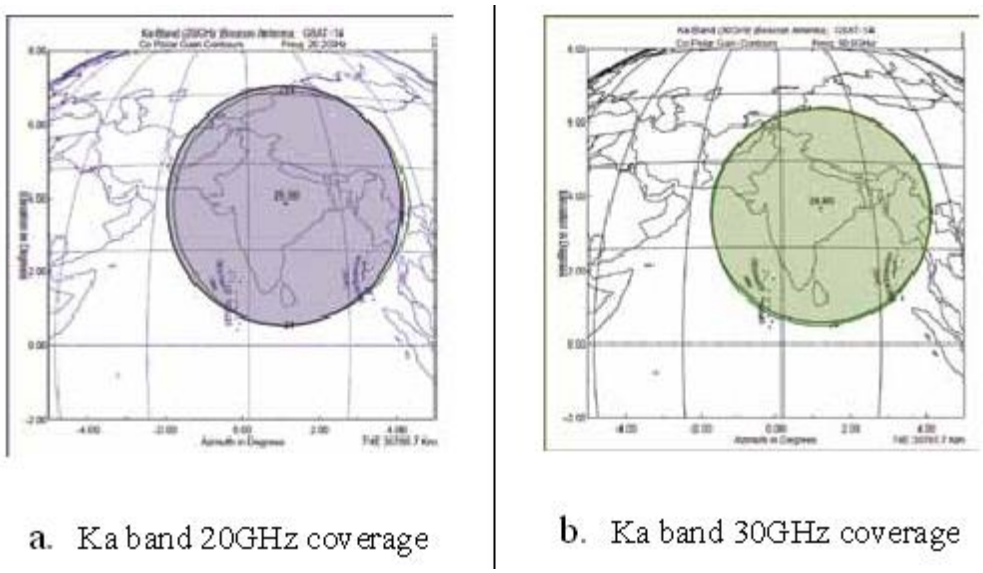

Figure 1.2-1: Ka Band Beacon Signal Coverage, Courtesy: ISRO

Indian Space Research Organization (ISRO), in collaboration with CNES and ONERA from France is going to carry out an experiment for the propagation of Ka Band radio waves beacon signal onboard the GSAT-14 satellite. For this reason, Space Applications Centre (SAC) has also planned to establish earth receiving stations for experiments at New Delhi and Ahmedabad in the first phase. Auxiliary equipments in addition to the beacon receiver will be a 20.2, 22.3, 30.5 and 31.5 GHz, 4 channel, sky-looking, Ka band Dicke Radiometer.

The digital electronics form the core of signal acquisition and data transmission in this Radiometer. This project aims at designing digital control and data acquisition electronics for

the ground-based radiometer (GBR). There are many companies that design the digital circuitry for such instruments. However, this attempt by SAC is an in-house development. This is a research and development project, which can further be extended to meet the project specific requirements. This research would also include the in depth study of the various basic blocks involved and the different technologies required in the realization of the desired design.

The presence of rain in the transmission path is the main cause for microwave system degradation, particularly when operating at frequencies greater than 10 GHz. Rain drops absorb and scatter radio waves, resulting in signal attenuation and reduction in the overall signal availability and performance. Thus an attempt is made towards studying the amount of signal attenuation in the Indian subcontinent region which experiences heavy rainfall during the monsoon season (June-September). Here the rain attenuation prediction model recommended by International Telecommunication Union Radio Communication sector (ITU) shall be used.

1.3. SENSOR DIGITAL CONTROL DESGIN:

The quest for highly integrated devices for product development offers more choices today than ever before. However, the considerations still remaining are power consumption, cost, time-to-market, volume and ease of development. In aerospace (sensor) applications there are special requirements that demand powerful, highly reliable design tools and methodologies. It is important that the tools necessary for the development of these applications not only understand the condition under which they operate, but also the special development requirements necessary to create them [3].

This thesis aims at designing digital control and data acquisition electronics for the Ground-Based Radiometer (GBR) to be designed for Ahmedabad and New Delhi receiving earth stations. The digital subsystems cater to the growing needs of data acquisition, data integration and formatting and buffer storage, all performed simultaneously. The system control and the real time data acquisition and processing are performed by the digital subsystem present within the sensor payload. The main functions of the digital subsystem can be briefed as below:

- High precision digitization of moderate speed received video signals and calibration signals of two channels.

- Provision of programmable features for functional and operational flexibility like gain/offset correction estimation.
- Initialization, command, control and configuration of receiver and other subsystems.

1.4. SENSOR REALIZATION TECHNOLOGIES:

With the advancement in technologies, design and construction of electronic devices has not only become simpler but their numbers have multiplied manifolds. For these reasons, newer avenues need to be searched that can provide numerous emerging technologies in the realization of these systems. Of the most recent developments in the field of sensors' digital subsystem design, the following options are sited below:

- Programmable System on Chip (PSoC)
- Field Programmable Gate Arrays (FPGAs)
- Application Specific Integrated Circuits (ASICs)

The sensors' digital electronics, in order to suit to the emerging applications, need to address few of the design related issues. Firstly they should be manufacturable at low industrial costs. Secondly, they should feature a good radiometric resolution, typically below 1 K, with small integration time in accordance with the specific application. At the end, reduction in size, weight and power consumption is a very important aspect in sensors network scenarios [4]. A solution to the aforesaid constraints is the miniaturization of the sensor, which can be scaled down to a single chip. Integrating a programmable processor and an adaptive sensor interface into one system-on-chip (SoC) combines analog and digital processing capability and rapid customization to different applications using the same integrated circuit. Single-chip integration of these components enhances performance while simultaneously reducing size, cost and power consumption [5]. Moreover, thermal stabilization system can also be easily implemented at chip-level.

However, from the project point of view, a detailed comparison and trade-off study has also been done between the various options available. Keeping in mind the above mentioned limitations and their chip-level solution, the use of programmable system on chip (PSoC) has been the first choice for the project.

1.5. SIGNAL ATTENUATION IN TRANSMISSION LINKS:

The design of a satellite communications system is a complicated process involving many inter-disciplinary interactions. In addition to this, signal link transmission in satellite communication comes with its own limitations. Of the many difficulties associated with signal link transmission, signal attenuation due to hydrometeors present in the atmosphere is of utmost importance. Thus it becomes necessary that the planning of RF/Microwave radio systems must include accounting for the propagation characteristics of the radio signal at that frequency range.

The growing demand of communications services has congested the currently available radio spectrum to such an extent that there is a need to go beyond and look for larger bandwidth and newer frequency bands above 20 GHz [6]. At these radio frequencies, the signal will be affected by various propagation impairments such as rain attenuation, cloud attenuation, tropospheric scintillation, ionospheric scintillation, water vapor attenuation, and rain and ice depolarization. Among all the propagation impairments, rain attenuation is the most important and critical parameter [7]. Rain attenuation results in outages that compromise the quality of signal quality and link availability, making it a prime factor to be considered in designing both terrestrial and satellite links [8]. It severely affects the communication network by degrading the centimeter and millimeter wavelengths (frequencies > 10GHz). They impose restriction on the path length of the radio communication channel to be used as well as limit the use of higher frequencies during line-of-sight microwave links and satellite communication. In tropical countries, like India, experiencing heavy rainfall, the knowledge of rain attenuation is extremely important in designing facilities for reliable ground and space based communication links [9].

The rain attenuation can be measured quite accurately by means of satellite beacon signals and radiometers [10]. However, since propagation experiments are carried out only in a few places in the world and for a limited number of frequencies and link geometry, their results cannot be directly applied to all sites. For this reason, several attenuation models based on physical facts and using available meteorological data have been developed to provide adequate inputs for system margin calculations in all regions of the world. Of the many models available, we choose to implement the *ITU-R P.618.8 Model*.

1.6. PROBLEM STATEMENT:

The above mentioned project aims at designing a digital control and data acquisition electronic circuit for a radiometer sensor system and realization of a ground-based radiometer system at Ahmedabad and New Delhi receiving earth stations. For the design of the digital electronics, four different technology options have been identified. Comparison and trade-off studies between the different options are being carried out for the selection of the best option. Furthermore, printed circuit board (PCB) development and actual hardware realization shall also be done during the research period.

From the application point of view, the loss of microwave radiometer satellite signal during transmission due to rain will also be done. The main purpose of setting up the earth station radiometer was to measure the communication link losses for GSAT-14 due to atmospheric interactions. The ITU model for calculation of rain attenuation prediction shall be used.

1.7. RESEARCH IDENTIFICATIONS:

1.7.1. RESEARCH OBJECTIVES:

- Identification of the digital electronics for a radiometer sensor.
- Comparison of the different hardware technologies identified for implementation of the digital unit of a radiometer sensor.
- Miniaturization of the digital electronics of the ground-based radiometer receiving earth station.
- Calculation of rain attenuation loss in the signal transmission link.

1.7.2. RESEARCH QUESTIONS:

- What are the basic blocks in the design of the digital circuitry of a ground-based microwave radiometer?
- What are the different specifications needed for the ADC to be used in the control circuit?
- What are the different design technologies used in realization of the digital electronics of a radiometer sensor?
- Among the hardware options, which is the best in all aspects, *i.e.*, cost, accuracy, speed, reliability and reproducibility?

- For the frequency bands of the Ground-based radiometer to be installed, what is the amount of the signal loss due to rain?

CHAPTER 2: LITERATURE REVIEW

2.1. MICROWAVE REMOTE SENSING:

With the advances in space technology, the use of microwaves has today become the heart of remote sensing. Microwaves, because of their cloud penetrating and all weather capability, is the answer to the question: Why to use microwaves? Apart from it, the ability to penetrate more deeply into vegetation covers and the information available from microwave imagery complementing the optical and infrared, make its use even more essential.

The science of microwave radiometry has established itself as an integral part in the general field of the environmental remote sensing. Also called as passive microwave remote sensing, microwave radiometry is the measurement of electromagnetic radiations emitted from the target and observed by the antenna. Microwave radiometry finds its applications in a wide domain ranging from astronomical studies, military applications and environmental monitoring.

2.1.1. MICROWAVE RADIOMETERS:

Microwave radiometers are highly sensible receivers designed to measure the incoherent thermal electromagnetic emission by material media. The signal received by a radar receiving antenna consists of energy scattered by the target after it has been illuminated by the radar transmitting antenna. In case of radiometers, the transmission source is the target itself. The energy received by the radiometer is due to the radiations self-emitted and/or reflected by the scene and collected by the antenna.

The output of the antenna is expressed in terms of its antenna temperature, T_A. The goal of the measurement is to relate the antenna temperature to the brightness temperature of the object under consideration. Thus the task of the microwave radiometer is to measure this antenna temperature with sufficient resolution and accuracy. The power P emitted by an object in thermodynamic equilibrium is a function of its physical temperature T, and in the microwave region P it is directly proportional to T [11].

2.1.2. GROUND BASED RADIOMETER:

The present task at hand is the designing of both digital and control electronics for the proposed GBR systems at Ahmedabad and New Delhi earth stations. As the GBR is designed to perform multi-channel High Precision Data Acquisition System (HPDAS) function, it is preferred to be mounted nearer to RF receiver unit, on the back side of the antenna, in the field. Thus keeping in mind the above constraints, the digital subsystem is miniaturized in terms of weight, power & volume. The Table 2.1-1 gives the design details of GBR.

Table 2.1-1: Technical Specifications of GBR

PARAMETERS	VALUES	
Type	Dicke Switching	
Operating Frequencies	20.2, 22.3, 30.5 and 31.5 GHz	
Polarization	Linear: Vertical and Horizontal	
Bandwidth	3dB: ±300MHz, 20dB: ±500MHz	
Dicke Switching Speed	1KHz	
Integration Time	1 sec	
Input Radiometric Range	10-350K	
NEΔT	Required: 0.3K	Goal: 0.1K
ADC ENOB	14 bits	

The system control and the real time data acquisition and processing are performed by the High Precision Data Acquisition digital subsystem. The basic back-end digital configuration for a radiometer system is shown below in Figure 2.1-1.

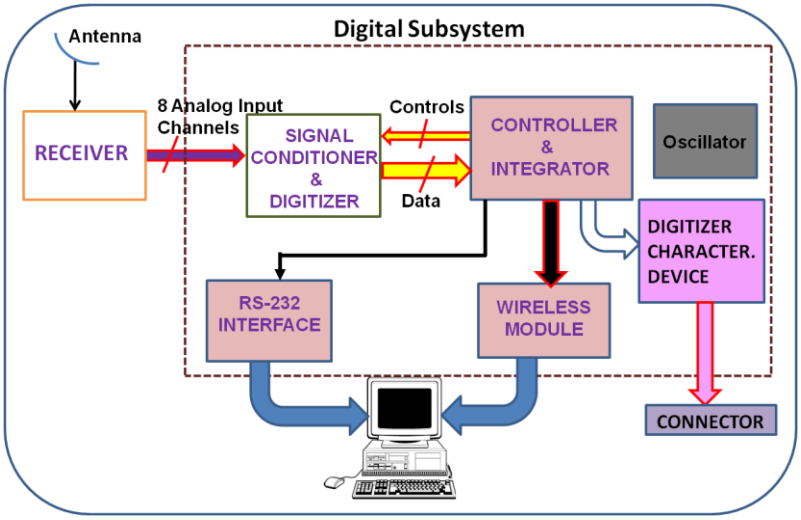

Figure 2.1-1: Block Diagram of Radiometer System

2.1.2.1. DICKE RADIOMETER:

The book by Niel Skou and David Le Vine [12] elaborately described the radiometric principles, types of radiometers available along with receiver types, etc. A brief excerpt is taken from the book about the Dicke Switching Radiometer which is proposed to be used in this project.

With fluctuations in atmospheric emission, and water vapor being the major culprit, adding to the noise in the output of a simple total-power receiver at frequencies of 5 GHz and up, one way to minimize these effects of fluctuations in both receiver gain and atmospheric emission is to make a differential measurement by comparing signals from two adjacent feeds. This method of switching rapidly between beams or loads is called Dicke switching. With the knowledge of the difference between the antenna temperature and some known reference temperature, the instabilities associated with the sensitivity of the measurement to gain and noise temperature is significantly reduced. This is achieved using the Dicke Radiometer (DR). The basic block

diagram of a Dicke Radiometer can be shown as below in the Figure 2.1-2:

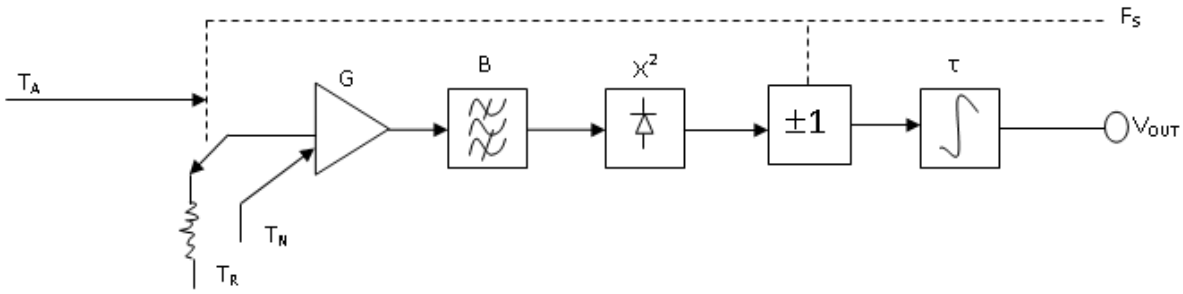

Figure 2.1-2: Block Diagram of Dicke Radiometer

The input of the radiometer is rapidly switched between the antenna temperature and the reference temperature. The switch frequency F_S is typically 1 kHz. The output of the square-law detector is multiplied by +1 or −1, depending on the position of the Dicke switch, before integration. The input to the integrator is altered between the two halves of F_S.

$$V_1 = c(T_A + T_N)G \qquad \{1\}$$

$$V_1 = -c(T_R + T_N)G \qquad \{2\}$$

Provided that the switch frequency F_S is so rapid that T_A, T_N, and G can be regarded as constants over the period, and that the period is much shorter than the integration time, the output of the radiometer is found as:

$$V_{out} = V_1 + V_2 = c(T_A - T_R)G \qquad \{3\}$$

Since only half of the measurement time is spent on the antenna signal (the other half is spent on the reference temperature), the sensitivity is poorer than for the total power radiometer. The sensitivity of the Dicke radiometer can be given as:

$$\Delta T = 2\frac{T_A + T_N}{\sqrt{B.\tau}} = 2\frac{T_R + T_N}{\sqrt{B.\tau}} \qquad \{4\}$$

2.1.2.2. NEΔT:

The objective of a radiometer is to measure power, in terms of noise. However, in many microwave applications, such as remote sensing of the Earth's atmosphere, it is common to express the power in the terms of equivalent temperature, called as the brightness temperature, T_B. The output of the antenna is expressed in terms of its antenna temperature, T_A. The goal of the measurement is to relate the antenna temperature to the brightness temperature of the object under consideration. This concept was highlighted in [13].

NEΔT, related to minimum resolvable temperature difference and was given by the equation:

$$NE\Delta T = \frac{T - T_B}{SNR} \qquad \{5\}$$

NEΔT depended on various factors such as spectral bandwidth and background temperature. Thus, an increase in NEΔT was manifested as a loss of detail in imagery.

2.1.2.3. ADC ENOB:

The heart of the High Precision Data Acquisition System (HPDAS) is the Analog-to-Digital Converter (ADC). To satisfy the dynamic range of temperature from 10º K-350º K in steps of 0.3ºK, the choice of ADC to be used is very important. The speed of the ADC to be used need not be high. However, the accuracy and precision of the measurement is highly essential. Thus the book by W. Kester [14] gave detailed understanding of every term related to ADCs. While ADC selection, the effective number of bits (ENOB) parameter was paid special attention.

An ADC is never able to achieve the ideal number of bits, falling short by 1 or 1.5 bits. The practical number of bits with which the ADC operates is termed as the *Effective Number of Bits (ENOB)*. Calculation of ENOB can be given by:

$$ENOB = \frac{SINAD - 1.76dB}{6.02} \qquad \{6\}$$

As the desired ENOB for the project is 14 bits, we test a 16-bit ADC.

2.2. SENSOR DESIGN:

In all remote sensing applications involving sensors, measurements are inter-related with other subsystems such as process control and instrumentation applications. The sensor transfers the signal from a given energy domain to the electrical domain. Afterwards the signal conditioning circuit, generally relying on the use of operational amplifies; perform some or all of the following tasks in the analog domain: output-to-voltage conversion, amplification, filtering, linearization and/or demodulation. The resulting analog signal is then digitized using an analog-to-digital converter. At the end, a digital system acquires, stores, processes, controls, communicates and displays the digital value with information about the measurand.

Today sensor outputs may be digitized directly by high resolution ADCs. Linearization and calibrations are then performed digitally, thus reducing cost and complexity. The digital electronics form the core of data acquisition and signal transmission of the various sensors used, both ground-based and space-borne. Thus various technologies in the realization of these systems are the need of the hour.

Ferran Reverter (2012) [15] reviewed the use of microcontrollers directly with the sensors, without requiring any analog circuitry. The paper discussed the options of interfacing resistor and capacitor sensors directly. Simple and low-cost circuits were designed using these technologies which have performed remarkably well for medium and high accuracies. A major disadvantage of these systems was that the use of resistors and capacitors slow the performance of the entire system due to longer time consumed in charging and dumping of the charges.

The document revision by BiPOM [16] discussed the usefulness of micro-controllers in complex circuitry design as well as in communication with any output device. With a host of advantages attached to micro-controllers like simple interfacing, high speed, low-cost for low resolution requirements and low programming overhead, they also find application in sensor design, such as temperature, humidity, pressure, etc. The document also discussed the analog-to-digital interfacing and noise considerations.

The study by Rahul Ranjan (2012) *et al.* [17] in their paper aimed at creating an intelligence monitoring system against theft by unidentified person using sensor technology. The project included embedded system based smart home design, security surveillance using ZigBee wireless communication module and internet based. This article described the embedded smart

home remote control system in the general, including the system overall design, system hardware platform and the realization of each part of interface circuit, data acquisition and processing, video acquisition and processing and GSM communication software program realization.

2.3. SENSOR TECHNOLOGIES:

2.3.1. FIELD PROGRAMMABLE GATE ARRAY (FPGA);

Ali Hayek (2012) *et al.* [18] highlighted the importance of flexibility and reliable computing solutions provided by FPGAs against the presently used standard microprocessor systems. The SRAM-based FPGAs can achieve desired safety integrity levels (SILs) at low design cost and time. Moreover, FPGAs, with galaxy of advantages such as faster time to market, almost nil non-recurring cost, simpler design cycles and most importantly field re-programmability, are thus described as the perfect choice for communication and sensor based applications.

A survey report on the designs and implementations of research sensor nodes that rely on FPGAs, either based upon standalone platforms or as a combination of microcontroller and FPGA was presented by Antonio de la Piedra *et al.* (2012) [19] in the paper. The paper presented a comparative study on the various FPGA architectures available, such as the standalone, combinations of microcontrollers and FPGAs and FPGA coprocessors. These were successfully implemented in designing sensor nodes.

A Lattice Semiconductor White Paper [20] gave an insight into the simple solution available for the limitations, in terms of power, cost and footprint sizes, through the FPGA approach. Users across all domains are thus now turning towards this cost-effective, low power requiring and reusable option of FPGA.

The usage of FPGA is not limited to only communication or interfacing with sensor design. This has been illustrated in a report by Synopsys Inc. [3]. Applications requiring powerful and highly reliable designs are possible using FPGA design and verification tools.

Spartan-3AN FPGA Family Data Sheet by Xilinx (2010) [21] illustrated the FPGA device used for the first phase of PCB design for the GBR. This chip consisted of 1400K system gates, 2816 configurable logic blocks (CLBs) with both LVDS and LVTT logic requiring 3.3V, 2.5V, 1.8V, 1.5V, and 1.2V for signaling. Macro-cells, D flipflops, counters, I/O banks and a galaxy of other

functionalities are hosted on this single chip. The basic diagram of the FPGA is illustrated in Figure 2.3-1with zoomed view of the internal structure.

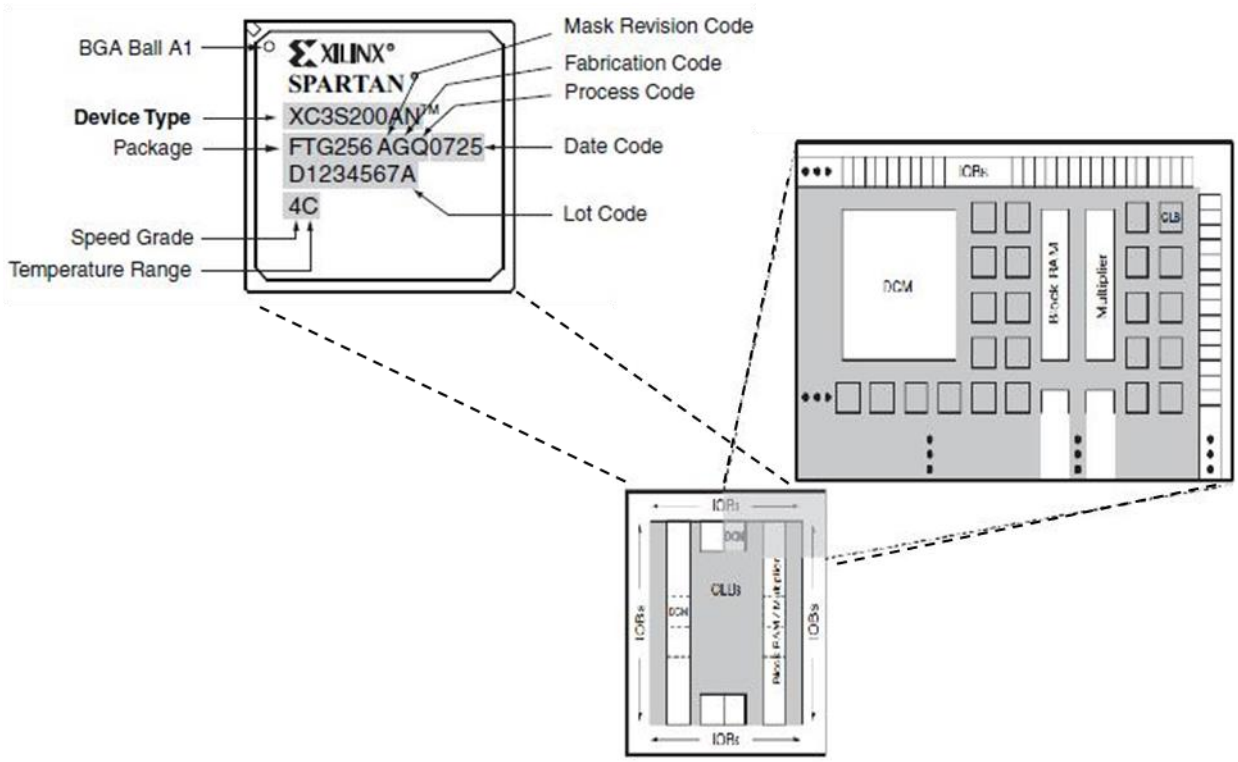

Figure 2.3-1: Structure of FPGA, Courtsey: SPARTAN FPGA Datasheet

2.3.2. APPLICATION SPECIFIC INTEGRATED CIRCUIT (ASIC):

An Application Specific Integrated Chip, or simply called as ASIC, is an integrated chip designed for a particular use, rather than for a general purpose use. ASICs seem to be deemed as the best option for high-volume applications. The cost and performance advantages reaped out of ASIC gives it an upper hand. The fact that ASICs are built for specific applications allows them to have a very high density of useful logic gates on the chip and use the resources optimally. Thus greater gate count and lower power consumption gives ASIC a competitive edge over FPGA.

ASIC designs come in a number of available options, such as *Classic Full Custom design*, *Standard Cell design*, *Gate Array design* and *Field Programmable Logic design*. By eliminating the need to cycle through an integrated circuit production facility, both time to market and financial risk can be substantially reduced in the Field Programmable Logic design. The two major classes of field programmable logic, Programmable Logic Devices (PLDs) and FPGAs, have emerged as cost effective ASIC solutions because they provide low-cost prototypes with nearly instant "manufacturing". This class of device consists of an array of uncommitted logic elements whose interconnect structure and/or logic structure can be personalized on-site according to the user's specification.

2.3.3. SYSTEM-ON-CHIP (SOC):

System-on-Chip (SoC) is basically a microcontroller with small FPGA on the same chip. It is more geared towards complete flexibility and user interaction. The general idea with a system-on-chip is to allow provide circuitry with multiplexers and other routing facilities such that the signal can be routed through a number of circuits to produce many useful types of stimulus/response pattern without the processor intervention. The basic diagram of *CY8C5868AXI-LP035 chip development board*, belonging to the CY8C58LP family describing all its components and signal interconnections is shown in Figure 2.3-2 below.

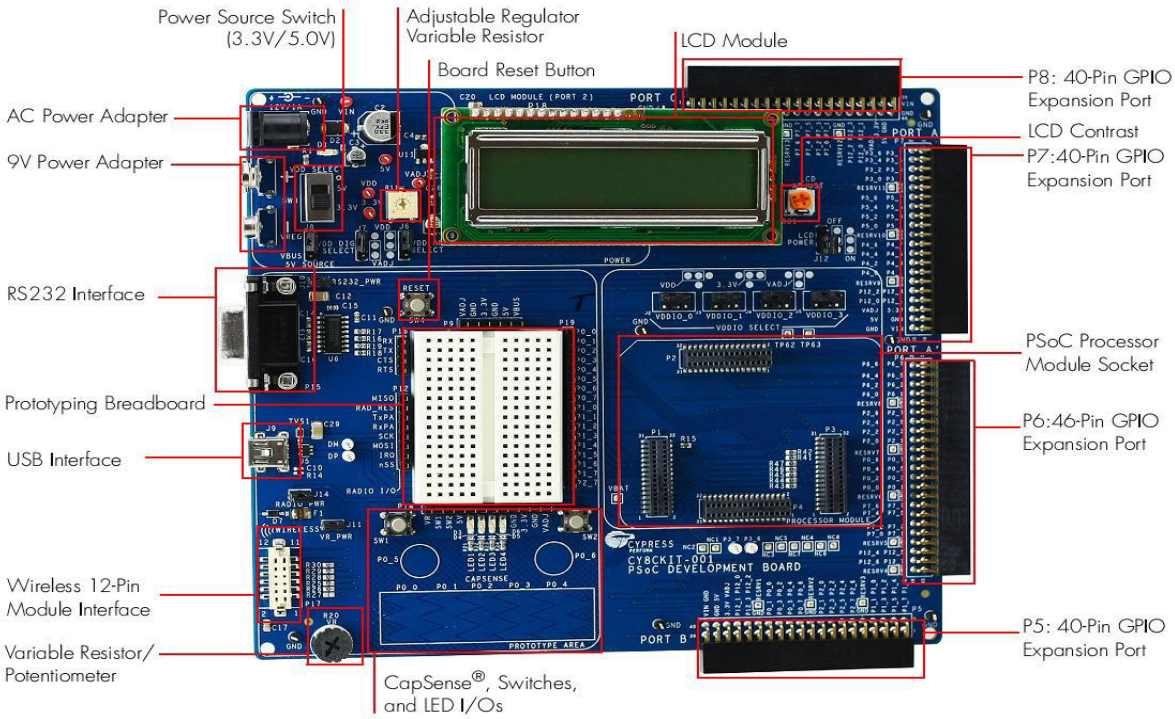

Figure 2.3-2: PSoC Development Board, Courtesy: Cypress MicroSystems

Presented in the paper by David Tomanek (2010) [22] titled "*What is PSoC?*" is the description of system on chip along with examples describing the various concepts. The necessity, structure and operation of the device created by Cypress MicroSystems was briefly discussed in the paper. The paper also reported about the usage, supporting softwares and compilers as well as the power management of the PSoC device.

With increasing technological development, a SoC can be successfully used in interfacing different activities using a personal computer. The technical note by J. Jayapandian (2006) [23] studied about how innovative programmable embedded hardware like Programmable System on Chip (PSoC) are solutions to complex embedded system designs. Simple designs used in industrial/laboratory applications were implemented using PSoC and design software like LabView. This approach also improved the experimental technique with good accuracy and reliability.

A paper by Qiong M. Li (2003) [24] showed the implementation of a configurable PWM Controller using PSoC. The highlight of PSoC is that unlike most of the microprocessor-based digital controllers that use fixed analog and digital peripherals, all the peripherals here were programmable. Even communication between the user and the controller was done using several communication protocols, like UART, SPI and I2C. Few drawbacks of PSoC like provision of only analog filters and the impracticality to implement pure analog protection due to the slew rate were also detected.

The development of a useful frequency based acquisition system, based on PSoC was reported by R. Aragonis *et al.* (2004) [25]. The frequency-based data acquisition method Implemented, using Indirect count methodology, in the circuit demonstrated the capability of PSoC being used in specific processing systems at affordable costs. Also illustrated in the report is the versatility of PSoC as a platform to acquire, condition, multiplex, process and transmit external analog data to different external processors, liberating the main processor of tedious works while allowing the system to spend time on processing instead of capturing data.

PSoC is a true system-level solution providing microcontroller unit (MCU), memory, analog, and digital peripheral functions in a single chip. It offers a modern method of signal acquisition, signal processing, and control with high accuracy, high bandwidth, and high flexibility. The dynamic reconfiguration capability of a PSoC was discussed in the paper by Doboli *et al.* (2009) [26]. Defining multiple controls using analog and digital configurations within the same device was experimentally proven in this paper.

F. Alimenti *et al.* (2008) [4] in their paper have focused on the different advancements in the field of remote sensing using the latest PSoC technology. The study tried to satisfy all the requirements and constraints associated with the design of a microwave radiometer sensor for forest fire detection and it was found that PSoC was a superior technology in terms of meeting the cost, power and performance requirements of the system as well as miniaturizing the chip in terms of size, weight, volume and power.

Integration of an 8-channel reconfigurable sensor interface with an 8-bit Σ-Δ A/D converter and a 16-bit sensor signal processor was presented by Jinwen Xi *et al.* (2006) [5] in the paper. Combined analog and digital processing capabilities of the SoC were used in integrating a programmable processor with an adaptive sensor interface. Rapid customization to different applications using the same integrated circuit feature was also provided in the same chip.

Operations ranging from sensor signal processing to execution of softwares to support interfacing configuration and calibration, ADC control and sensor data processing were all carried out in the single chip. With simplified RISC architectural design, the SoC was able to communicate with different input/output devices also.

2.4. RAIN ATTENUATION LOSS IN SIGNAL TRANSMISSION:

2.4.1. RADIOWAVE PROPAGATION AND TRANSMISSION:

Report of the NMO courses provided by the NavyMars Institute (1998) [27] gave a detailed report on Electromagnetic waves, the induction a nd radiation fields associated with them and also about the radio waves, their propagation and transmission. In depth knowledge about the polarized radio waves, how these waves undergo reflection, refraction and diffraction due to the atmosphere and the different types of propagation paths taken by radio waves. This report also highlighted how transmission losses affect radio wave propagation, especially how electromagnetic, man-made/natural interference, and ionospheric disturbances also affect radio wave propagation. Other important topics covered in the report were tropospheric and ionospheric scattering of electromagnetic waves, with details about radio waves. The different operational frequency levels and their predictions based on atmospheric condition, like temperature inversion, were also touched upon in the report.

2.4.2. LOSSES IN ATMOSPHERIC TRANSMISSION OF RADIO WAVES AND ASSOCIATED MODELS:

From the presentation made by Kamran Ahmed [28] on the basic effects of propagation anomalies were identified which further influence the communication satellite system performances. The losses were broadly categorized under: Atmospheric, Ionospheric and Rain Attenuation losses. For a slant path, the primary Free-space-loss was calculated to be:

$$FSL\ (\lambda) = \left(\frac{4\pi R}{\lambda}\right)^2 \qquad \{7\}$$

Where, R = distance between receiver and transmitter antennas

λ = wavelength of the operating signal

Along with this, other losses such as the beam-spreading loss, polarization loss, scintillation loss, weather loss, etc. were briefly described.

A white paper series by LightPointe [29] discussed the underlying processes that impact the radio signal propagation important in calculation of the statistical system availability for a point-to-point radio transmission. With a short description about the various losses encountered in the path of signal transmission, the equation in calculation for a Radio Link Budget was discussed:

$$B_{TLB}(dB) = T_{dB} + G_{TX}(dB) + G_{RX}(dB) - R_{dBm} \quad \{8\}$$

Where, T_{dB} = Transmission power
G_{TX} = Gain of Transmission Antenna
G_{RX} = Gain of Receiver Antenna
R_{dB} = Receiver Sensitivity

The post-graduation thesis of Samuel P. Mason (2011) [30] analyzed the near surface propagation losses at 1.78 GHz for the experiment site, Near Earth Propagation-6 (NEP-6), Panama City, Florida. Various instruments ranging from towers, probes and sensors were used to collect the data which was at a later stage processed. The report concluded that meteorological variance did not seem to have a concrete impact on propagation loss. However, the antenna height played a direct role in propagation loss.

K. Sudhakar and M.V. Subramanyam (2011) [31] in their paper studied microwave transmission through the atmosphere and its effects due to various atmospheric parameter variations. During the course of the work, fluctuations in the angle-of-arrival of the signal from targets were observed for microwave and millimeter waves due to presence of perturbers like dust and smoke. Measurable signal parameters such as intensity and phase fluctuations showed a 2dB peak-to-peak fluctuation.

Signal distortion due to variations in atmospheric conditions and the factors responsible for degradation of this signal were highlighted in yet another paper by K. Sudhakar and M.V. Subramanyam (2013) [32]. Weather conditions of rain and suspended particle such as water vapor and fog, adversely affect the signal propagation at frequencies greater than 10 GHz were discussed. To obtain the amount of signal loss, the ITU gaseous absorption model along with ITU models on “Attenuation by Hydrometeors, in Particular Precipitation, and Other Atmospheric Particles” were used. These models estimate the amount of signal loss by

calculating the total specific attenuation rates. For a wide spectrum of frequencies and different oxygen and water vapor density profiles, plots were generated to show the signal deteoration along the horizontal path.

2.4.3. RAIN ATTENUATION LOSS PREDICTIONS AND ASSOCIATED MODELS:

T. Shiomi [33] has mentioned about how perturbers such as rain and obstacles affect the formulation of link budget for a satellite broadcasting system, in order to quantify the system parameters of a transmission channel. In the absence of water and water vapors in the atmosphere, calculations of the effect of weather on radio wave propagation would be comparatively simpler. However, due to the presence of some form of water (vapor, liquid, or solid) these are taken care of in all calculations.

Attenuation because of raindrops is greater than attenuation because of other forms of precipitation. This loss can be accounted for absorption, in which the raindrop, acts as a poor dielectric and absorbs power from the radio wave and dissipates the power by heat loss or by scattering [33]. With increase in frequencies above 100 MHz, raindrops cause greater attenuation by scattering than by absorption as shown in Figure 2.4-1. Also, at transmission frequencies below 5 GHz a radio signal typically does not experience high levels of attenuation even at higher rain rates. However, attenuation at higher millimeter wave frequency levels can be very high and can contribute significantly to signal fade. At frequencies above 6 GHz, attenuation by raindrop scatter increases with increase in frequency.

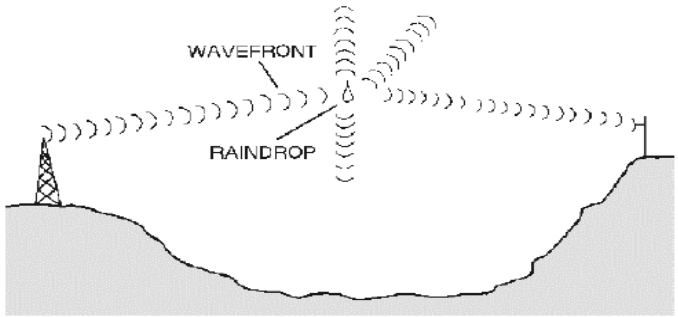

Figure 2.4-1: RF Energy loss from Scattering due to Raindrop

The book by T. Pratt *et al.* [34] describe the depolarization of radio waves is due to the shape of raindrops as shown in Figure 2.4-2. Due to the forces of the atmosphere, the raindrops which were initially thought to be spherical in shape, undergo deformation and finally become disc-like shapes. Rain scatter occurs when the transmitting antenna beam passes through a rain cell, and the raindrops scatter a portion of the radio waves. The resulting scattering acts as an interference to other communication systems operating in the same frequency band.

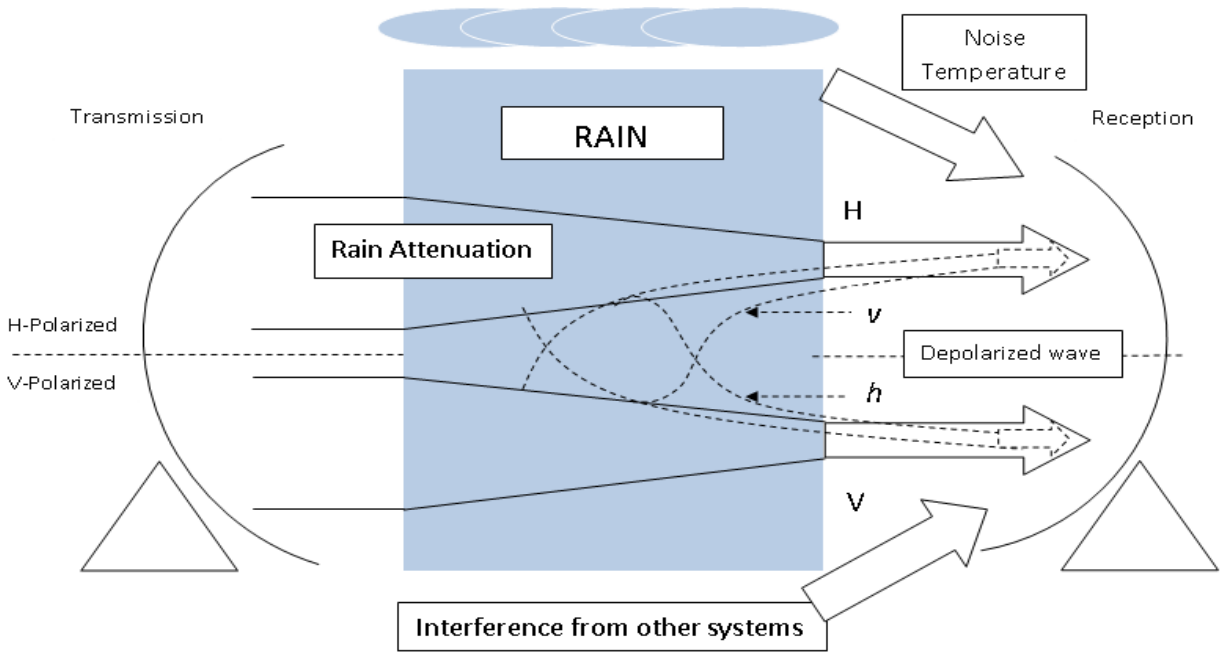

Figure 2.4-2: Interference due to Rain cell causing Depolarization, Courtesy: *Satellite Communications*, Pratt et al.

The paper by Wei Zhang and Nader Moayeri (1999) [35] (IEEE 802.16 Broadband Wireless Access Working Group) described the power-law form of rain specific attenuation in calculating rain attenuation statistics. The power-law form is written as:

$$A = kR^{\alpha} \qquad \{9\}$$

Where, A= Specific Attenuation rate

R = rain rate (mm/hr)

K and α = power law constants, depending on frequency, raindrop size distribution, rain temperature, and polarization.

Again, For linear and circular polarization, the parameters are defined as:

$$k = \frac{[k_H + k_V + (k_H - k_V)cos^2\theta.cos2\tau]}{2} \quad \{10\}$$

$$\alpha = \frac{[k_H\alpha_H + k_V\alpha_V + (k_H\alpha_H - k_V\alpha_V)cos^2\theta.cos2\tau]}{2k} \quad \{11\}$$

Where, θ=path elevation angle

τ=polarization tilt relative to the horizontal (for circular polarization, τ=45˚)

Variations in k and α are on the basis of rain rate and different rain drop-size distribution of Gamma, Log-normal, Laws and Parsons and Marshall and Palmer, which were also provided in tabular format.

The values of the power parameters, k_H, k_V, α_H and α_V were given by the Recommendations ITU-R P-838.3 (1999) [36] report. The values are given in a tabular form in Appendix.

There are two main methods for predicting the rain attenuation on the radio wave path: physical and empirical methods.

<u>Physical Methods:</u> Physical methods the theoretical methods or analytical models which recreate situations similar to reproduce the physical behavior involved in attenuation process. As physical methods do not use all the input parameters, it has a number of numerical analysis methods to provide solutions to intractable mathematical functions and formulations. Although time consuming, the physical method is reliable because the results obtained from such experiments are real problem based.

Empirical Methods: It is based on measurement database stations in different climatic zones within a particular zone. The knowledge of the qualitative behavior of absorption and scatter in homogenous scattering media form the base for the different empirical models. Since a physical method does not always require all the input parameters for analysis, the empirical models are the most preferred. Some of the examples of empirical models are Crane's Global model, Crane's Two-component model, International Telecommunication Union Recommendation (ITU-R) models, Specific Attenuation Model (SAM) by Stutzman and Dishmna and Dissanayake, Allnutt and Haidara (DAH) model.

The final report by COST 255 (2002) [10] elaborately described the various models for rain attenuation studies. According to this report rain attenuation can be precisely measured by means of satellite beacon signals and Radiometers. But the limitations of frequency, link geometry and sporadic distribution of test sites make it difficult for obtaining accurate results. Thus, the use of different attenuation models comes into play. From among a host of rain attenuation models, some of the most commonly used are listed below:

1. Crane Global Model
2. Crane Two-component Model
3. Specific Attenuation Model (SAM) by Stutzman and Dishmna
4. Dissanayake, Allnutt and Haidara (DAH) model
5. International Telecommunication Union Recommendation (ITU-R) model, 618.8

With a requirement of rain rate statistics at 1-minute integration time for the prediction of rain attenuation in satellite and terrestrial links at any probability of exceedance, a method for the calculation of the same was provided in the report by the International Telecommunication Union Recommendation (ITU-R P837-6) (2013) [37]. The rainfall rate R_p, exceeded for any given percentage p of the average year and for any given location is calculated using the ITU-R P-837.6 model. The latitudes and longitudes were divided into grid size of 1.125º and bilinear interpolation technique was used to obtain the values of P_{r6}, M_t *and* β, for any given (lat, long). Then for calculation of R_P, the following set of equations was used.

$$M_c = \beta M_t \; and \; M_s = (1-\beta)M_t \qquad \{12\}$$

$$R_p = \frac{-B \pm \sqrt{B^2 - 4AC}}{2A} \qquad mm/hr \qquad \{13\}$$

Where, $A = a*b$, $B = a + c*\ln(P/P_O)$ and $C = c*\ln(P/P_O)$

$a = 1.09$, $b = (M_C+M_S)/21797P_O$ and $c=26.02b$

Above mentioned were the different rain attenuation prediction models. However, the most important input to these models is $R_{0.01\%}$, rain rate at 0.01% exceedance. Thus for obtaining $R_{0.01\%}$, firstly the long term rain rate is converted into short integration time of about 1-minute. Long integration-time rainfall rate is not advised due to its failure to capture high-intensity short-duration rain events and also it is not recommended for communication system design. Therefore, 1-min integration time has been accepted worldwide as the most desirable in the attenuation prediction studies [38]. Once converted into 1-minute integration time, the rain rate at *p*% probability of exceedance is downscaled to 0.01% in order to be used as input to the attenuation models. This study was presented in a Hydrology Project Training Module (2002) [39]. Further included in the module were checking of homogeneity of rainfall data sets, computation of basis statistics, fitting of frequency distribution and duration curves, etc.

The paper by J. S. Mandeep and S. I. S. Hassan (2008) [40] illustrated the importance of conversion of long integration time data to 1-minute and its utility in the accurate rain attenuation prediction. The paper highlighted the various methods of conversion, such as: Segal method, Burgueno *et al.* method, Chebil and Rahman method, Joo *et al.* method and the most widely used Moupfouma and Martin method. As most precipitation in Southeast Asia originated from large mesoscale cloud masses, errors at 0.01% probability occurrence were most likely to occur for frequent short-duration precipitation events. While Joo *et al.* method was found to be least useful in tropical countries, Chebil and Rahman's model showed minimum errors of <6% at 0.01% probability of occurrence. Although Moupfouma and Martin's method closely followed the measured rainfall-rate data at 0.1% and 0.01% probability of occurrence, the Segal model provided the best estimate.

A conversion method for probability of 1-minute rainfall rate from that for longer integration time for a 3-year long rainfall dataset provided by ETRI was proposed by Joo Hwan Lee *et al.* (1994) [41] in their paper. The study considered two kinds of distribution for the analysis of measured rainfall data: mean and statistical distribution. The conversion was also carried out by: calculating the relationship of time probability between 1-min and t-min distribution for the same rain rate or obtaining the relationship between 1-min and t-min rain -rates for equal

probability. A linear and a logarithmic regression model were proposed with the following set of equations:

$$R_1(p) = aR_\tau(p) + b \quad for\ 5.0\% \leq p \leq 0.01\%\ (linear\ scale) \qquad \{14\}$$

$$\log R_1(p) = a \log R_\tau(p) + b \quad for\ 5.0\% \leq p \leq 0.01\%\ (log - normal\ scale) \qquad \{15\}$$

Similar study was again made by Joo Hwan Lee *et al.* (2000) [42] in their paper. In this study 2 year rainfall measurements by ETRI were conducted using Optical Rain Gauge (ORG) to obtain Probability Density Functions (PDF) and Cumulative Density Functions (CDF) using Moupfouma distributions.

$$PDF, f(r) = a\frac{e^{-ur}}{r^b}(u + \frac{b}{r}) \qquad \{16\}$$

$$CDF, P(r \geq R) = a\frac{e^{-uR}}{R^b} \qquad \{17\}$$

Coefficients for the Moupfouma CDF were also derived for the various time integration of rainfall data. The paper concluded with a new conversion method for various integration time data based on available ETRI 2-year measurements. Again the data was validated with data conversion methods for 1-minute rain rate distribution.

A.P.Gallois *et al* .(1989) [43] described an investigation in which attenuation predictions were calculated using a number of models in the slant path for sites spread all over Europe. Seven different models were used in the study, namely: ITU-R, Crane's Global and Two-component, Misme and Waldteufel, Rue, Leitao and Watson and Capsoni *et. a1.*'s Exponential Cell Model. With inputs to the model as rainfall, rain height and site specifications, contour maps were plotted using the basic specific attenuation equation. The study concluded with near similar values of attenuation for all the sites under experiment with % rms deviation ranging from 11.61-47.29%. Resemblance in prediction of attenuation was estimated for near future calculations.

The comparative study between the ITU-R and Crane models was presented by William Myers (1999) [44]. For long term fade probability calculations, differences in estimates were seen for

both the models. However, both the models could not accurately predict attenuation for short term rainfall events. Differences in results were also noticed due to location variations.

J. A. Garcia-Lopez *et al.* (1988) [45] presented four desirable features of simplicity, accuracy, usage and homogenous behavior for calculating the rain attenuation predictions to be used in satellite radio-link engineering. The proposed model used in the paper was the ITU-R. This model described the specific attenuation rain rate which is frequency, polarization, elevation angle and equivalent path length dependant. For the different test sites with varying climatic conditions across the globe, the method is limited to low rain intensities having low elevation angles.

Zhao Qingling and Jin Li (2006) [46] has presented the idea of measurement of rain specific attenuation with simultaneous measurement of rain rate distribution. The rain attenuation measurements are done taking into consideration the dropsize distribution at 35 GHz and 103 GHz. With the knowledge of important dropsize distribution models like Laws-Parsons, Marshal-Palmer, Joss and Sekhon-Srivastava as well as the Crane's model of rain attenuation, a comparison was made. There is an exponential decrease of 0.2r in the probability that rain rate would exceed 'r'mm/hr during different rain events. With the statistics of rain attenuations in agreement with previous studies, Qingling, concluded that rain restricts the path of radio frequency and its knowledge is important in the design of a reliable earth-space as well as terrestrial communication link.

L. D. Erniliani *et al.* (2004) [47] highlighted the importance of rain rate prediction and rain attenuation studies in designing facilities for reliable ground and space based communication links. With Columbia selected as their study area, contour maps for rain rates and attenuation were developed using interpolation and kriging method. Moreover, a comparative study was also made taking into account models developed by ITU, Rice and Holmberg and Chebil. These models are used in the calculation of point rain rates, cumulative distribution function for rainfall and attenuation studies. This study made use of the available local climatological data. The study concluded that with an average deviation of 30% in modeled and measured values, not all models can work equally well in all climatic conditions.

Tools for the prediction of rain rate and rain attenuation in the form of contour maps for varying climatic conditions across Nigeria using an enormous rainfall data spanning over 30 years was done by J. S. Ojo *et al.* (2008) [48]. Data used for the study was obtained from local

climatological parameters. The rain rate prediction model which approximates a log-normal distribution at the low rates, and a gamma distribution at high rain rate, developed by Moupfouma and Martins was used. J. Chebil's model for calculation of $R_{0.01\%}$, was made which served as an input to the rain rate model. Further, the famous ITU-R model for attenuation prediction was used for completion. Kriging method using MATLAB was implemented in construction of contour maps. The result from these maps served as important data in the preliminary design for both terrestrial and earth-satellite microwave links, and also provided a broad idea of rain attenuation to microwave engineers for the projected launching of other future communication satellites.

P. A. Owolawi *et al.* (2012) [8] presented the study of 19 different sites spread over South Africa for experimental rain rate measurement using ITU-R model. Planned for use in both microwave and millimeter broadband wireless networks, the specific attenuation and total path attenuation for rain rates at 0.01% exceedance were measured for horizontal, vertical and circular polarized signals over 1-400 GHz frequency spectrum. In general, it was observed that the fade depth progressively increased starting from the vertical polarization, circular polarization and the highest fade depth is observed in horizontal polarization for different experimental sites. Further, the outcomes of the experiment were extended to setting up of Line-of-Sight microwave links.

2.4.4. CALCUALTING RAIN ATTENUATIONS IN TROPICS:

A review of literature on the rain attenuation at millimeter wavelengths and rain rate prediction models for analysis of various systems particularly for the Indian subcontinent was made by R. Bhattacharya *et al.* (2007) [6] . The paper has considered rain attenuation, analysis of intense and moderate rain rates over Indian locations, surface point rain-rate prediction, slant path attenuation statistics, attenuation and brightness temperature and water vapor attenuation. Various models for rain attenuation prediction were compared and contrasted. Following the pattern of rain rate, the calculation of attenuation using Gracia-Lopez model was found suitable for northern India. Models were also introduced that calculated the attenuation on the basis of rain-drop size distribution and were found to be highly regionalized.

Yussuff Abayomi I.O. and Nor Hisham Haji Khamis (2012) [49] discussed the signal fading and associated rain attenuation studies at millimeter wavelengths. With rainfall classified into three categories and the tropic and sub-tropic regions divided into four major categories,

existing rain attenuation mitigation techniques like Frequency diversity, Site diversity, Time diversity, Power control and Reconfigurable antenna patterns were broadly discussed. Tropical Rainfall Measurement Mission (TRMM) data served as rainfall data input for the different attenuation models like SAM, DAH and ITU-R models. SAM and DAH models showed high degree of correlation for all the frequency bands considered for slant-path attenuation for 0.01% percentages of time exceedance. However good performance was shown using ITU-R model due to the assumption of uniformity in the rainfall distribution along the slant path.

Illustrated in the study by Rafiqul MD Islam *et al.* (2012) [50] was the enhanced approach for calculation of rain attenuation cumulative distribution function. Operating at 15 GHz and spread over six different geographic DIGI-MINI LINKS across Malaysia, the study calculated new coefficients for CD calculations. From the model the attenuation measurements were under- and over-estimated at lower and higher rain rates respectively. However, the modified ITU-R model showed close resemblance to the measured data. For data validation purpose, five Brazilian and seven Nigerian locations were also identified.

The impact of rain playing a havoc in the path of signal transmission for tropical countries like India, falling in the K-region of attenuation level, was discussed by Mukesh Chandra Kestwal *et al.* (2014) [51] . In the paper, an exponential model for calculation of excess path attenuation was recognized, which converted the rainfall into rain rates and the SAM model was run on these data. 20 years of rainfall data was collected for the test site, Almora, and attenuation values were obtained for frequencies 10, 20, 30 and 60 GHz. From the estimated values of the total atmospheric attenuation , it was derived that with increase in frequency of the signal, the attenuation also increases. Attenuation was also dependent on the rain rate at the location. From the results obtained, it was proposed that similar studies can be extended for different regions affected by torrential rain.

Nazar Elfadil *et al.* (2005) [52] has investigated rain attenuation prediction models for the design of microwave terrestrial line-of-sight systems. Attenuation values were calculated using the *Rainsoft.m* MATLAB program which incorporated the ITU-R Rec.530 Prediction and Global Crane Prediction Models. Rain attenuation plots were developed for three raindrop size distributions as well as for different polarization effects using the two models. The report showed that path loss varied normally with raindrop size distribution and rain rate. At the end it was concluded that Global Crane prediction model overestimated the values for vertical

polarization and ITU-R Recommendation 530 Prediction Model was preferred for rain with 99.99% of link availability due to much lower prediction on attenuation.

From among the various types of propagation impairments, rain attenuation is the most critical. Thus the paper by M. Sridhar *et al.* (2012) [7] is an attempt towards these studies. Disdrometer data was used to record rainfall intensity and measure the rain rate at 1-minute integration time. ITU-R P-837.6 and ITU-R P-618.6 models were implemented for calculation of probability of rain rate exceeding for an average year and rain attenuation prediction values, respectively. The KL University at Guntur was selected as the experiment site. The conclusions from this study were that with increase in rain rates and frequencies of signal propagation, the corresponding rain attenuation values also increased. Also the attenuation decreased for increase in the time exceedance of rainfall at a particular frequency for the location.

Animesh Maitra and Kaustav Chakravarty (2005) [53] have attempted to estimate instantaneous attenuation from rain rates obtained from optical rain gauge data using the Specific Attenuation Model (SAM). The Ku-band signal at 11.72 GHz from the NSS-6 geostationary satellite was studied. A complete experimental setup was developed at University of Calcutta consisting of antenna receivers, signal generators, attenuator and spectrum analyzer. Effective path lengths calculated from SAM were found to be slightly greater than the actual path length, which contributed to greater model values at higher rain rates.

An outage prediction model was proposed by Uzma Siddique *et al.* (2011) [54]. In addition to a comparative study between the proposed outage model and ITU-R P-530.7, cumulative distributions of microwave attenuation and the relationship between specific attenuation and rainfall rate were done in the report. From the study it was derived that Pakistan can no longer be considered under a single region (‘K’ region of rainfall intensity with 42 mm/hr rain). A deviation of 0.05%-3% was observed between ITU standard model and the proposed solution. Also the proposed solution could calculate worst month average which was significant in the planning of mobile communication networks.

Although the various ITU-R models provide a good estimate of rain attenuation in the temperate regions, they somewhat undervalue these calculations for tropical climate. With this idea, M. R. Islam & A. R. Tharek (1999) [9] studied the simple specific attenuation model with modified power coefficients. It was found in the study that the modeled and measured values did not

match, with large deviation between them. Thus re-evaluation of these ITU-R models was proposed for tropical countries.

Similar studies have also been carried out by Sharul Kamal.A.R *et al.* (2001) [55] where they have reported that attenuation studies made with models valid for temperate regions do not show good performance for tropical regions. Rainfall data obtained from two sources; TRMM and local rain gauges, served as inputs to the different attenuation prediction model. Predicted rain attenuations were underestimated by these models and the TRMM data showed lesser attenuation values as compared to satellite receiver. Moreover, it was also concluded that ITU-R models can be used to study the slant-path rain attenuation prediction data.

Many studies have also been done regarding the rain attenuation prediction along the satellite link path taking into consideration the rain drop size distribution. A. Maitra (2004) [56] has also highlighted the importance of drop size distribution (DSD) to indicate the variability in the pattern of rain attenuation for tropical countries. Attenuation models for three Indian stations of Dehradun, Guwahati and Kolkata were used in terms of log-normal distribution of DSD represented by:

$$N(D) = \frac{N_T}{\sigma D\sqrt{2\pi}} * \exp\left[\frac{-0.5(\ln D - \mu)^2}{\sigma^2}\right] \qquad \{18\}$$

Where, N= No. of drops

D= Diameter in unit volume

And N_T, μ and σ are considered as rain rate dependent distribution parameters.

It was observed that the rain attenuation values calculated using DSD at these locations significantly varied from each other depending on the geographical positions as well as from the calculated ITU-R model.

S. Das *et al.* (2010) [57] have also discussed the difference in attenuation values between ITU-R model and those taking into account DSD for four different climatic condition test sites. For different rain rates, significant variations in attenuation were observed between the two models. The paper concluded that for lower rain rates and frequency range of 10-30 GHz the ITU-R

model performed well but overestimated the attenuation values at rain rates greater than 30 mm/hr. Thus in the design of terrestrial and earth-space satellite communication transmission links, the DSD is an important parameter to be kept under consideration.

CHAPTER 3: STUDY AREA AND RESOURCES REQUIRED

3.1. STUDY AREA:

The areas under study are the two earth stations, at Ahmedabad (AES) and New Delhi (DES). Our area of interest is the antenna used at these stations. Being one among the IRNSS Reference Stations (INRES), the station and antenna details associated with AES and DES are given below in the table 3.1-1:

Table 3.1-1: Table illustrating the IRNSS Reference Station (INRES) details

STATION PARAMETERS	Ahmedabad Earth Station (AES)	Delhi Earth Station (DES)
Station code:	ISRO0303	ISRO0463
Latitude (deg)	23.02356 ºE	77.23 ºE
Longitude (deg)	72.515 ºN	28.61 ºN
Station height above MSL (m)	48.77	293
Antenna height above MSL (m)	49.77	294
Antenna Polarization angle (deg)	21.7º	19.6º
Antenna Elevation angle (deg)	63º	56.4º

3.2. DATA SET USED:

Point rainfall data at the two earth stations were obtained from the Automatic Weather Station (AWS) available at the stations. The AWS rainfall data was obtained for a 5 year period from 2010-2014. The Indian subcontinent receives maximum rainfall in the monsoon months of June-September (JJAS). The AWS gives information about air temperature, atmospheric pressure, humidity and rain for the particular location of installation. Thus hourly rainfall data for AES and DES for the 122 days long Indian monsoon was obtained.

3.2.1. ANCILIARY DATA:

The ancillary data used in the rain attenuation prediction model are obtained from the antenna details at the respective earth stations. The auxiliary data include the station location (latitude

and longitude), its height above the sea level, the antenna height and its elevation and polarization angle.

3.2.2. SOFTWARES USED:

- Cypress PSoC Creator2.1
- MATLAB
- Zuken's CADSTAR
- Microsoft Office

CHAPTER 4: METHODOLOGY

4.1. DIGITAL CIRCUITRY DEVELPOMENT:

In the digital control subsystem design for the ground-based radiometer antenna, we have taken into consideration a number of options. These range from the choice of ADC to data interfacing. The block diagram given below in Figure 4.1-1 shows the steps that need to be followed in this process.

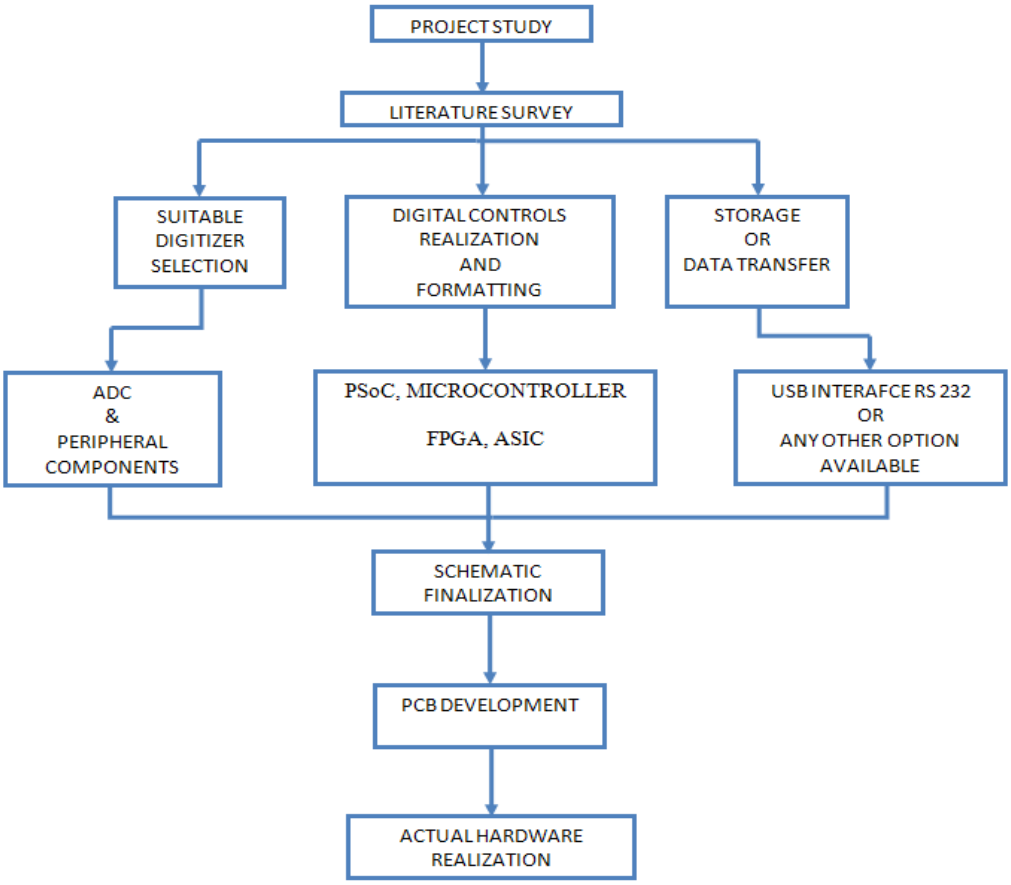

Figure 4.1-1: Methodological flow diagram for digital control electronics design

4.1.1. DIGITAL SUB-SYSTEM CONFIGURATION:

With reference to the basic block diagram of the digital sub-system shown above in Figure 2.1, the received data has the following characteristics features: single ended, 0 to +5V, base band signal of 1KHz bandwidth and termination with 100 K. For the purpose of a radiometer, the board is designed to provide very accurate and precise data at the cost of data rates. Careful choice of ADC peripheral components is properly done, so as to achieve 16 bits digitizer resolution. Voltage Reference device is provided externally as it is not in-built into the digitizer device. Considering the key specification of temperature coefficient (TEMPCO) to be as low as possible & stable for longer duration , REF43 device from Analog Devices is selected for +2.5V voltage reference for the two digitizers. A standalone source of 4 MHz frequency is also used to generate all the timings controls required for digital sub-system. The two channel digitized data is fed simultaneously to digital controller & integrator for signal processing. After an integration time of 1-sec, individual channel data is serialized & proper data packet carried out in processor itself. For obtaining the data, RS-232 device is also interfaced with same processor & serial data will be transferred to a Personnel Computer. As the entire system is proposed to be mounted in the field, a wireless communication module is proposed to be incorporated into the subsystem. Thus for this purpose the digital sub-system also contains ZigBee based wireless communication device. Power supply for the components is generated within the PCB using a LDO, provided by a 12V battery, connected just outside the package. Utmost care is taken in filtering to remove the noise & ripples and achieve the desired digitizer performance. Shown below in Figure 4.1-2 is the control and integrator module for the above mentioned digital subsystem.

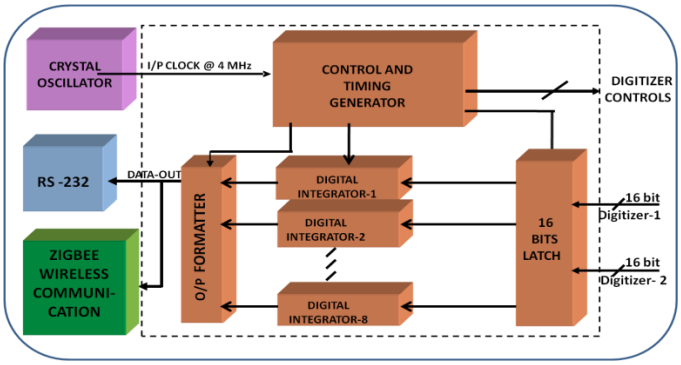

Figure 4.1-2: Block diagram of Controller and Integrator module

4.1.2. DIGITIZER SELECTION:

Since the HPDAS handles the sensor data acquisition and processing requirements, like integration of large number of input channels, its primary function is the data acquisition involving high precision analog to digital conversions (ADCs). The choice of the right digitizer, the digital processing activity as well as compatibility of both is done through literature survey. Thus, the following options are discussed for ADC selection in the HPDAS. Again these parameters are determined through the different ADC tests. Details of these tests are mentioned below.

- Digitizers in a single package: **ADS1278** from Texas Instrument having 8 separate ADCs in a single package with common controls available in commercial grade.
- Individual digitizers in separate packages: **ADC161S626** from National Semiconductor having 1 channel ADC available in very tiny plastic package but humidity and corrosion prone.
- Inbuilt PSoC digitizer: **CY8C58LP family** from Cypress PSoC. The PSoC has only one Σ-Δ ADC built having only one channel. So for the realization of the eight-channel GBR we may either use eight PSoCs or use one in a multiplexing mode. This multiplexing can be done in two modes: ***cross-talk mode*** and ***isolation mode***. As the implementation of multiplexing technique requires a large setup consisting of test-beds and power supply, the testing, although proposed, has not been done yet. This test aims to find out the multiplexer's different specifications before it can be interfaced with the ADC for use.

The comparative block diagram of for the three available design options are presented below as Figures 4.1-3, 4.1-4 and 4.1-5.

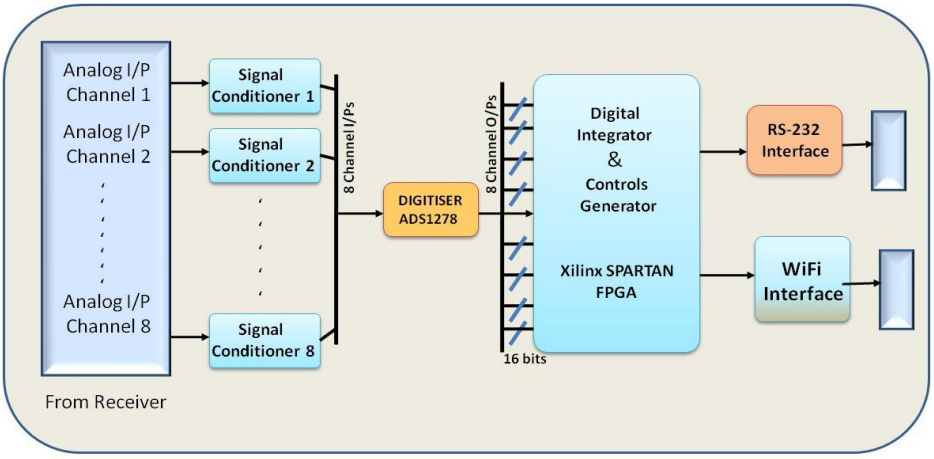

Figure 4.1-3: Digitizer selection option 1- Single packaged ADS1278

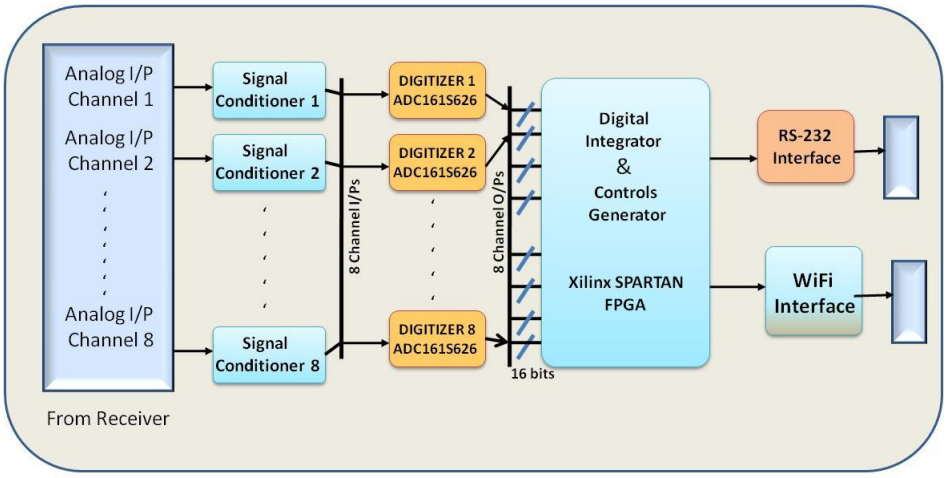

Figure 4.1-4: Digitizer selection option 2- Individual digitizer in separate package, ADC161S626

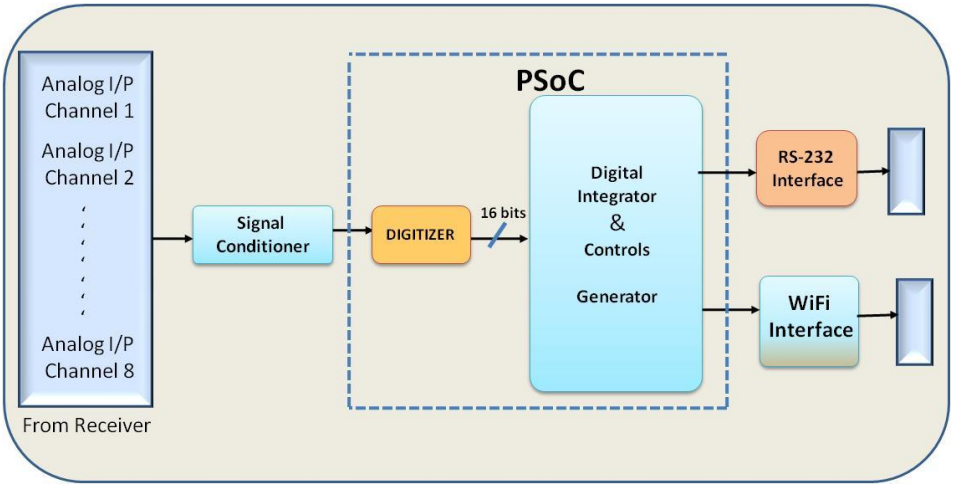

Figure 4.1-5: Digitizer selection option 3- ADC inbuilt in PSoC

In the selection of any ADC, the different specifications that need to be considered are: Analog Band width, Resolution, Sampling Clock, Integral Non Linearity (INL), Spurious Free Dynamic Range (SFDR), Signal to Noise Ratio (SNR), Total Harmonic Distortion (THD), Effective Number of Bits (ENOB), along with equal importance given to material used, package of components and power consumption.

4.1.3. ADC TESING:

The performance of an ADC will be never ideal. During operation, a n-bit ADC never achieves the entire n bits and falls short by a 1-1.5 bits. Thus the actual number of bits with which the ADC operates is called as the *Effective Number of Bits (ENOB)*. This loss in bits during operation can be accounted due to the errors associated with the ADC. Of the number of errors present, some important ones are listed below.

- **Quantization error:** With the sampling of an ADC done at every clock instant, the difference of up to ±1/2 LSB between the actual analog input and the exact value of digital output is termed as the quantization error. However accurate the ADC maybe, it will always have the quantization error. The quantization error is a function of time and can be given by:

$$RMS\ quantization\ error = \frac{q}{\sqrt{12}} \qquad \{19\}$$

Where, $q = 1\ LSB = \frac{V_{FS}}{2^n}$

- **Aperture jitter:** With the application the clock, it is not necessary that the input signal is always sampled at every clock event. The sample-to-sample variation at every clock instant introduces an error, called as the aperture jitter. Measured in pico seconds, the clock jitter depends on the material used in the quartz oscillator. Over the time with long-term ADC use, causing aging effect which in turn also affects the aperture jitter.
- **PCB Development errors:** PCB designing, component layout and grounding of the signals also introduce errors within the design. Both analog and digital components should be kept separately within the board. Apart from this, special care should be taken for grounding of the signals. Separate analog and digital grounding create a case of *ground bounce*. Thus both grounds should be connected to the power source at the *star point*.
- **Component selection errors:** All the components used in the board should be of high quality including the shielded cables.
- **Instrument errors:** However small, some error is always associated with the instruments used. Proper calibration can minimize the error, but cannot remove it.
- **Power supply errors:** Special attention needs to be paid towards the power sources used in operations. Earthing of devices and instruments should be done with utmost care using proper cords and cables.

4.1.3.1. STATIC TESTS:

An ADC does not have a unique voltage input corresponding to each output code- there is a small input voltage range equal to 1/2 LSB in width (for an ideal noiseless ADC) that will produce the same digital output code. This is called as the quantization uncertainty, and it can be the source of confusion when specifying and measuring ADC static transfer characteristics. Any shift from this value during transition adds missing codes to the results. The static absolute accuracy of an ADC can be described in terms of three fundamental kinds of errors. They are

offset errors, gain errors and non-linearity errors. There are many methods to measure the static errors of an ADC- the proper choice depends upon the specific objectives of the device.

Offset and Gain error:

In an ideal A/D converter, an input voltage of q/2 (0.5LSB) will just barely cause an output code transition from zero to a count of one. Similarly the final transition code is obtained at FS-1.5LSB. Any deviation from these values are called *Zero Scale Error, Zero Scale Offset Error, or Offset Error*. Offset error is a constant and can easily be factored or calibrated out. This error can be positive or negative when the first transition point is higher or lower than ideal, respectively. Positive or negative offset errors are due to the inherent device properties, the dye properties and inbuilt resistors used.

For the measurement of offset error, a DC input is given to the ADC with different steps within the full scale range. For an n-bit ADC, the code corresponding to a given DC voltage is given using the equation:

$$Code = \frac{V_{dc} * (2^n - 1)}{V_{FS}} \qquad \{20\}$$

At the step voltages, ADC samples are collected and the corresponding codes are noted down. At both the lower and higher end sides of the voltage, samples are taken which should correspond to 0000 and FFFF codes. From the Figure 4.1-6(a) shown below, we can calculate the offset errors associated with an ADC. Although given for a 3-bit ADC, the terminologies can be extended for an n-bit ADC.

Any deviation of the ADC characteristics from the ideal slope of the ADC transfer function is defined as the *Gain Error,* shown in Figure 4.1-7(b). Like the offset, gain error can be both positive and negative. The gain error is expressed in percentage.

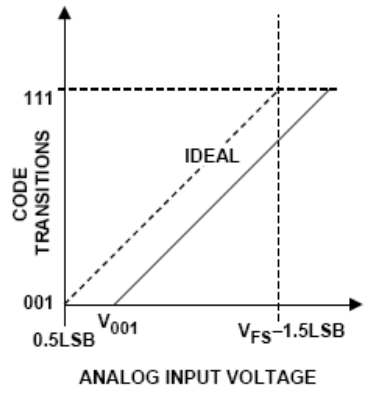

(a)

$$Offset\ Error = V_{001} - 0.5LSB$$

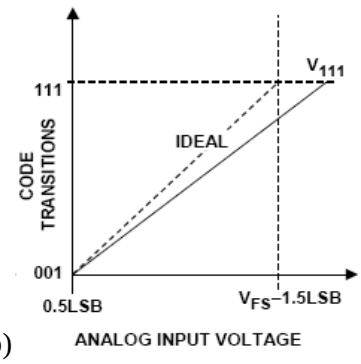

(b)

$$Gain\ Error_{only}(\%) = 100\left(\frac{V_{111} - 0.5LSB}{V_{FS} - 2LSB} - 1\right)$$

Figure 4.1-6: Offset and Gain Error Calculation, Courtesy: Analog-Digital Conversion

Differential and Integral Non-Linearity Error:

When the input voltage changes from one voltage level to the adjacent voltage level, an ideal ADC steps up or down ±1/2 LSB without skipping a count or holding on the same count. The *Differential Non-Linearity (DNL)* error can be termed as the maximum deviation from the ideal step size of ±1/2 LSB between ADC counts corresponding to two adjacent input voltage levels, across the entire input range. Expressed in multiples of LSB, the DNL is an important specification because a more negative differential non-linearity error can lead to missing codes in the ADC. Differential non-linearity is due to encoding process and may vary considerably depending on the ADC encoding architecture. These DNLs in the ADC transfer function produce distortion products which not only depend on the amplitude of the signal but also the positioning of the DNLs across the ADC transfer function.

Analogous to the linearity error of an amplifier, the *Integral Non-Linearity (INL)* error is defined as the maximum deviation of the actual characteristics of the converter from the ideal straight line characteristics. The magnitude of linearity error is the maximum deviation from a "best straight line", with the output swinging through its full-scale range. INL is expressed in % of the full-scale range. The overall non-linearity of an ADC is due to the integral non-linearity of the front-end and SHA as well as the overall integral non-linearity in the ADC transfer

function. Overall integral non-linearity produces distortion products whose amplitude varies as a function of the input signal amplitude. The Figure 4.1-7 below shows an example of an ideal ADC output (blue line) with an ADC with INL (red line).

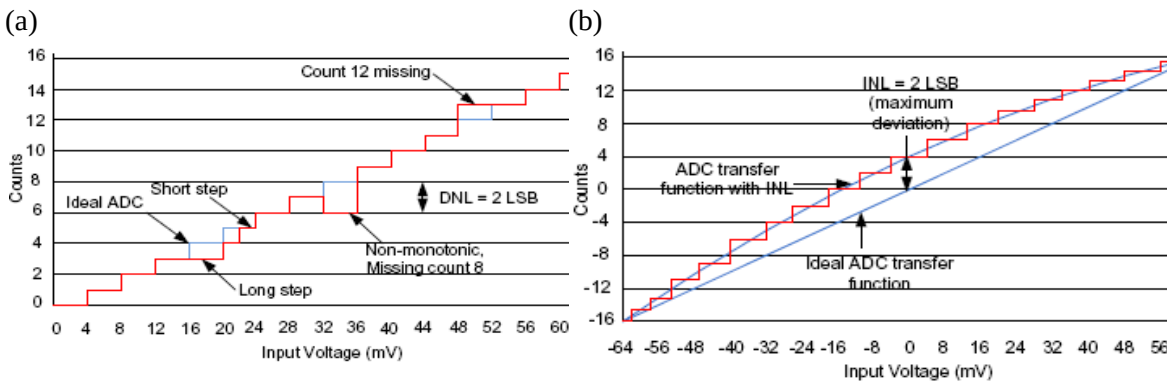

Figure 4.1-7: Differential and Integral Non-Linearity Errors, Courtesy: Analog-Digital Conversion

4.1.3.2. DYNAMIC TESTS:

The only errors (ac or dc) associated with an N-bit ADC are those related to the sampling and quantization processes. The maximum error an ideal converter makes when digitizing a signal is ±1/2 LSB. In addition to the quantization process using dc signal, quantization error for any ac signal spanning more than a few LSBs can be approximated by the uncorrelated saw-tooth waveform having peak-to-peak amplitude of q, the weight of an LSB. With widespread growth in ac testing of ADCs, ac specifications such as SNR, SINAD, ENOB, THD, SIAND, etc., have become integral parts of all sampling ADC datasheets. Of the numerous ADC ac specifications few are sighted below. These specifications are vital to emerging applications in communications, where wide dynamic range is of utmost importance.

Signal to Noise Ratio:

Signal-to-Noise Ratio (SNR) is the ratio of the rms signal amplitude to the mean value of the root-sum-squares (rss) of all the spectral components. It does not include the signal harmonics and the dc components, leaving only the noise terms. Plotted generally for the first 5 harmonics

because of their dominance, SNR plots degrade at high frequencies. The equation for calculating the SNR can be given as:

$$SNR = 6.02N + 1.76dB \qquad \{21\}$$

Signal-to-Noise and Distortion Ratio:

Similar to the SNR, the Signal-to-Noise-and-Distortion Ratio (SINAD) is also the ratio of the rms signal amplitude to the mean value of the root-sum-square of all the spectral components, including the harmonics, but excluding the dc. SINAD is a good indication of the overall dynamic performance of an ADC as a function of input frequency because it includes all components which make up the noise (thermal noise included) and distortion.

Effective Number of Bits:

As discussed earlier, an ADC is never able to achieve the ideal number of bits, falling short by a few. The practical number of bits with which the ADC operates is termed as the *Effective Number of Bits (ENOB)*. Calculation of ENOB can be given by:

$$ENOB = \frac{SINAD - 1.76dB}{6.02} \qquad \{22\}$$

If the input signal is less than full-scale, the above equation must be corrected as follows:

$$ENOB = \frac{SINAD - 1.76dB + Level\ of\ Signal\ below\ Full\ Scale}{6.02dB} \qquad \{23\}$$

Total Harmonic Distortion:

Defined as the ratio of the rms value of the fundamental signal to the mean value of the root-sum-square of its harmonics (only the first 5 are significant), Total Harmonic Distortion (THD) is specified with the input signal close to the full-scale. However THD can also be specified for any specified voltage level. Like SFDR, THD is also used to test the quality of signals.

Spurious Free Dynamic Range:

Used in a communication application, *Spurious Free Dynamic Range (SFDR)* of an ADC is defined as the ratio of the rms signal amplitude to the rms value of the peak spurious spectral content measured over the bandwidth of interest. SFDR is a quality testing parameter and considers all sources of distortion, regardless of the origin. It is generally plotted as a function of signal amplitude, expressed relative to the signal amplitude (dBc) or the ADC full-scale (dBFS) shown in Figure 4.1-8.

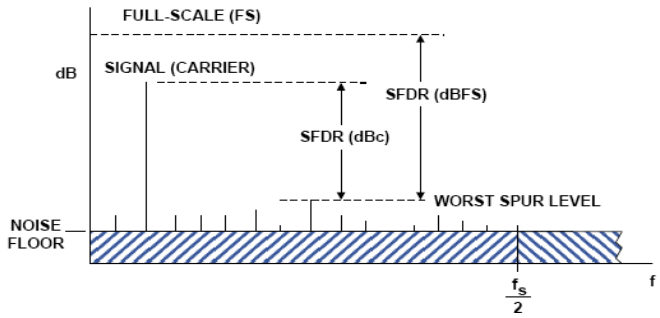

Figure 4.1-8: Spurious Free Dynamic Range

In order to test an ADC for the Static Test a DC signal was required. For the generation of DC signal we have used ***Model 532 GPIB Remote Controlled Precision DC Source/Generator from Krohn-Hite Corporation***. A PSoC program to obtain the samples for a given input voltage was written using ***PSoC Creator 2.1***. Using the ***LabView*** code, an integrated circuit design was made which included input being given to the PSoC kit from the DC source through GPIB and output being written to a .txt file through the COM port. The UART was used for making the connections. Once the input signal was switched on, voltages at 0.1V step size were generated. For the 16 bit ADC used, a total number of 8192 samples were obtained for each level. The codes obtained for the different input voltages are given below.

A ***MATLAB*** code was then run which would count the scattered codes and their number from the ideal value for a particular voltage. The maximum scattered code corresponding to the voltage was noted down and plotted against the voltage using MATLAB. Before plotting, an ideal ADC transfer function was drawn. Now with the two plots together, we had a rough estimate of the offset voltage. Again, the above equations used to calculate the offset error. The

same procedure was followed for both the offset and gain error calculation. The entire MATLAB code is presented in Appendix 1.

Similar procedure was followed for the Dynamic Testing using AC signal. A ***Function Generator*** was used to generate AC signal of 2V peak-to-peak. Signal from the generator was connected as an input to the ***PSoC Evaluation Board*** for testing. Program using PSoC Creator2.1 was written which took AC input to generate codes. A ***COM-PORT*** connection was made between the PSoC and the local computer which would receive the digital codes for the corresponding AC inputs using ***Hyper Terminal Transfer***. From the codes obtained, ADC noise analysis and dynamic parameters calculations were done. Figure 4.1-9 below shows the process flow for ADC Static and Dynamic tests.

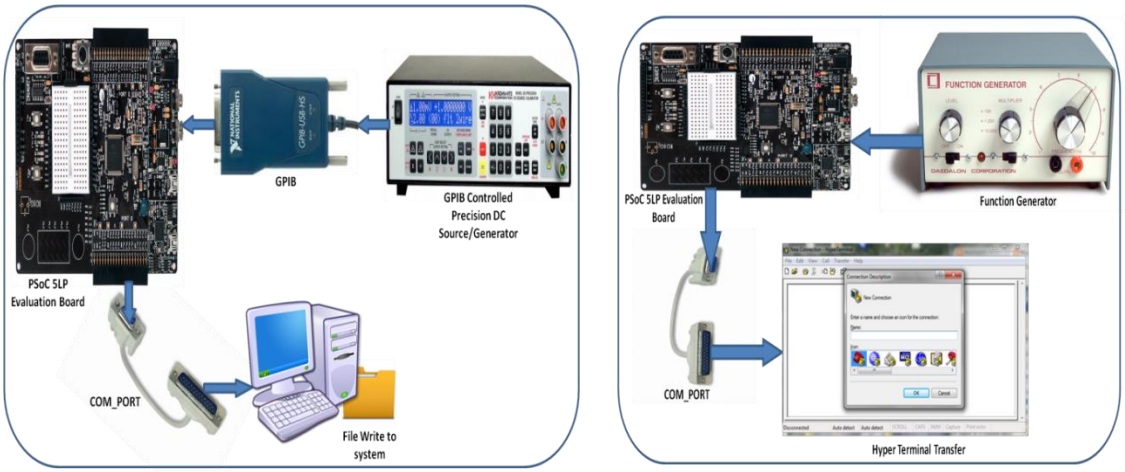

Figure 4.1-9: Process Flow for ADC Static and Dynamic Test

4.1.4. SPARTAN FPGA:

In the first phase of designing the digital control electronics for the GBR, an option of integrating packaged digitizers with FPGA is tested. For this the ADS1278 from Texas Instrument is interfaced with Spartan FPGA from Xilinx having an inbuilt PROM, which reduces the size of the PCB. The ADS1278 is a 8 channel, 24 bits Delta-Sigma ADC available in a 84 pin ceramic flat package, with high temperature range. As per the requirements of the

project only two channels and 16 bits of the ADC have been used. This reduction in the number of bits is called as *truncation*. Features like re-programmability, simpler design, almost nil NREs (non-recurring expenses) of the FPGA make it our first choice for the project. The connections of ADC with FPAG for design of the controller and integrator module is shown below in Figure 4.1-10.

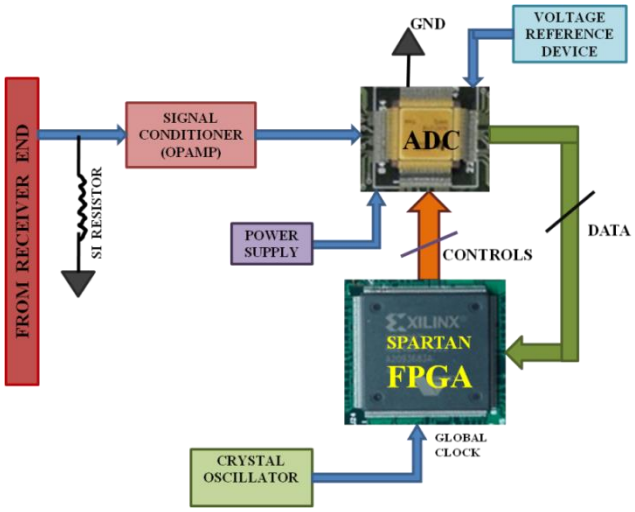

Figure 4.1-10: Block Diagram of ADC1278 Interfacing with SPARTAN FPGA with Controls

Since the project aims at comparing the design aspects of various sensor technologies available in the market, the option of using a Programmable System on Chip (PSoC) has also been proposed. However, due to time constraints, the PSoC has only been used to create a controller and integrator module (described later). Implementation of the PSoC in schematic has so far not been done, but is definitely aimed for.

4.1.5. DATA INTERFACE:

4.1.5.1. UART MODULE WITH RS 232 INTERFACE:

The UART User Module is an 8-bit Universal Asynchronous Receiver Transmitter that handles duplex RS-232 compliant data format serial communications over two wires. Received and transmitted data format includes a start bit, optional parity, and a stop bit. The RS-232 is the most widely used standard for serial interface communications. Due to its cheap, freely

available and widespread use even over higher speed standards, RS232 is popular till date. Application Programming Interface (API) firmware routines of any device are provided to initialize, configure, and operate the UART. Even in the design of the control circuitry using the FPGA, data interfacing is done using RS232. Figure 4.1-11 below illustrates the basic block diagram of a UART connection.

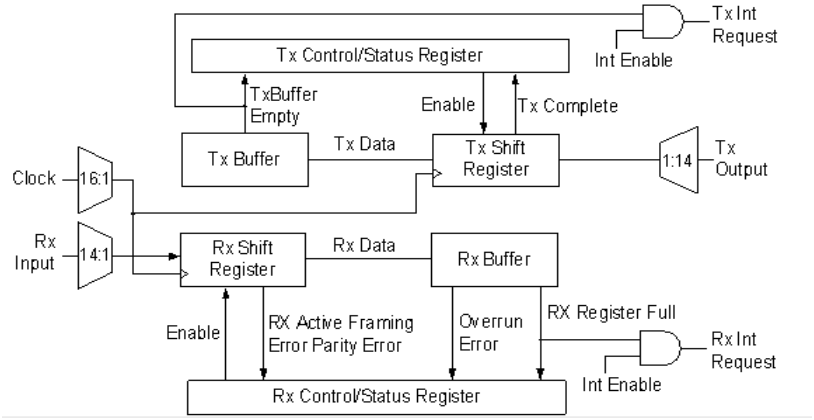

Figure 4.1-11: Block Diagram of UART with RS232

Moreover, interfacing between PC and PSoC chip to be used in the second phase of experiments in GBR design, the RS232 is recommended for use. The UART User Module implements a serial transmitter and receiver. The UART maps onto two PSoC blocks designated TX and RX, in the PSoC Designer Device Editor. The TX PSoC block provides transmitter functionality and the RX PSoC block provides receiver functionality. RX and TX operate independently. Each have its own Control and Status register, programmable Interrupts, I/O, Buffer register, and Shift register. They share the same enable, clock, and data format. Enabling and disabling is performed using the API provided functions. The UART User Module clock is shared by both the RX and TX components. The clock frequency selected must be eight times the frequency of the required data bit rate. The clock is configured using the PSoC Designer Device Editor. The data received and transmitted is a bit stream that consists of a start bit, eight data bits, an optional parity bit, and a stop bit. The parity may be set to none, even, or odd, and is set using the PSoC Designer Device Editor or using the UART API.

A PSoC program is written to interface an ADC with the local computer using a UART for transferring of data and control. Snapshots of the program used for data interfacing using RS232 connection with the UART is shown below in Figure 4.1-12. Again, Hyper Terminal connection found within the computer is used for transferring the obtained digital codes as shown in Figure 4.1-13.

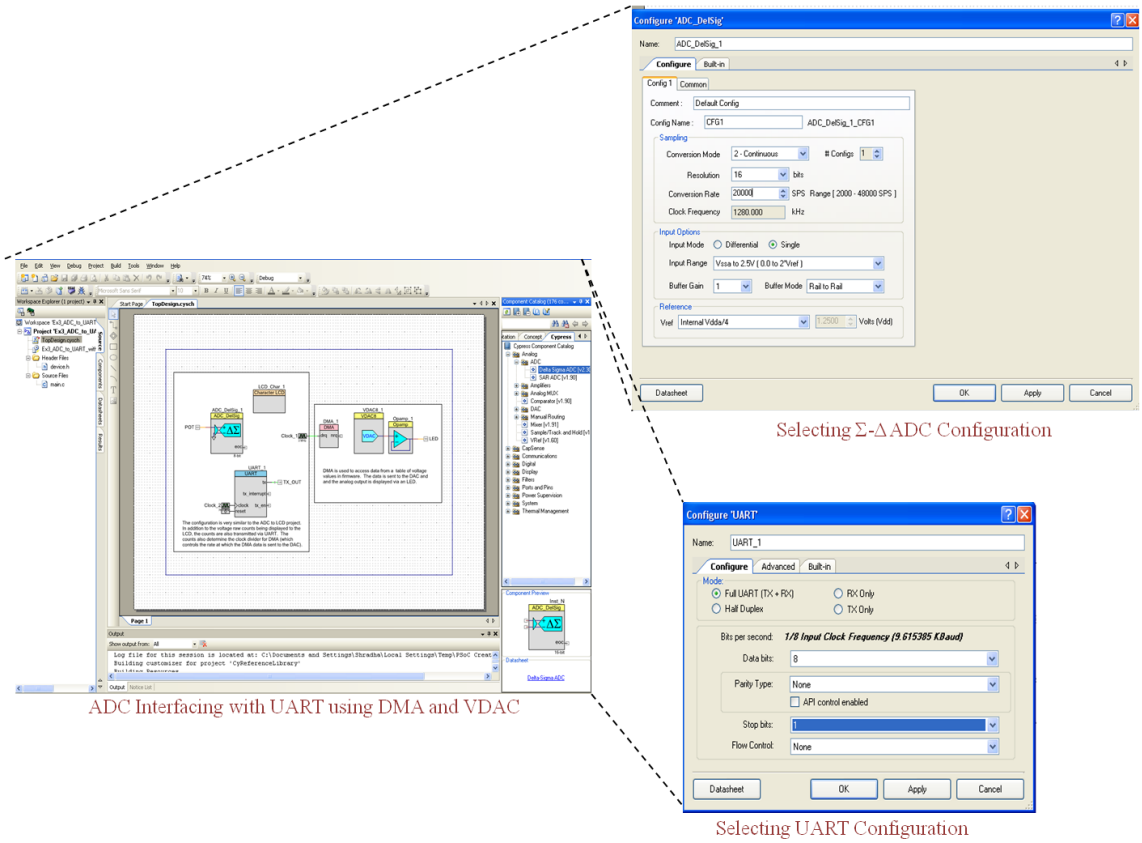

Figure 4.1-12: Testing of UART Connection with PSoC using PSoC Creator2.1 Software

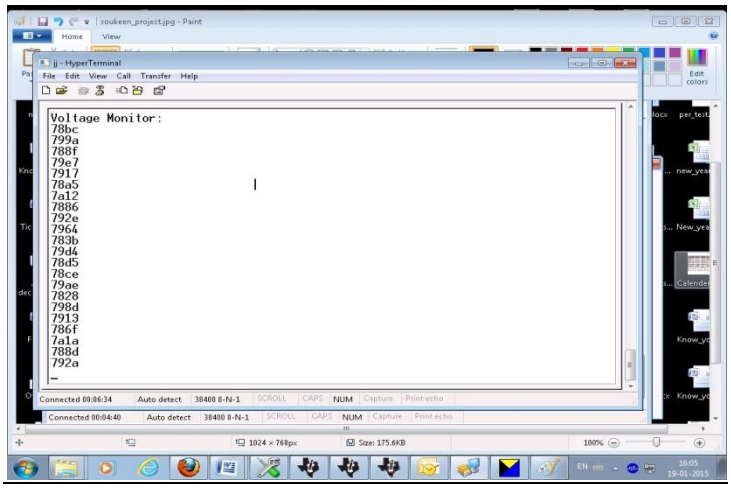

Figure 4.1-13: Digital codes collected using RS232 and seen on desktop via Hyper Terminal

4.1.5.2. ZIGBEE WIRELESS MODULE:

With the radiometer module designed to be placed behind the antenna inside the earth station, in the field, a newer technology of wireless data communication has been proposed. This wireless network transfer is intended to be done using the ZigBee wireless module.

ZigBee is a wireless technology developed as an open global standard to address the unique needs of low-cost, low-power consumption, and low rate, wireless M2M networks targeted towards automation and remote control applications. The specification is a packet-based radio protocol intended for low-cost, battery-operated devices that allow devices to communicate in a variety of network topologies and can have battery life lasting several years. The ZigBee standard operates on the ***IEEE 802.15.4*** physical radio specification and operates in unlicensed bands including 2400, 900 and 868 MHz.

In order to use ZigBee protocol, it has to be implemented in the hardware. ZigBee Transceiver chip identified is ***IEEE 802.15.4 chipset, CC2530 SOC from Texas Instruments*** containing a 8-bit microcontroller and MAC processor along with RF interface in a small QFN40 package. The CC2530 chipset comes with 256 KB of flash which holds the entire microcontroller code. In order to realize the target of Tile Tele-commanding between multiple units, it is required to

develop Application Software for CC2530 SOC; then this application software has to be programmed into the internal flash memory which will store the application software; and to verify the desired functionality by testing this code. For all these activities, various developments and testing tools are required which includes the following:

- IAR Embedded Workbench
- Flash Programmer, and
- RF Packet Sniffer

As proposed in the project, a provision for wireless network communication was also provided using the ZigBee module. Available in separate package, the ZigBee module was mounted on the test board and its interfacing with the PSoC was done using programming. Two test boards were prepared which were used for the purpose of transmitting and receiving the signals. Similar to the RS232 interface using the UART, codes were written in PSoC Creator2.1 which upon execution gave codes that were wirelessly accessible using the ZigBee. Sample codes were collected and the Hyper Terminal connection module was used for view on the computer.

4.1.6. CONTROLLER AND INTEGRATOR CIRCUIT USING DIGITIZER:

As the main function of the digitizer is to act both as a controller and an integrator, the in-built Σ-Δ ADC present in the PSoC chip was programmed to function as an integrator. The lone **Σ-Δ ADC** present was used in single end mode for **16 bits** at **16 kHz** clock frequency. The Figure 4.1-14 shown below shows the Top Design layout of ADC acting as an integrator and controller using the PSoC Creator2.1 software. The associated code is given in Appendix.

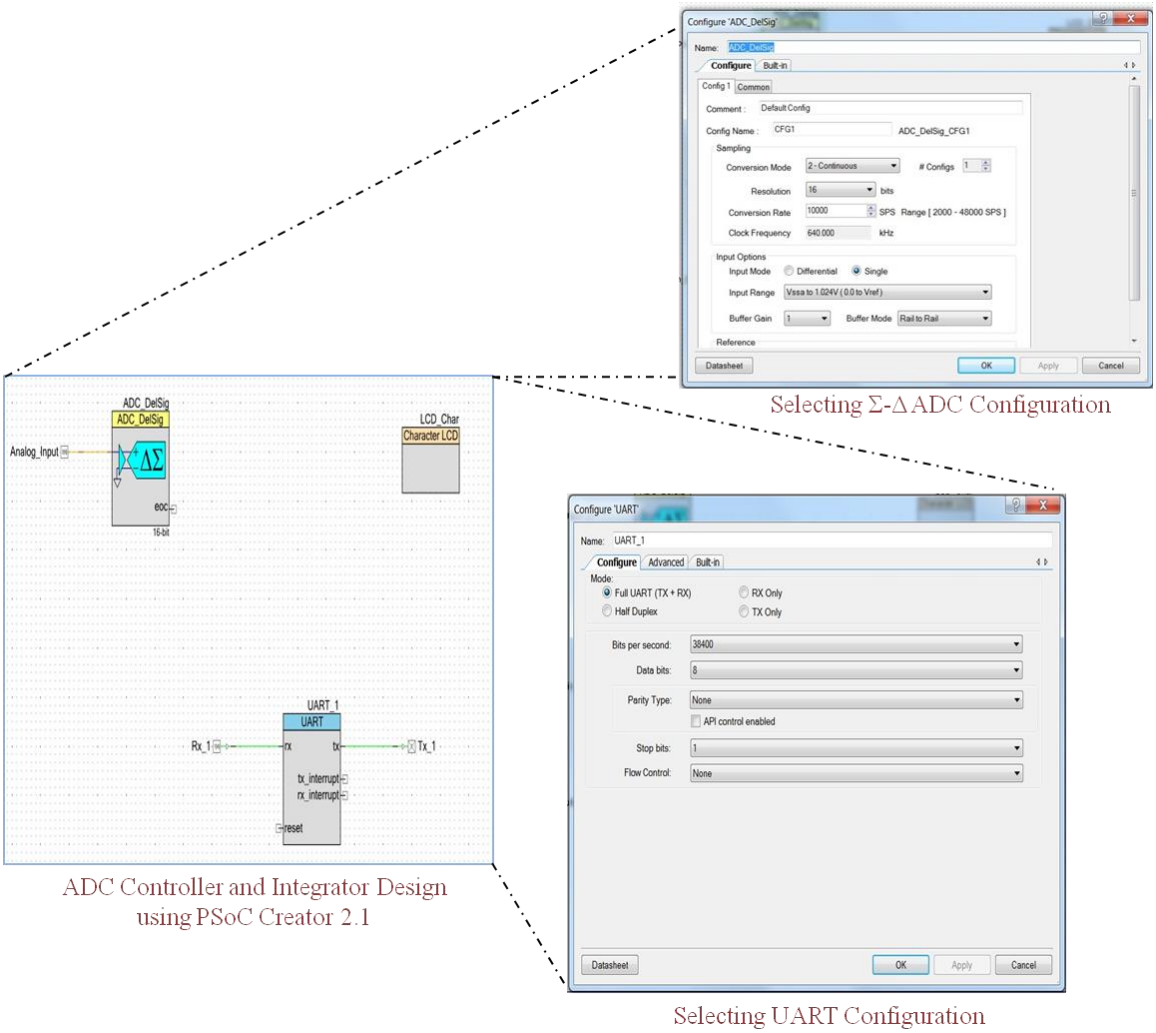

Figure 4.1-14: Testing of PSoC's inbuilt ADC using PSoC Creator2.1 software

4.1.7. PREPARATION OF SCHEMATIC FOR GBR BOARD:

In the design of any digital circuitry, the schematic preparation is one important step, involving the identification of the different electronics components, in-detail study of their datasheets to know its controls and finally the interconnection between these components in order to

complete the circuit. Similar is the case with the GBR project at hand. Below given are the schematic blocks of the different electronics components used, like SPARTAN FPGA, ADS1278, USB INTERFACE and most importantly the POWER SUPPLY to the board.

4.1.7.1. SPARTAN FPGA: POWER SUPPLY, I/O BANKS AND PROM CONFIGURATION:

The Spartan FPGA (U11) has 4 I/O banks each with 9 pins requiring 3.3V supply. For the internal functioning of the macrocells, dedicated 1.2V supply is provided at the VCC_INT pins as in Figure 4.1-15. The auxiliary pins also require a 3.3V supply, similar to the IOBs. The ground pins corresponding to each supply are earthed, providing an electrical stability to the board. Also shown to the right, are the bypass-capacitor banks for the two supplies.

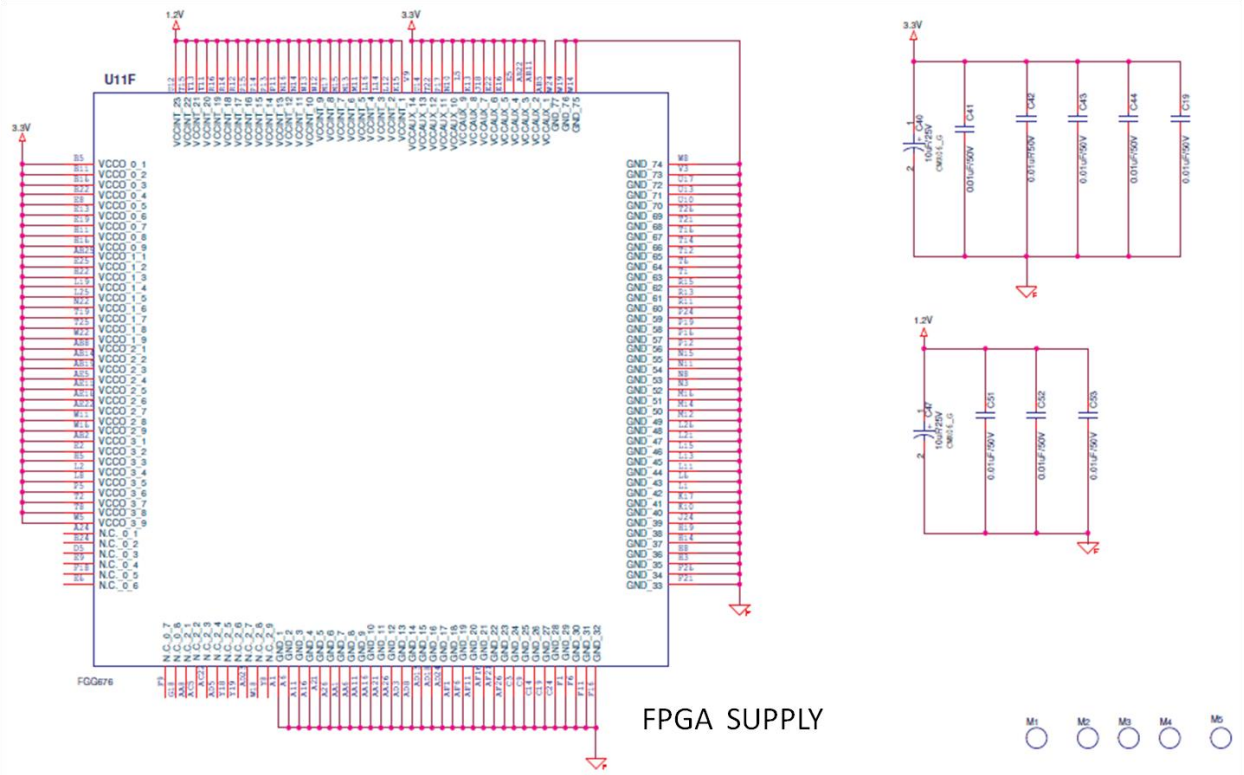

Figure 4.1-15: Schematic diagram of FPGA, showing its I/Os and power inputs

The next Figure 4.1-16 shows the 4 I/O banks present within the FPGA (U11B, U11C, U11D and U11E) along with the 16 MHz crystal oscillator connection (U14) responsible for providing the global/master clock control to the FPGA device. The various controls and data lines for the dedicated banks, going into and out of the FPGA, have been identified and marked. The banks of the FPGA have been assigned different dedicated pins for various operations and controls. Like for example, for the control of the digitizer, ADS1278, ADC_INPUT, ADC_STROBE, ADC_CLK, DIN and DOUT pins are given to the FPGA. Communication with PROM also requires MODE selection pins (MODE0, MODE1, MODE2), SYNC pin, oscillator clock (OSC_CLK), etc. given to the FPGA. Likewise, data interfacing with RS232 and wireless ZigBee module also have data, clock and strobe pins provided for interconnection. Keeping in mind few pins for future use, SPARE0 to SPARE7 pins are kept.

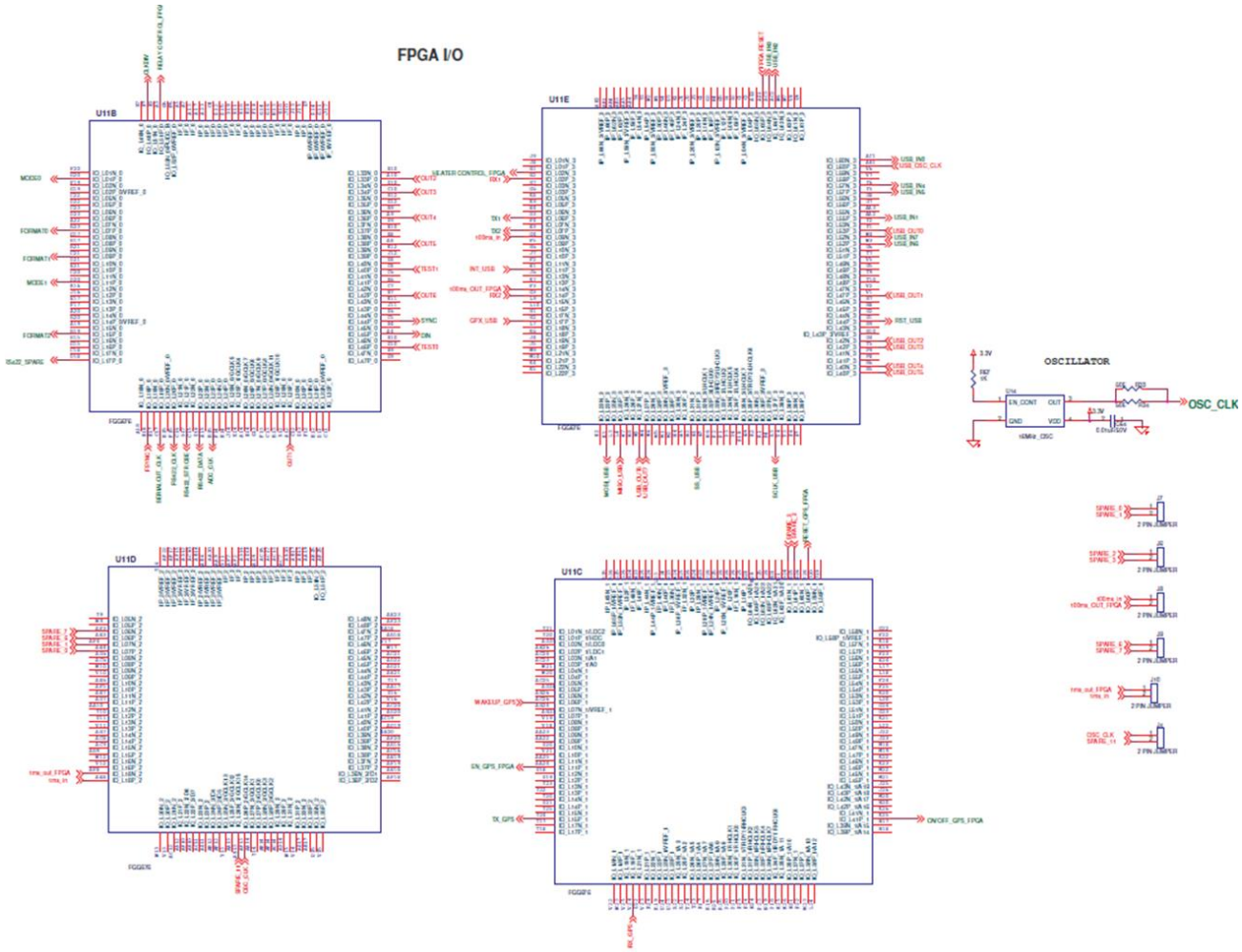

Figure 4.1-16: Schematic diagram of FPGA I/O banks along with crystal oscillator

Communication of the FPGA with other devices for controls and data signals is done through the PROM (U11A). Unlike other Xilinx FPGAs, one advantage associated with the Spartan FPGA is that the PROM is built inside it, thus saving additional board space. The PROM has the flags to all the dedicated signals, such as INIT, TDI, TDO, DONE, CCLK, etc. Upon receiving the signal from the PROM, the FPGA acts accordingly. The jumper pins J3, J1 and J5 provided at the right side of the Figure 4.1-17 shows the different mode selection, M0, M1 and

M2 respectively. As the PROM has a certain lifetime of operation, commands can also to be given to the FPGA, bypassing the PROM. Such provision is made using the JTAG and Trans-Receiver connections. Schematic symbols ST1, ST2 and U5 show the connections of the JTAG and Trans-Receiver respectively.

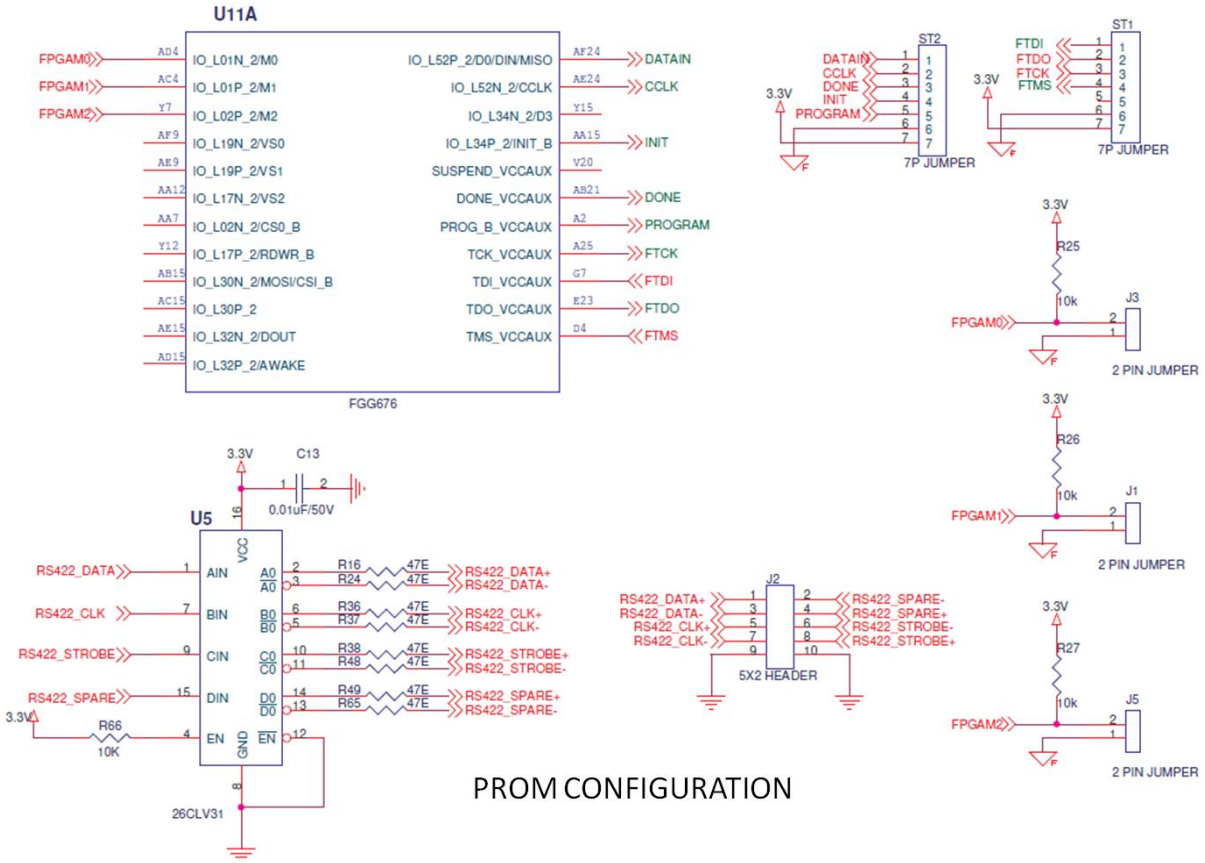

Figure 4.1-17: Schematic diagram of FPGA's PROM Configuration

4.1.7.2. ADS1278, POWER SUPPLY AND USB INTERFACE:

ADS1278, denoted by U15, is used as the digitizer for control and integration purpose. It has 3 different power supplies 5V, 3.3V and 1.8V for its different control and data activities. ADC receives analog data from the back-end of the receiver terminal through the connector K2, for

power and analog interconnections. Two channels of single ended input is fed to the ADC along with conditioned signal using the U8A and U8B unity gain buffers. A separate voltage reference, U10, chip is also included for the ADC. Figure shown below, gives the schematic of the ADC with its interconnections with the power connector, analog inputs, voltage reference, outputs and control signals. Banks of pull-up and pull-down capacitors are also shown in Figure 4.1-18.

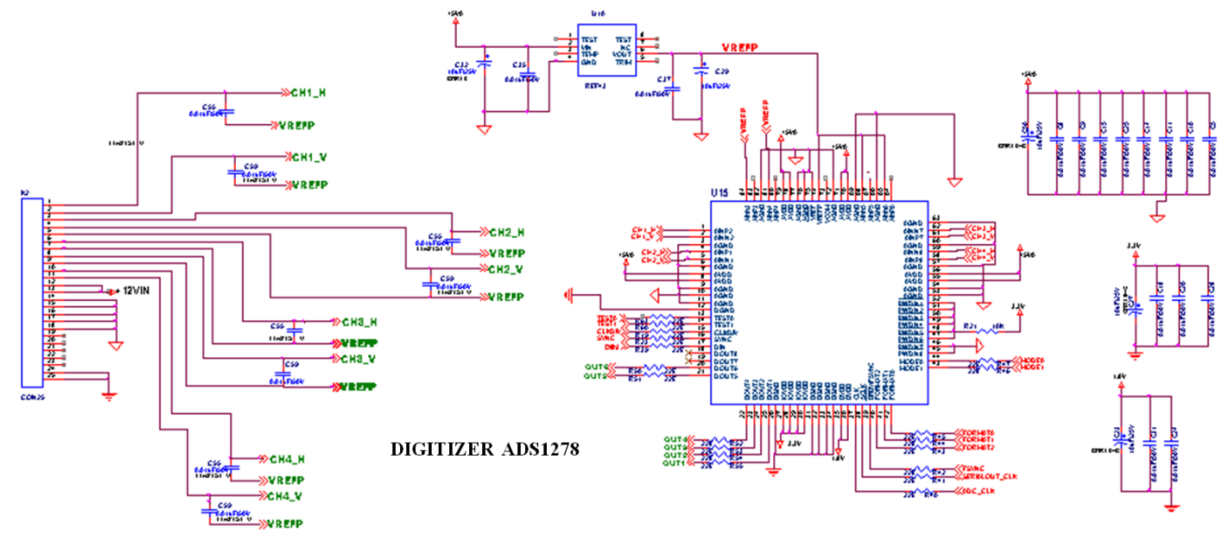

Figure 4.1-18: Schematic diagram of ADS1278 showing connector and capacitor banks

The power supply of 12V is provided through the K2 connector, shown in the above figure. However, for the different power requirements in the board, provision of voltage regulators, termed as *Low Droop-out Voltage* (LDOs) are made. These units (U1, U2, U3 and U4) convert the 12V to the required 5V, 3.3V, 1.2V and 1.8V respectively. The values of the resistors and capacitors used, in series and parallel combinations, within the circuit of the LDOs determine the output voltage for a fixed input as shown in Figure 4.1-19.

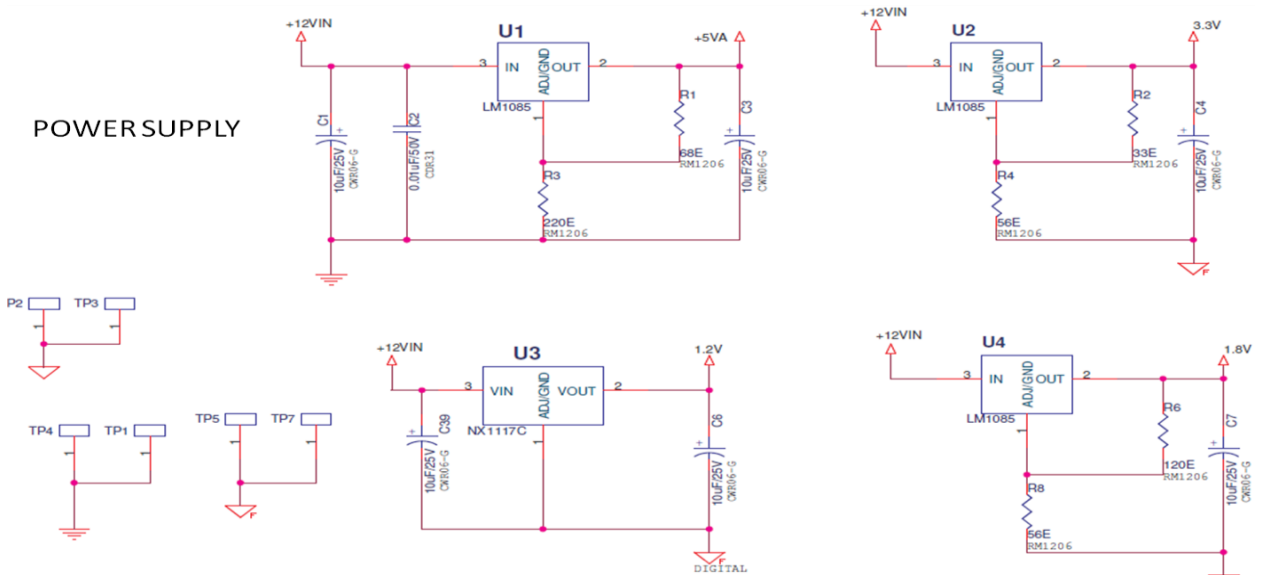

Figure 4.1-19: Schematic diagram of the power supply connections via Low Droop-Outs (LDOs)

Finally at the end, the schematic for the USB interface (U6) is shown. RS232 is used for data interfacing between the system and the local computer for data transfer as in Figure 4.1-20.

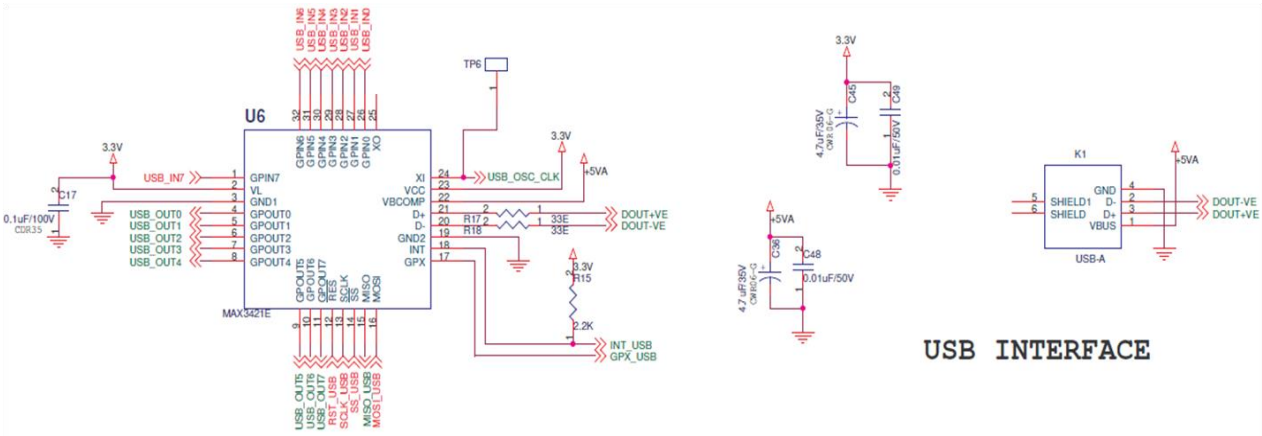

Figure 4.1-20: Schematic diagram showing USB for data interfacing

4.1.7.3. DESIGN OF PCB USING SOFTWARE, ZUKEN'S CADSTAR:

With the finalization of the schematic, the actual job of PCB design starts with the PCB layout. Using Zuken's CADSTAR software, the schematic is mapped into the PCB layout. This process is called as *ECO-UPDATE".* The eco-update contains all information related to the different components to be used, a generation of Bill-of-Materials (BoM), components' PCB footprint selection and designated information related to the reference and component names. A PCB may consists of two or more layers as per project specification.

Once the schematic is transferred to the PCB, the placement and routing of the components begins. Size and shape of the PCB along with its package is decided. Quality Assurance and Quality Control (QA & QC) guidelines are followed in relevant component placement as well as to maintain the overall reliability of the board. Placement of holes and studs, for mechanical stability of the board, are decided. Connector positions are also finalized.

As the board is designed to carry various electronic components and electrical connections, calculations overall power consumption of the board is made. These calculations take into account the voltage and current requirements of different components and their placement in the board. With so many components present on the board, heat generated from them is an important aspect to be taken care of. For the sake of it, proper heat dissipation arrangements are made. Components are always operated on low stress levels as per the QA & QC guidelines. Thermal vias, chotherm sheets, studs below component dye, etc. are a few options available for management of thermal stress.

As mentioned earlier, a PCB is made up of number of layers, with the number depending upon the complexity of the board. The top and bottom layers are used for the component placement, where as routing between the components is done in top, bottom and in between layers also. For the provision of power supply to the board, a separate arrangement of power layer is made. For different voltage levels, different layers can be made, or else division of the layer into different voltage levels can also be done. For electrical neutrality of the board, the corresponding ground layer is also made. For mixed signal boards, provision for analog ground (AGND) and digital ground (DGND) is also provided. The Figure 4.1-21 below shows the two important PCB layers. The left image is of the TOP_ELEC with TOP_SILK and the right image shows the BOTTOM_ELEC with BOTTOM_SILK. TOP_ELEC layer shows almost all the components and their placement on the board. Routing done on the top layer are also visible. However, with

a few components like resistors and capacitors soldered on the bottom layer, the BOTTOM_ELEC does not show the components. But few routes are also seen on the bottom layer.

(a) (b)

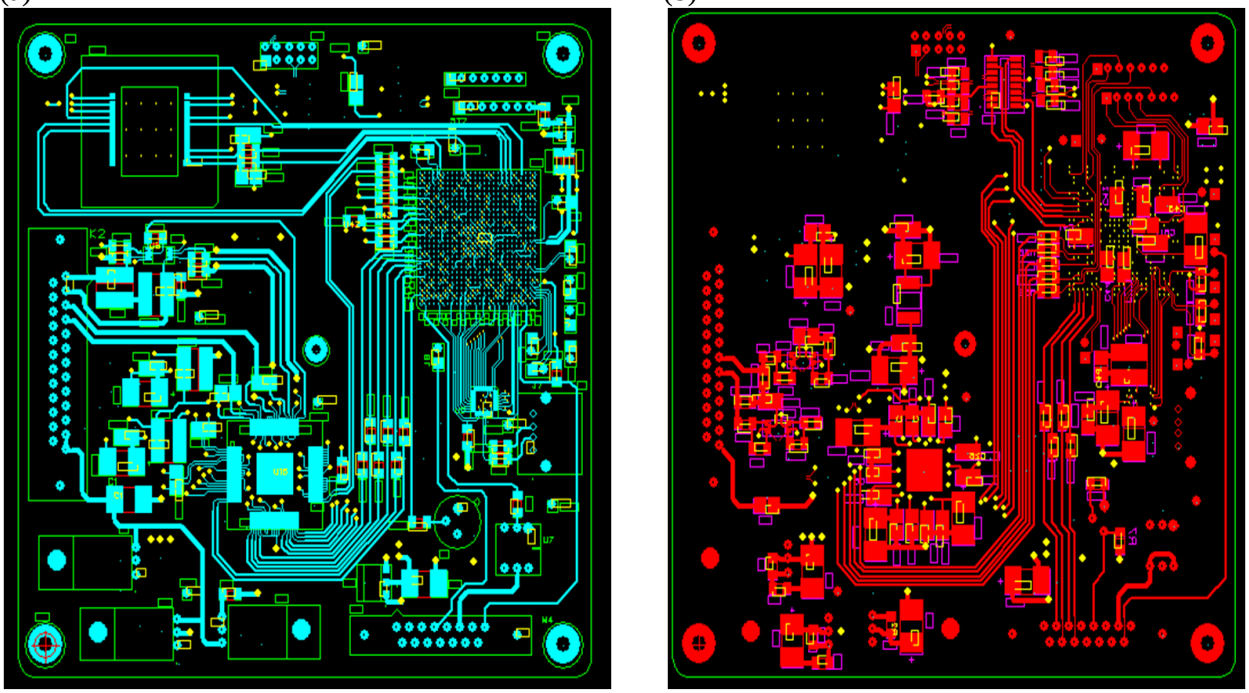

Figure 4.1-21: PCB layout diagram showing (a) TOP_ELEC and (b) BOTTOM_ELEC layers

4.2. RAIN ATTENUATION CALCULATIONS:

It is evident from the literature surveys made that millimeter range waves are affected by precipitation, especially due to rain. It has also been noticed that the attenuation increases with rainfall rate, as well as with an increase in frequency, there is a significant increase in the attenuation levels. The rain attenuation prediction loss is also dependent on raindrop size distribution, rain rate, frequency and regions. However, the rain-drop size distribution is not taken into account in this study of estimation of rain attenuation in the signal transmission link. The following methodological flow diagram in Figure 4.2-1 shows the processes involved in calculation of rain attenuation in the signal transmission link and a comparative study between the two Earth-stations

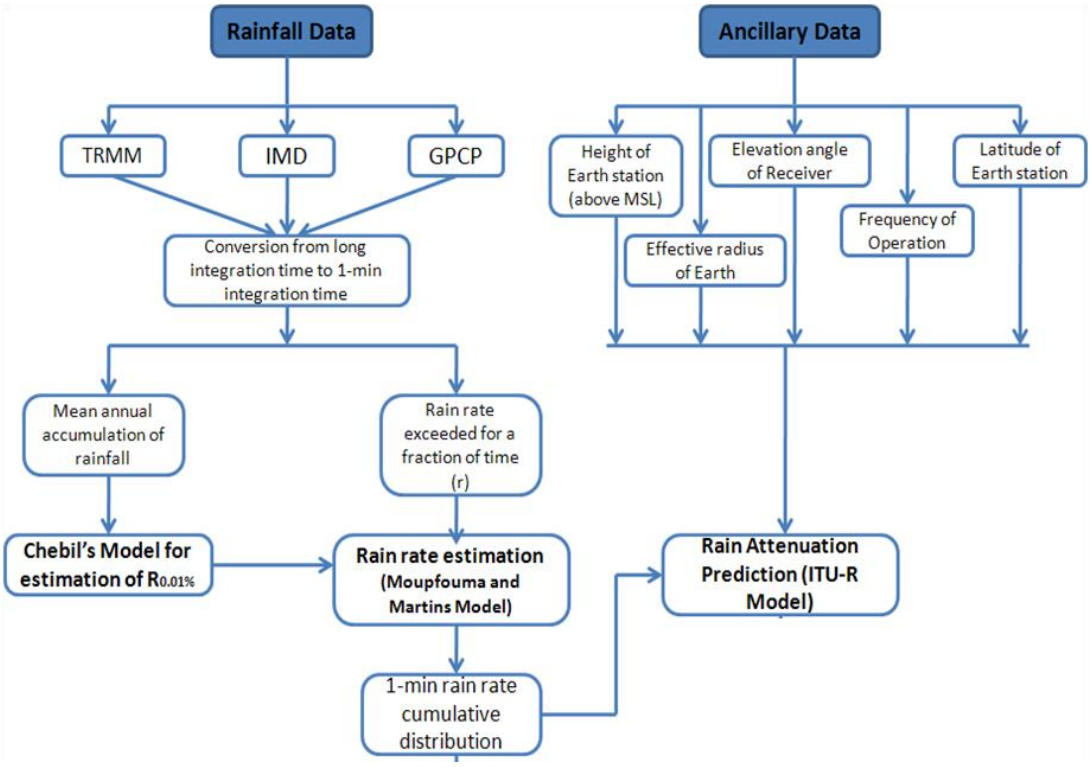

Figure 4.2-1: Methodology flow diagram showing Rain Attenuation Calculations

4.2.1. RAINFALL DATA RETRIEVAL:

The rainfall data for the two earth stations, the Ahmedabad (AES) and New Delhi earth stations (DES), under study was obtained from the respective Automatic Weather Station (AWS) data. The details for the stations are given below:

- ISRO0303_15F12F (SAC, Ahmedabad)
- ISRO0463 (GD-SEOG-D, DES)

The rainfall data procured on an hourly basis from the AWS was converted to a daily data by averaging over the entire period of acquisition as in Figure 4.2-2. This data obtained was the rain rate (mm/hr). Similar averaging technique was applied on the calculated daily data over a particular month for a period of 5 years. The cumulative distribution of rainfall over AES and DES were for an integration time of 60 minutes. But for the rain data to be used in the attenuation model, it was necessary to convert the available data to a shorter integration time, of about 1-minute. For this purpose the model proposed in Characteristics of precipitation for propagation modeling, ITU-R P-837.6.

R	S	T	U	V	W	X	Y	Z	AA	AB	AC	AD	AE	AF	AG	AH
	Date	Daily rainfall (in mm)	Rain_Rate (mm/hr)	Rain_Rate (mm/min)	Date	Daily rainfall (in mm)	Rain_Rate (mm/hr)	Rain_Rate (mm/min)	Date	Daily rainfall (in mm)	Rain_Rate (mm/hr)	Rain_Rate (mm/min)	Date	Daily rainfall (in mm)	Rain_Rate (mm/hr)	Rain_Rate (mm/min)
	JUNE, 2010				JULY, 2010				AUGUST, 2010				SEPTEMBER, 2010			
	6/1/2010	0	0	0	7/1/2010	670	67	1.1166667	8/1/2010	4848	372.9231	6.2153846	9/1/2010	670	335	5.5833333
	6/2/2010	50	2.0833333	0.034722	7/2/2010	1362	71.684211	1.1947368	8/2/2010	5387	448.9167	7.4819444	9/2/2010	2347	335.2857	5.5880952
	6/3/2010	120	5	0.083333	7/3/2010	2776	115.66667	1.9277778	8/3/2010	7366	526.1429	8.7690476	9/3/2010	1011	337	5.6166667
	6/4/2010	120	5	0.083333	7/4/2010	3050	132.6087	2.2101449	8/4/2010	10152	597.1765	9.9529412	9/4/2010	2022	337	5.6166667
	6/5/2010	120	5	0.083333	7/5/2010	1534	139.45455	2.3242424	8/5/2010	182	15.16667	0.2527778	9/5/2010	680	340	5.6666667
	6/6/2010	147	6.125	0.102083	7/6/2010	1891	145.46154	2.424359	8/6/2010	368	16	0.2666667	9/6/2010	2076	346	5.7666667
	6/7/2010	988	41.166667	0.686111	7/7/2010	2920	153.68421	2.5614035	8/7/2010	282	17.625	0.29375	9/7/2010	2439	348.4286	5.8071429
	6/8/2010	702	54	0.9	7/8/2010	811	38.619048	0.6436508	8/8/2010				9/8/2010	2190	365	6.0833333
	6/9/2010	1296	54	0.9	7/9/2010	7	1	0.0166667	8/9/2010	2067	159	2.65	9/9/2010			
	6/10/2010	1296	54	0.9	7/10/2010	58	3.4117647	0.0568627	8/10/2010	3498	159	2.65	9/10/2010	405	405	6.75
	6/11/2010	1296	54	0.9	7/11/2010	88	4	0.0666667	8/11/2010	4563	190.125	3.16875	9/11/2010	3300	412.5	6.875
	6/12/2010	1296	54	0.9	7/12/2010	44	4	0.0666667	8/12/2010	4600	200	3.3333333	9/12/2010	2516	419.3333	6.9888889
	6/13/2010	1296	54	0.9	7/13/2010	48	4	0.0666667	8/13/2010	4400	200	3.3333333	9/13/2010	2968	424	7.0666667
	6/14/2010	1296	54	0.9	7/14/2010	111	4.625	0.0770833	8/14/2010	3654	203	3.3833333	9/14/2010	2568	428	7.1333333
	6/15/2010	1202	54.636364	0.910606	7/15/2010	207	9	0.15	8/15/2010	5544	231	3.85	9/15/2010	3440	430	7.1666667
	6/16/2010	1265	55	0.916667	7/16/2010	207	9	0.15	8/16/2010	5082	231	3.85	9/16/2010	2580	430	7.1666667
	6/17/2010	1523	66.217391	1.103623	7/17/2010	213	9.6818182	0.1613636	8/17/2010	5544	231	3.85	9/17/2010	1290	430	7.1666667
	6/18/2010	1608	67	1.116667	7/18/2010	220	11	0.1833333	8/18/2010	5544	231	3.85	9/18/2010	430	430	7.1666667
	6/19/2010	737	67	1.116667	7/19/2010	264	11	0.1833333	8/19/2010	5382	234	3.9	9/19/2010	1720	430	7.1666667
	6/20/2010	871	67	1.116667	7/20/2010	264	11	0.1833333	8/20/2010	5389	256.619	4.2769841	9/20/2010	860	430	7.1666667
	6/21/2010	1541	67	1.116667	7/21/2010	271	11.291667	0.1881944	8/21/2010	4303	268.9375	4.4822917	9/21/2010			
	6/22/2010	1523	66.217391	1.103623	7/22/2010	1054	43.916667	0.7319444	8/22/2010	821	273.6667	4.5611111	9/22/2010			
	6/23/2010	1523	66.217391	1.103623	7/23/2010	554	79.142857	1.3190476	8/23/2010	1415	283	4.7166667	9/23/2010	4730	430	7.1666667
	6/24/2010	1541	67	1.116667	7/24/2010	1647	164.7	2.745	8/24/2010	1133	283.25	4.7208333	9/24/2010	10320	430	7.1666667
	6/25/2010	1608	67	1.116667	7/25/2010	1387	231.16667	3.8527778	8/25/2010	284	284	4.7333333	9/25/2010	9460	430	7.1666667
	6/26/2010	737	67	1.116667	7/26/2010	2461	307.625	5.1270833	8/26/2010	853	284.3333	4.7388889	9/26/2010	10320	430	7.1666667
	6/27/2010	871	67	1.116667	7/27/2010	4346	310.42857	5.1738095	8/27/2010	570	285	4.75	9/27/2010	10320	430	7.1666667
	6/28/2010	1541	67	1.116667	7/28/2010	7482	311.75	5.1958333	8/28/2010	1735	289.1667	4.8194444	9/28/2010	10320	430	7.1666667
	6/29/2010	938	67	1.116667	7/29/2010	7125	323.86364	5.3977273	8/29/2010	1240	310	5.1666667	9/29/2010	10320	430	7.1666667
	6/30/2010	1139	67	1.116667	7/30/2010	7824	326	5.4333333	8/30/2010	977	325.6667	5.4277778	9/30/2010	10320	430	7.1666667
					7/31/2010	3260	326	5.4333333	8/31/2010	996	332	5.5333333				
			1487.6635	24.79439			3381.7826	56.363043			7738.716	128.97859			10852.55	180.87579

JJAS_2010

Figure 4.2-2: Conversion of daily rainfall data from AWS to 60 min integration time

4.2.2. CONVERSION OF RAINFALL DISTRIBUTION FOR VARIOUS INTEGRATION TIME:

In order to predict reliable rain attenuation for a given location, an appropriate distribution of rainfall rate for the site is required. And furthermore, the distribution is must be based on long-term measured data with 1- minute integration time. Long integration-time rainfall rate is not advised due to its failure to capture high-intensity short-duration rain events and also it is not recommended for communication system design. Therefore, 1-min integration time has been accepted worldwide as the most desirable in the attenuation prediction studies. The *Rain Rate*

Statistics Conversion MATLAB program provided by ITU-R P837.6 is used for this purpose as shown in Figure 4.2-3.

The inputs to the software are given below:

- T-minute integrated P(R): percentage exceedance value between (0-100%)
- T-minute integrated P(R): rain rate values (mm/hr)
- Source integration time (minutes)
- Station details (latitude and longitude)

A provision of direct data input using .csv file is also given along with direct user input.

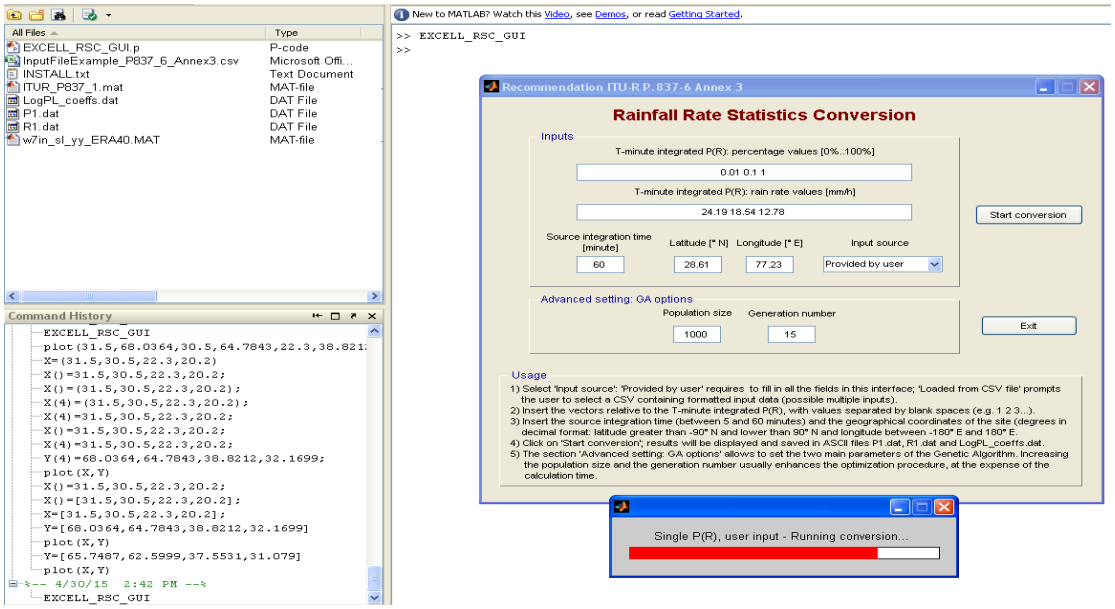

Figure 4.2-3: Screen-shot showing Rainfall Rate statistics converting 60 minute to 1 minute

Once the conversion is complete, a figure is generated depicting both the T-minute integrated input P(R) (blue line) and the 1-minute integrated P(R) estimated by the SW (red line), like shown in Figure 4.2-4.

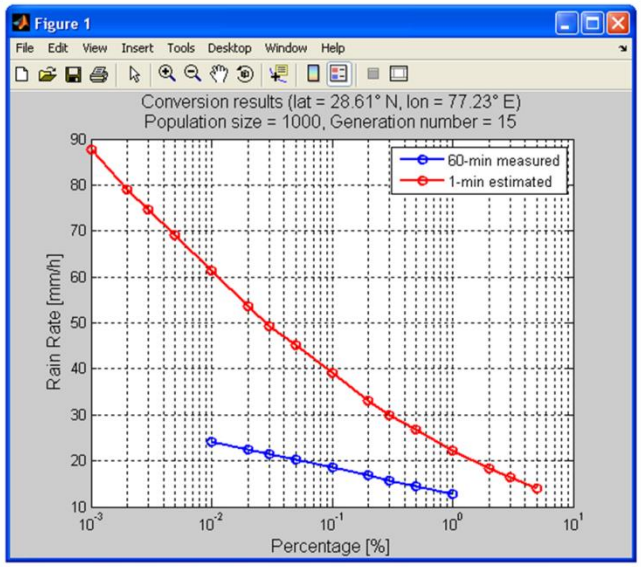

Figure 4.2-4: 1 minute rainfall conversion data

The software also produces additional data related to the coefficients of the power-law equation $[P(R) = P_o \ln\frac{R_a}{R}]$ followed in the conversion shown in Figure 4.2-5. An explanation of the various parameters is listed below:

- ***P1.dat*** and ***R1.dat***: they contain respectively the probability and rain rate vectors of the estimated 1-minute integrated P(R)
- ***LogPL_coeffs.dat***: it contains the values of the log-power law expression defining the estimated 1-minute integrated P(R)

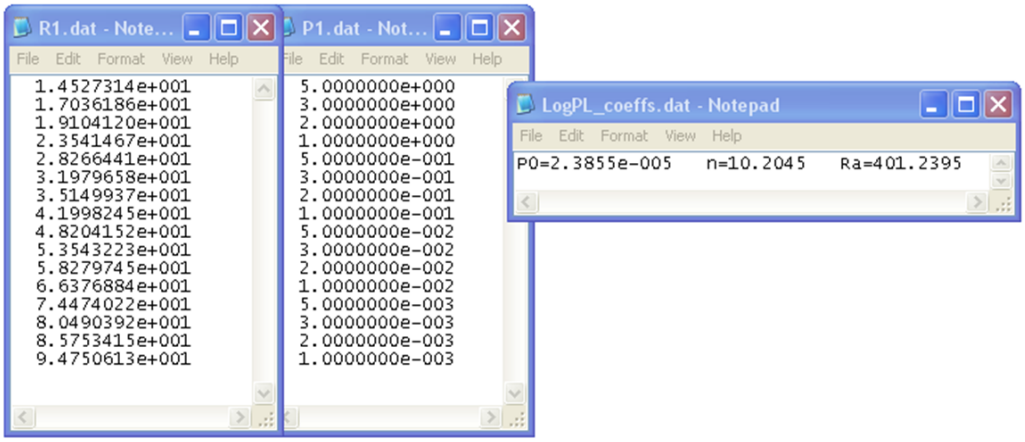

Figure 4.2-5: Power law coefficients

4.2.3. RAINFALL ATTENUATION PREDICTION MODEL, ITU-R P618-8:

ITU-R P 618.6 Model: Basically used for comparing the measured rain attenuation with ITU-R predictions, this model is a step-by-step procedure for calculating rain attenuation cumulative distribution function over the satellite link. The ITU-R model is a step-by-step procedure for calculating rain attenuation cumulative distribution function over the satellite link [58]. The ITU-R model provides the most accurate statistical estimate of attenuation on slant paths. This model provides global rain statistics by dividing the earth into rain regions and assigning a rain rate to each region along with the probability of that rain rate being exceeded. It can be used for the frequencies from 4 - 55 GHz and 0.001 - 5% percentage probability range. The model uses the rain rate at 0.01% probability level for the estimation of attenuation and then applies an adjustment factor to the predicted rain fade depth for other probabilities [59]. Attenuation predictions require first the estimation of a surface rain rate distribution and second the prediction of the radio wave attenuation value distribution, given by the rain rate distribution [60]. The model has been derived on the basis of the log-normal distribution, using similarity principles. Inhomogeneities in rain, in both horizontal and vertical directions are accounted for in the prediction [61]. The limit of the model being the number of station-years of measurements available and not all stations fulfilled the one minute integration time requirement. The geometry is shown below in Figure 4.2-6:

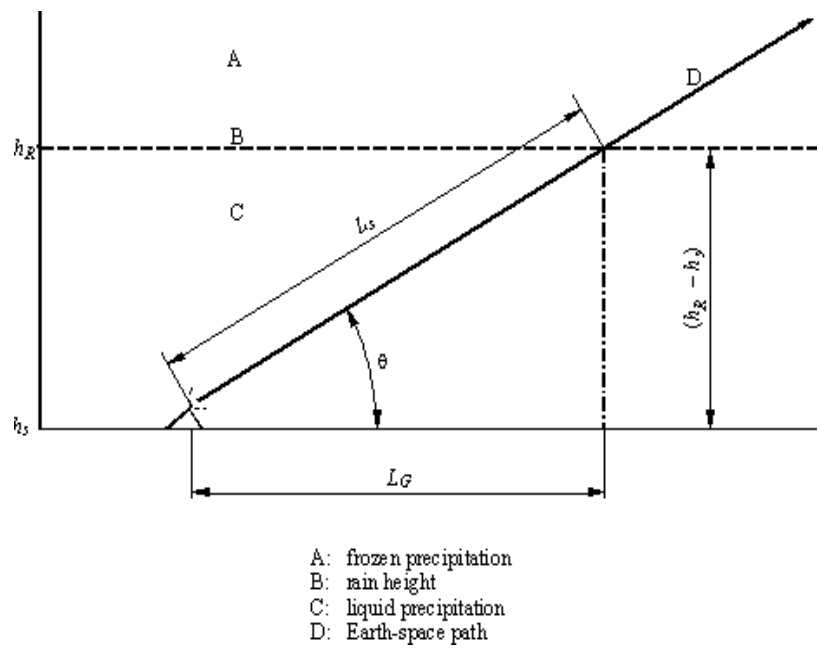

Figure 4.2-6: Schematic presentation of an Earth-Space path giving the parameters to be input into attenuation prediction process

The various steps involved in the model are given as follows:

1. Freezing height during rain (H_R) calculated from the absolute values of latitude and longitude of the Earth station.

$$H_R = 0.36 + h_O \qquad \{24\}$$

Where, h_o=0˚ isotherm height above mean sea level and can be obtained from Isotherm chart provided by "*Rain height model for prediction methods, Recommendation ITU-R P.839-3, ITU-R P Sers., Int. Telecomm. Union, Geneva, 2001*"

2. Slant path length (L_S) below rain height

$$L_S = \frac{H_R - H_S}{sin\theta} \qquad \{25\}$$

Where, H_S = altitude of earth station above mean sea level, in km

θ = elevation angle between the horizontal path and slant path

3. Horizontal projection of slant path (L_G)

$$L_G = L_S \cos\theta \qquad \{26\}$$

4. $R_{0.01\%}$ obtained from 1-min integration of rain rate data by using the frequency dependent regression coefficients provided in ITU-R P.838 Recommendation and using "*Specific attenuation model for rain for use in prediction methods", Recommendation ITU-R P.838-3, ITUR P Sers., March 2005*"
5. The specific attenuation $\gamma_{0.01}$ (dB/km) for 0.01 % of time

$$\gamma_{0.01} = kR_{0.01}{}^{\alpha} \qquad \{27\}$$

6. Path reduction factor ($r_{h,0.01}$) horizontally adjusted for 0.01% of the time

$$r_{h,0.01} = \frac{1}{1 + 0.78\sqrt{\left(\frac{L_G\gamma_{s,0.01}}{f}\right)} - 0.38\{1 - \exp(-2L_G)\}} \qquad \{28\}$$

Horizontally adjusted rainy slant path length is calculated from:

$$L_{h,0.01} = \begin{cases} \frac{L_G r_{h,0.01}}{\cos\theta} \; ; \; \rho > \theta \\ \frac{H_R - H_S}{\sin\theta} \; ; \; \rho \leq \theta \end{cases} \qquad \{29\}$$

Where, $\rho = \tan^{-1}\{\frac{H_R - H_S}{L_G\gamma_{h,0.01}}\}$

7. Vertically adjusted path reduction factor ($r_{v,0.01}$)

$$r_{v,0.01} = \frac{1}{1 + \sqrt{\sin\theta}\,[31\left(1 - \exp\left(\frac{-\theta}{1+\sigma}\right)\right)\frac{\sqrt{L_G \gamma_{0.01}}}{f^2} - 0.45]} \quad \{30\}$$

Where, $\sigma = \begin{cases} 36 - \varphi\,; \varphi < 36° \\ 0 \quad\quad ;\ \varphi \geq 36° \end{cases}$

8. Effective path length (L_{eff})

$$L_{eff} = L_{h,0.01} r_{v,0.01} \quad \{31\}$$

$$and, A_{0.01} = \gamma_{0.01} L_{eff} \quad \{32\}$$

The predicted attenuation exceeded for other percentages %p of an average year may be obtained from the value of $A_{0.01}$ by using the following extrapolation:

$$A_{\%p} = A_{0.01}[\frac{p}{0.01}]^{-\{0.655+0.033\ln p - 0.045\ln A_{0.01} - z\sin\theta(1-p)\}} \quad \{33\}$$

Where, p = percentage probability of interest and z is given as,

$$p \geq 1\%, z = 0 \quad \{34\}$$

$$p < 1\%, z = \begin{cases} 0 & ;\ \varphi \geq 36° \\ -0.005(\varphi - 36) & ;\ \theta > 25°\ and\ \varphi < 36° \\ -0.005(\varphi - 36) + 1.8 - 4.25\sin\theta & ;\ \theta < 25°\ and\ \varphi < 36° \end{cases}$$

With the 1-minute integration time of rainfall data, as the primary input to the attenuation model, the attenuation of signal transmission link due to rainfall was calculated. Ancillary information like antenna details was also made available from the respective earth station. For the ITU-R P618.8 model, calculation of 0º isotherm height was made by bilinear interpolation shown in Figure 4.2-7. From the above bilinear interpolation calculations, the 0º isotherm heights for AES and DES were found to be **4.921282933 km** and **4.9158523 km** respectively.

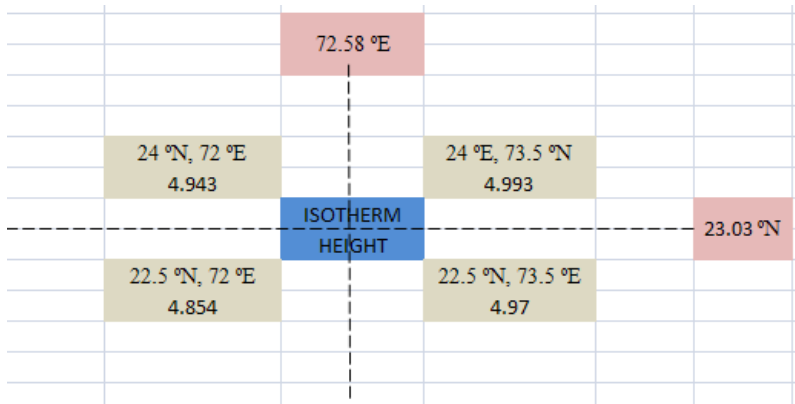

Figure 4.2-7: Bilinear Interpolation for calculation of 0 deg isotherm height

Prior to the MATLAB program for ITU-R P618.8 model, specific attenuation parameters, k_H, k_V, α_H and α_V, were calculated for a range of frequency (1-400 GHz) at a step size of 0.1 GHz as seen in Figure 4.2-8.

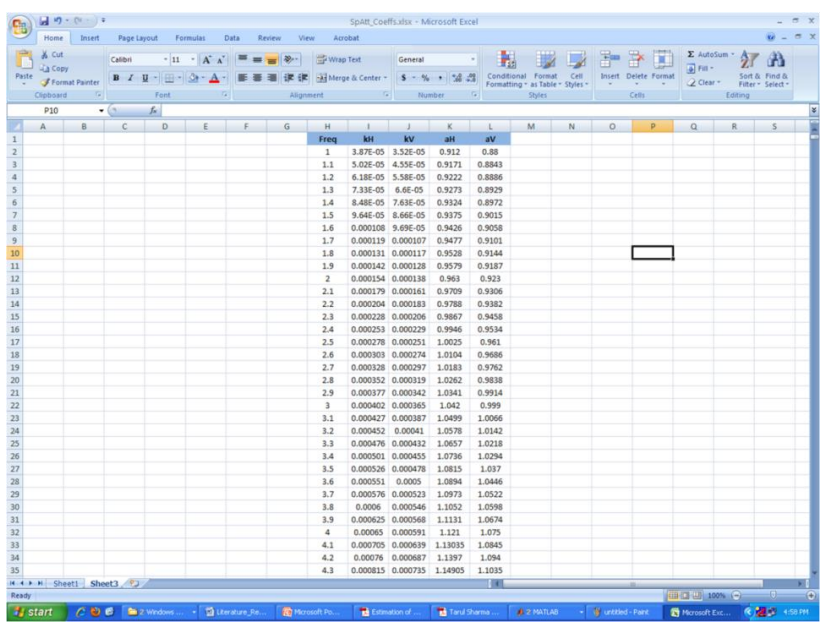

Freq	kH	kV	aH	aV
1	3.87E-05	3.52E-05	0.912	0.88
1.1	5.02E-05	4.55E-05	0.9171	0.8843
1.2	6.18E-05	5.58E-05	0.9222	0.8886
1.3	7.33E-05	6.6E-05	0.9273	0.8929
1.4	8.48E-05	7.63E-05	0.9324	0.8972
1.5	9.64E-05	8.66E-05	0.9375	0.9015
1.6	0.000108	9.69E-05	0.9426	0.9058
1.7	0.000119	0.000107	0.9477	0.9101
1.8	0.000131	0.000117	0.9528	0.9144
1.9	0.000142	0.000128	0.9579	0.9187
2	0.000154	0.000138	0.963	0.923
2.1	0.000179	0.000161	0.9709	0.9306
2.2	0.000204	0.000183	0.9788	0.9382
2.3	0.000228	0.000206	0.9867	0.9458
2.4	0.000253	0.000229	0.9946	0.9534
2.5	0.000278	0.000251	1.0025	0.961
2.6	0.000303	0.000274	1.0104	0.9686
2.7	0.000328	0.000297	1.0183	0.9762
2.8	0.000352	0.000319	1.0262	0.9838
2.9	0.000377	0.000342	1.0341	0.9914
3	0.000402	0.000365	1.042	0.999
3.1	0.000427	0.000387	1.0499	1.0066
3.2	0.000452	0.00041	1.0578	1.0142
3.3	0.000476	0.000432	1.0657	1.0218
3.4	0.000501	0.000455	1.0736	1.0294
3.5	0.000526	0.000478	1.0815	1.037
3.6	0.000551	0.0005	1.0894	1.0446
3.7	0.000576	0.000523	1.0973	1.0522
3.8	0.0006	0.000546	1.1052	1.0598
3.9	0.000625	0.000568	1.1131	1.0674
4	0.00065	0.000591	1.121	1.075
4.1	0.000705	0.000639	1.13035	1.0845
4.2	0.00076	0.000687	1.1397	1.094
4.3	0.000815	0.000735	1.14905	1.1035

Figure 4.2-8: Specific Attenuation coefficients calculation (1-400 GHz)

Now the ITU-R P618.8 model was written using MATLAB taking the 1-minute rainfall data, auxiliary antenna data, etc. to estimate rain attenuation predictions. A screenshot of the program is given below in the Figure 4.2-9.

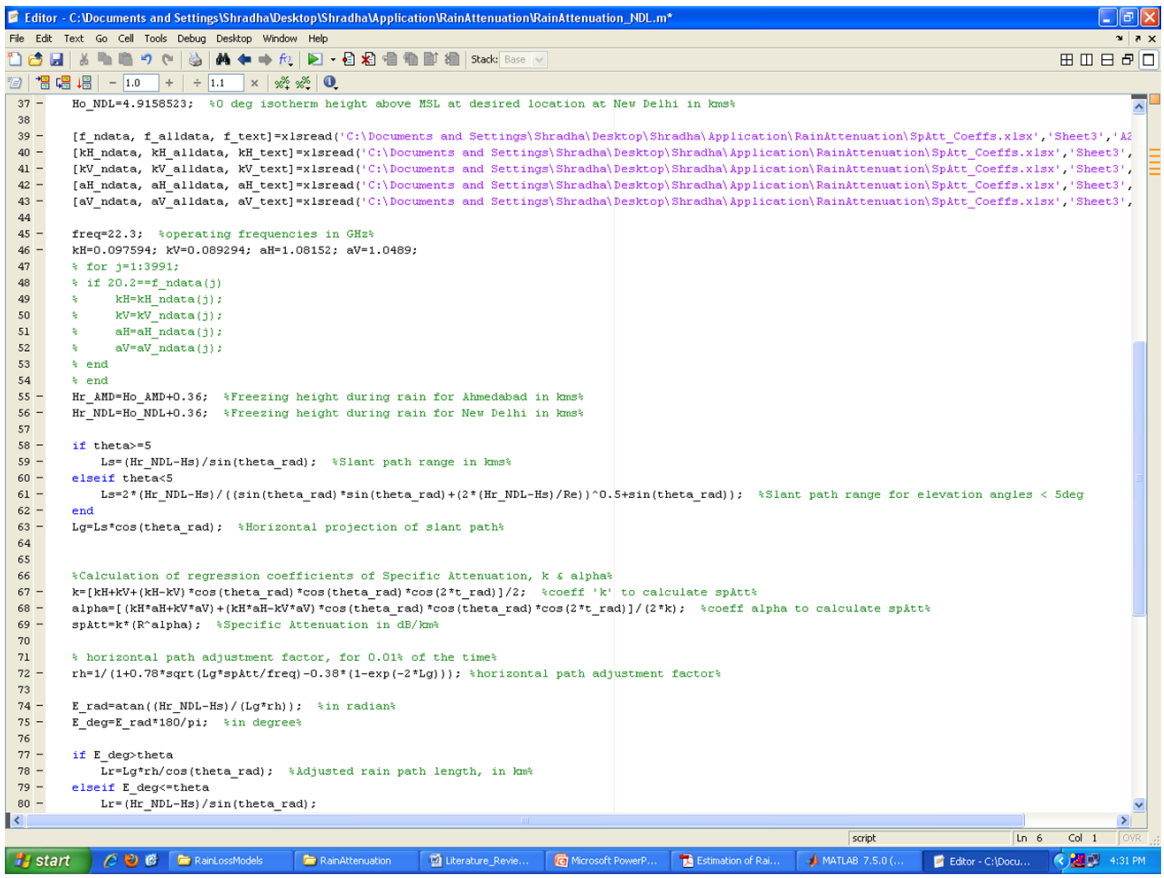

Figure 4.2-9: Snapshot showing implementation of MATLAB program for attenuation calculations

CHAPTER 5: RESULTS AND DISCUSSION

5.1. SENSOR DESIGN TECHNOLOGIES COMPARISON:

Sensor communication applications not only require high performance processing but also flexible and reliable computing. Today, standard microprocessor systems are still application oriented and aren't suitable by implication for reliability-related and safety-related applications. In order to achieve a certain safety integrity level (SIL), several measures, methodologies and especially additional components should be considered, which leads to more and more complex systems. For this reason, new application devices should be targeted. With newer upcoming sensor development technologies available in the market, the Table 5.1-1 below shows a comparative study between the three technologies, namely:

- Field Programmable Gate Array (FPGA)
- Application Specific Integrated Circuit (ASIC)
- Programmable System on Chip (PSoC)

Table 5.1-1: Comparative table showing three different sensor design technologies

Sl.No.	DESIGN PARAMETERS	FPGA	ASIC	PSoC
1.	SPEED	Slower in comparison with ASICs	ASIC rules out FPGA in terms of speed	Slower than ASICs
2.	COST	For smaller applications, FPGAs are very cost-effective	But with projects involving complex and large volume designs, ASIC is more preferred to FPGA	Expensive as compared to both FPGA and ASIC
3.	SIZE/AREA	Size of FPGAs is quite larger than the corresponding ASIC design due to large number of LUTs involved	Smaller in size/area than FPGAs	Small and compact
4.	POWER REQUIREMENTS	With a large unwanted circuitry involved, power wastage in FPGA is on the	ASIC designs allow for power optimization to the fullest.	Operate in low power modes

		higher side		
5.	TIME TO MARKET	FPGAs have very small and simple design cycle, thus requiring little time to market	ASICs have longer time to market as compared to FPGAs	Extended design cycle take longer time to market
6.	TYPE OF DESIGN	Mixed signal designs along with only analog signals cannot be implemented n FPGAs	Mixed signal designs can be implemented using ASICs	Can be used for mixed signals
7.	CUSTOMIZATION	FPGA customization is not possible.	Full customization is possible using ASIC	Customization of user modules possible
8.	PROTOTYPING	Because of the re-usability property, FPGAs are available for ASIC prototyping	Prototyping feature not available in ASICs	Prototyping kits available at low cost
9.	NON RECURRING ENGINEERING/ EXPENSES	FPGAs are very cost effective.	NRE is higher in ASICs.	Higher NREs
10.	SIMPLER DESIGN CYCLE	Due to the software that handles the routing, placement and timing, FPGAs have simpler and smaller designed cycles than ASICs.	Design cycles of ASICs more intense and complex than FPGAs.	Simpler design cycle
11.	REUSABLILITY	FPGAs can be used for different applications because of the re-programming property, hence increasing the re-usability.	With no prototyping feature, ASICs are not preferred for reusability.	Prototyping and customization features allow the reuseability of the device

5.2. ADC TEST AND DIGITIZER COMPARISON:

As already discussed, the design of a digital control circuitry for a ground-based radiometer involves the integration of various parameters. These parameters include the selection of the digitizer, the sensor design technology to be used, data interfacing options, etc. At the first

place, in the selection of the perfect digitizer, the ADC AC and DC characteristics are tested. For the same, three different ADC options were considered, namely:

- Single packaged ADC from Texas Instrument (ADS1278)
- Separate packaged individual ADC from National Semiconductors (ADC161S626)
- Inbuilt PSoC ADC from Cypress (CY8C58LP family)

5.2.1. ADC TESTS:

Since the first two options of digitizer selection were already tested and used in previous projects, our main aim was to test the Σ-Δ ADC in PSoC. The Figure 5.2-1 given below shows the results of the static test showing the actual code vs. ideal code values and the code histogram.

INPUT DC VOLTAGE (in V)	IDEAL CODE $\left(\frac{V_{dc}*(2^n-1)}{V_{FS}}\right)$	ACTUAL CODE	CODE (in Hex)
0.00778	248.956	15	000F
0.1	3199.9511	3063	0BF7
0.3	9599.85351	9461	24F5
0.5	15999.7558	15857	3DF1
0.7	22399.658	22254	56EE
1.0	31999.5117	31854	7C6E
1.2	38399.414	38251	956B
1.5	47999.2675	47845	BAE5
1.8	57599.121	57445	E065
2.043	65375.0024	65213	FEBD

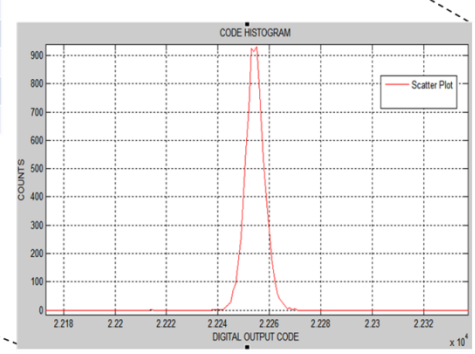

Figure 5.2-1: Code histogram showing actual and ideal code

Using the MATLAB code, tests have been carried out and the offset and gain errors were found to be **0.00778 V** and **-0.62099%** respectively in Figure 5.2-2. As the error is very small, the plot has been zoomed in to show a clear deviation from the ideal characteristics.

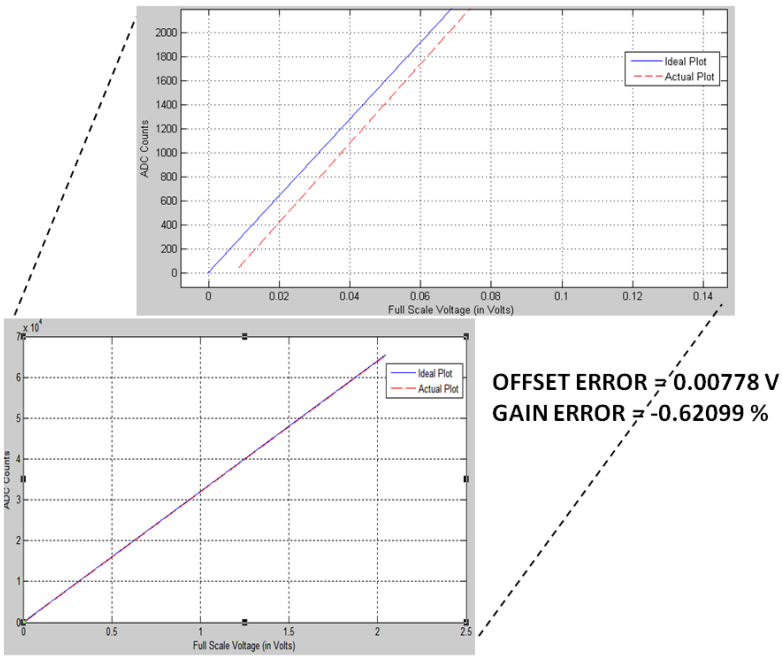

Figure 5.2-2: MATLAB plot ADC DC characteristic, with gain and offset error

Due to certain limitations associated with the PSoC ADC, it was not the prime option for the digitizer selection. Use of PSoC would have required additional multiplexer circuit or use of 8 PSoCs for realization of the 8-channel GBR. Thus due to time constraints and prioritization of other test results, the dynamic tests have not been performed on the PSoC ADC. However, in the due course of the project, similar tests would be carried on, which shall define its performance characteristics.

5.2.2. DIGITIZER COMPARISON:

The Table 5.2-1 below shows a comparative study between the three ADC options available in terms of the digitizer specifications.

Table 5.2-1: Comparative table on Digitizer options

Sl. No.	DIGITIZER SPECIFICATION	ADC161S626	ADS1278	PSoC (as per datasheet)
1	**Make**	National Semiconductors	Texas Instruments	Cypress MicroSystems
2	**Architecture**	SAR	Delta-Sigma	Delta-Sigma
3	**Analog Bandwidth**	26MHz (Full power)	62KHz	
4	**Analog i/p Voltage Range**	0 to +5V	0 to +5V	0 to +5V
5	**Sampling Clock**	250 ksps	128 ksps	48 ksps
6	**Resolution**	16 bits	24 bits	16 bits
7	**Diff. Non Linearity (DNL)**	-0.5 /+0.8 LSB		± 1 bit
8	**Integral Non Linearity (INL)**	± 0.8 LSB	± 0.0012 % FSR	± 2 bits
9	**Signal to Noise Ratio (SNR)**	88 dB	106 dB	-
10	**Signal to Noise Ratio + Distortion (SINAD)**	88 dB	100 dB	48 dB
11	**Total Harmonic Distortion (THD)**	-104 dB	-108 dB	-
12	**Spurious Free Dynamic Range (SFDR)**	108 dB	109 dB	-
13	**Common Mode Rejection Ratio(CMRR)**	85dB	108 dB	35 dB
14	**No. of Analog channel**	One	Eight	One
15	**Data O/P format**	2's compliment	2's compliment	
16	**Power**	5.3mW	245 mW	
17	**Package**	10 pin Plastic	84 pin Ceramic FP	100 pin TQFP

5.3. DATA INTERFACING:

5.3.1. RS232 USING UART:

Once the analog inputs have been fed into the digitizer from the receiver end, and conversion been done into digital codes, the data needs to be received at the output terminal. This transfer using a USB device to a personal computer for further processing, is called as data interfacing.

Data interfacing can be both transmission and receiving of data. For this, the globally accepted RS232 link using an UART is used.

Earlier projects done at MSDPD/MRSA/SAC have already tested the compatibility of RS232 with the device used and found successful results. So, the work at hand was to check the compatibility of RS232 with the PSoC device. The PSoC evaluation board has a provision for data interfacing, which has been used for test purpose. A program, using PSoC Creator 2.1, was written which displays the raw voltage count as the digital output for changing ADC input using the LCD. Counts were also transferred to the local computer, using the UART, and view using the Hyper Terminal communication accessory as seen in Figure 5.3-1.

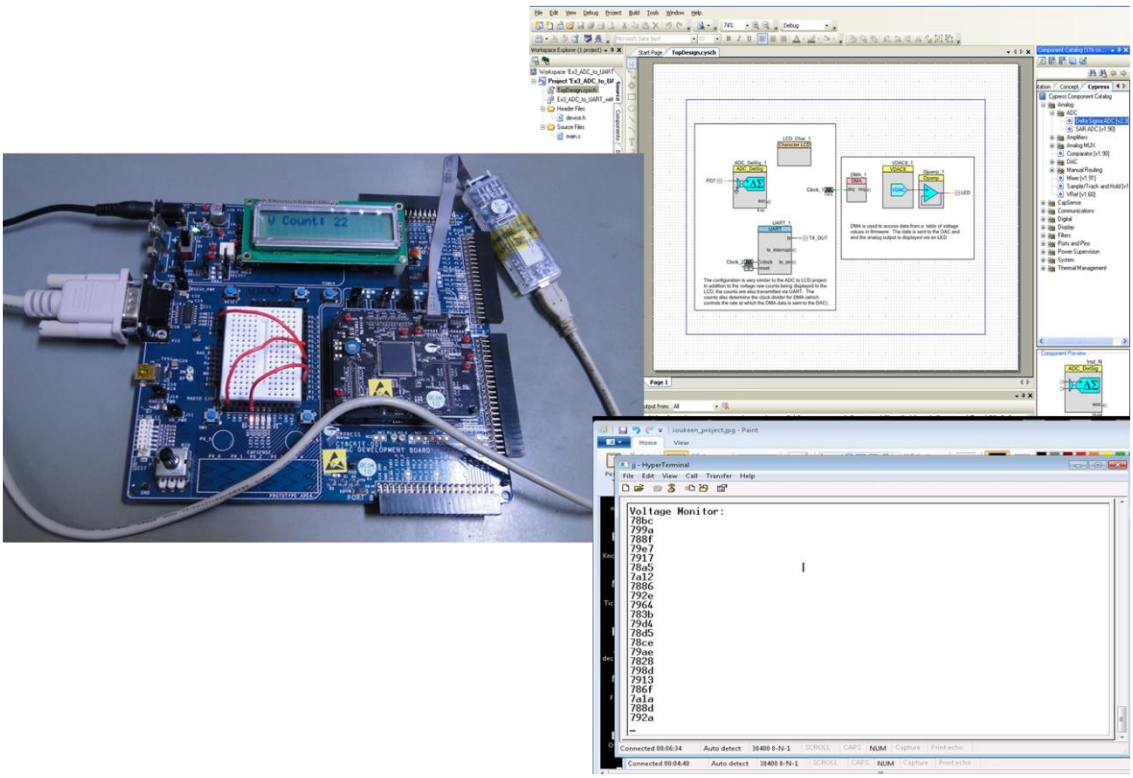

Figure 5.3-1: Data interfacing through RS232 and UART

5.3.2. WIRELESS COMMUNICATION USING ZIGBEE MODULE:

As the GBR is proposed to be mounted behind the antenna, in the field, a way of communication apart from the RS232 is said to be the wireless network using ZigBee. This test for wireless data interfacing is done for the first time in the study, using the PSoC. After being tested successful with the PSoC evaluation board, it will be interfaced with the GBR board in due course of time. For the time being, only testing for wireless communication has been performed.

Data transmission using ZigBee basically consists of three major components-PSoC development board, ZigBee transmitter module and ZigBee receiver module. Once data is available at PSoC development board's UART, it is transmitted to ZigBee transmitter module's UART through RS-232 communication as shown in Figure 5.3-2.

ZigBee transmitter module has 8051 microcontroller and radio module. When data is available at its UART, 8051 microcontroller is interrupted and data is transferred to radio module's buffer register. Now data is available to radio module for further transmission. Data is transmitted to ZigBee receiver module under microcontroller's control from radio module. ZigBee receiver also has 8051 microcontroller and radio module for data reception. As soon as data is available at radio module's input, 8051 is interrupted for data reception. Now microcontroller transmits data to PC through its UART module using RS-232 communication.

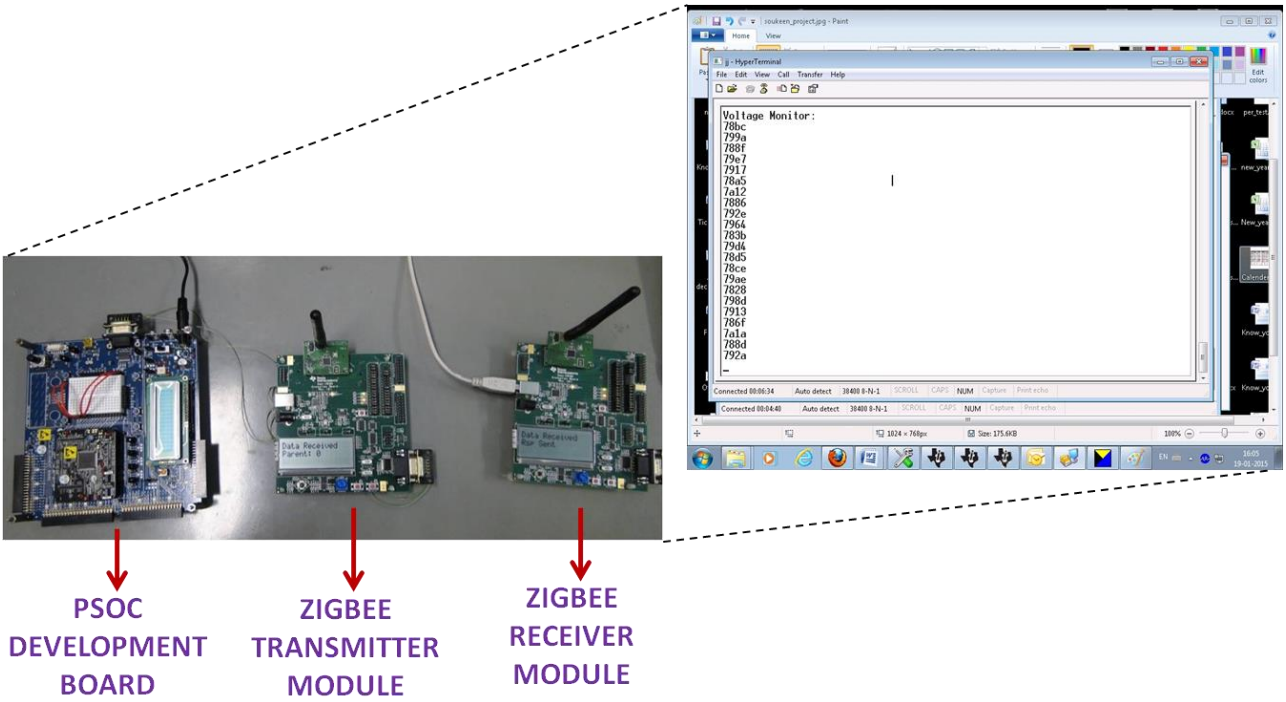

Figure 5.3-2: Data interfacing through wireless ZigBee module

5.4. FINAL HARDWARE REALIZATION:

With the finalization of schematic for the HPDAS and layout design of the board being done using Zuken's CADSTAR, the PCB was sent for loading. A series of checks were undertaken by the supervisor before the board was sent to the DESIGN CENTRE for the development of the PCB. The following steps are necessarily undertaken for PCB design:

- A copy of documents related to all layers, like the TOP_SILK, TOP_ELEC, COPPER, BOTTOM_SILK, etc. in the PCB design
- A GERBER (.grb) file is generated in the CADSTAR software. This file has all necessary details
- Like the GERBER file, a NETLIST (IPC-D 356 Report) is also generated after PCB layout, which checks for every net detail.

- CAM 350 software checks if all the rules pertaining to PCB design are correctly followed, like placement details, routing, etc.
- After getting clearance from the CAM 350, the layout is sent for manufacturing.

Once the PCB was received after manufacturing, checks were conducted to see if there were any short-circuit in the board. After clearance test, the board mounted with the required components. Smaller elements, like resistors, capacitors, small ICs, etc. were done in the lab. However, bigger and important components like the FPGA, digitizer ADS1278, connectors, power regulators, etc. require precise placement without causing any damage to the board. A dedicated department, called as the PFF at SAC is solely used for this purpose.

The Figure 5.4-1 below shows the HPDAS board for the Ground-based Radiometer project, with the different components highlighted and marked.

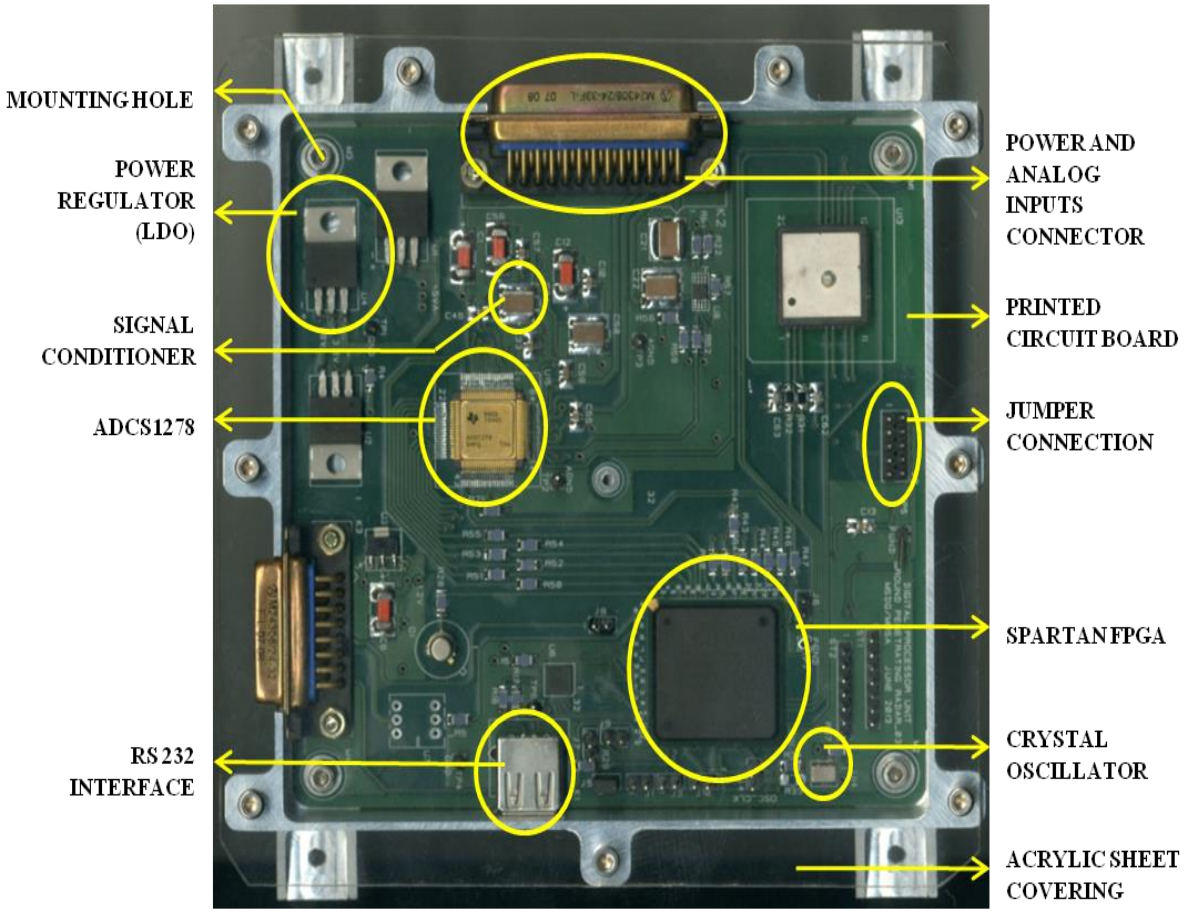

Figure 5.4-1: HPDAS board of GBR showing the different components mounted

This Figure 5.4-2 below shows the interconnections made between the digital subsystem board and the antenna receiver board inside one package. The harnesses used different interconnections can clearly be seen from this image.

Figure 5.4-2: Interconnection of HPDAS board with other electronic module via harness

5.5. RAIN ATTENUATION PREDICTIONS:

Any signal transmission path is affected by the presence of atmospheric hydrometeors. Calculations of the effect of weather on radio wave propagation would have been comparatively simple if there were no water or water vapor in the atmosphere. However, some form of water (vapor, liquid, or solid) is always present and must be considered in all calculations. Rain plays a very important role in the transmission link, degrading the signal level with increase in rain rate and frequency of propagation of the signal. In the present study, models have been run which calculated the rain attenuation prediction losses at the proposed frequencies of operation for the Ground-based Radiometer to be set-up at Ahmedabad and New Delhi earth receiving stations.

The statistical analysis done using MATLAB by calculating cumulative distribution function for every month showed that the rainfall rate is highest during the monsoon months of June-September. From above literature surveys it was evident that the rain attenuation will be

predominant during the above period of the year. '*Characteristics of precipitation for propagation modeling*', *ITU-R P837.6* gave the conversion for any integration time, the value of 1-minute of rain rate for any percentage of time exceedance. The *ITU-R P618.8* model, '*Propagation data and prediction methods required for the design of Earth-space telecommunication systems*' used for rain attenuation prediction was used to determine the attenuation value for the given rain rate.

The rainfall rate was calculated using the ITU-R P. 837.6 model and the variation of the rainfall rate (mm/hr) is shown in the Figure 5.5-1 below, for different time exceedance percentages. At 22.23 GHz operating frequency, it can be observed that the maximum rainfall rate was 130 mm/hr and 85.57 mm/hr for AES and DES respectively at 0.001% time of an average year.

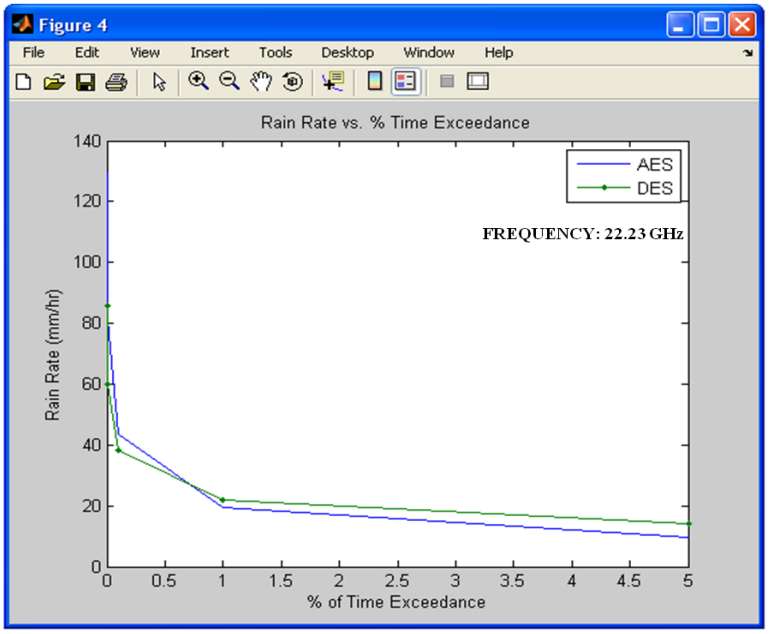

Figure 5.5-1: Rain Rate vs. % time exceedence curve for AES and DES

The rainfall rate was 81.5147 mm/ hr and 60.01 mm/hr exceeded for 0.01% of an average year, with 1-min integration time for AES and DES respectively. The obtained rainfall rate with different % time exceedance of average year will be compared and studied with practical

rainfall rates measured. The Table 5.5-1 below gives a detail about the rain rate (mm/hr) and attenuation caused (dB) at the different percentage exceedance of time for an average year.

Table 5.5-1: Rain rate and Attenuation data for different % Time exceedance at 22.235 GHz

	Ahmedabad Earth Station (AES)		**Delhi Earth Station (DES)**	
% Time Exceedance	Rain Rate (mm/hr)	Attenuation (dB)	Rain Rate (mm/hr)	Attenuation (dB)
0.001%	130	50.0804	85.57	47.9545
0.01%	81.5147	38.7453	60.01	35.8212
0.1%	43.8	26.3803	38.1	28.9167
1%	19.4	14.6331	21.88	19.4915
5%	9.579	7.3087	13.99	13.1056

It can be inferred from the values that with increase in the rain rate, the attenuation also increases. As can be seen, from the table, that AES has received higher rainfall for the given time duration, the attenuation values corresponding to 0.01% time exceedance for AES and DES are 38.7453 and 35.8212 respectively. Given below, the Figure 5.5-2 shows the attenuation and rain rate values at 22.23 GHz for the various % of time exceedance. This plot clearly shows that attenuation is directly proportional to the rain rate, i.e., with increase in rain rate, attenuation increases. Although plotted only for one frequency of 22.23 GHz, similar trend can be seen for the rest of the operating frequencies of the ground-based radiometer.

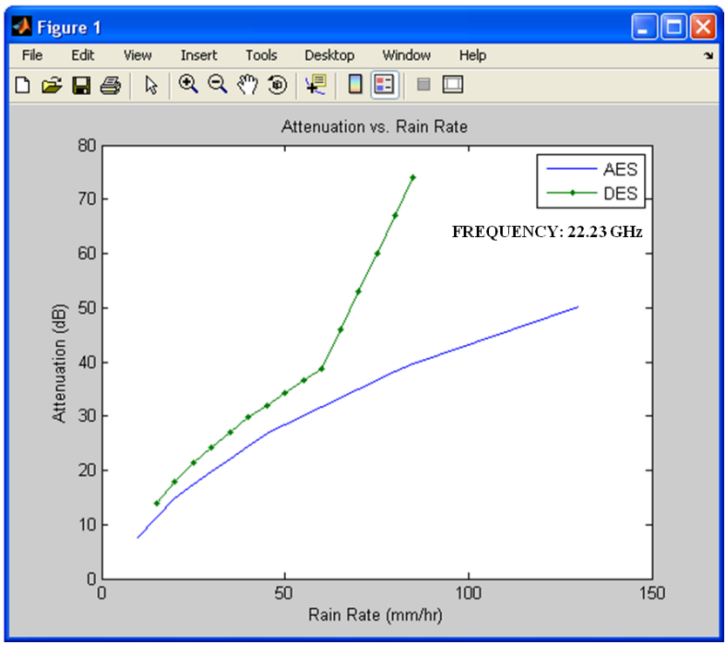

Figure 5.5-2: Attenuation vs. Rain Rate @ 22.235 GHz

For the earth stations AES and DES, at rain rates of 81.5147 mm/hr and 60.01 mm/hr, the attenuation of the signal is obtained using ITU-R P. 618.8 Recommendation for the frequency range of 20-32 GHz. From the Figure 5.5-3 below, it is evident that the attenuation increases with increase in frequency at a given rain rate.

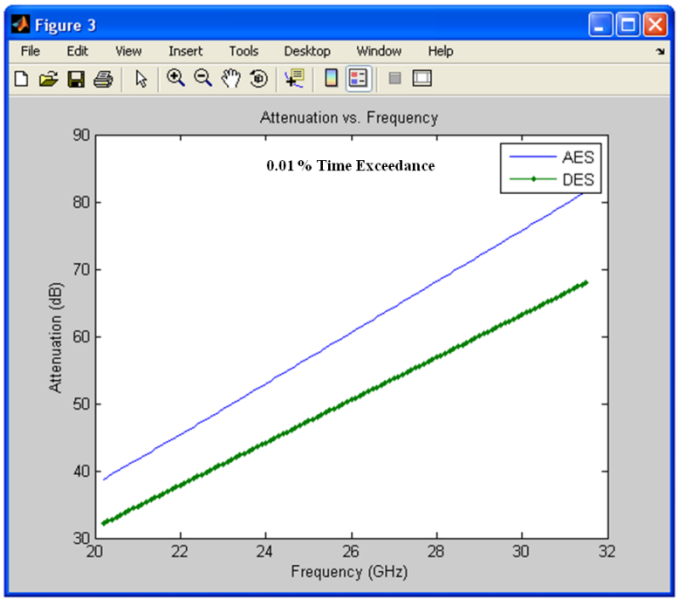

Figure 5.5-3: Attenuation vs. Frequency at 0.01% time exceedance

The rain attenuation was calculated for 0.001% to 5% of time exceedance percentages of an average year as shown in Figure 5.5-4. The attenuation is 38.7453 dB and 35.8212 dB with 0.001% and 7.3087 dB and 13.1056 dB with 5% exceeded time of an average year.

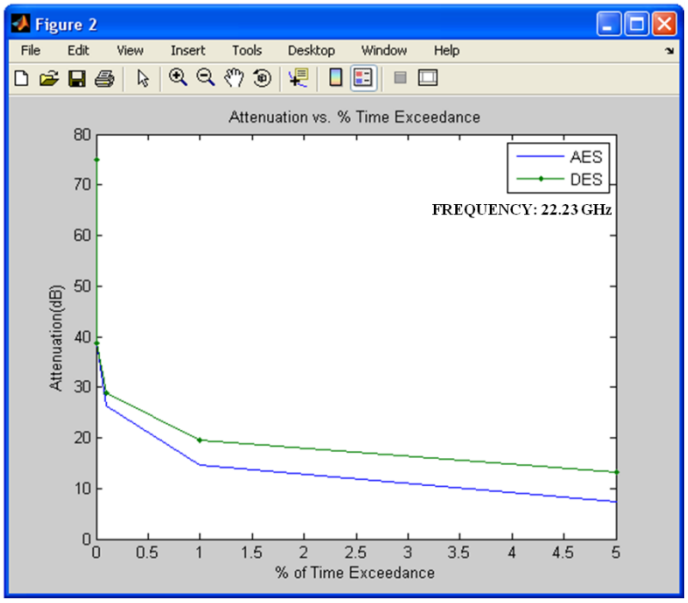

Figure 5.5-4: Attenuation vs. % Time exceedance @ 22.235 GHz

CHAPTER 6: CONCLUSION AND RECOMMENDATIONS

6.1.CONCLUSIONS:

From the results obtained with necessary assumptions, depending on the research questions associated with this study, flowing conclusions have been made.

- What are the basic blocks in the design of the digital circuitry of a ground-based microwave radiometer?

  Any sensor design is a combination of different blocks, all interfaced together to create one system. Similarly, the ground-based radiometer system is also composed of different subsystems. The signal after being received at the antenna, through the reflector, feed horn and receiver, is given as an input to the digital subsystem. The main blocks of the digital subsystem consist of the signal conditioner and digitizer, the controller and integrator circuit, a digitizer characterization circuit and data interfacing (including both RS232 and ZigBee wireless module option). Along with the above components, crystal oscillator (for clock generation) and connector is also available.

- What are the different specifications needed for the ADC to be used in the control circuit?

  The heart of any digital system is the analog to digital converter. However, the selection of ADC is a daunting task as it needs to consider the project requirement, speed, cost, weight, volume, etc. For the choice of an ADC, it needs to have the required ENOB after being integrated into the circuit for use. The different ADC specifications include offset and gain error, differential and integral non-linearity error, signal-to-noise ratio, signal-to-noise and distortion ratio, effective number of bits, total harmonic distortion and spurious free dynamic range.

- What are the different design technologies used in realization of the digital electronics of a radiometer sensor?

  With advances in the field of design technologies, newer options in sensor design technologies are available. Each of them comes with their own set of advantages and disadvantages. Earlier, microcontrollers were used to perform complex circuitry designs. But now they have been overshadowed by FPGAs, ASICs and the latest in the market being PSoC.

  The field-programmable gate array (FPGA) is a semiconductor device that can be programmed after manufacturing. It contains programmable logic components called as “logic blocks” and programmable interconnect. Instead of being restricted to any predetermined hardware function, a FPGA allows you to program product features and functions, adapt to new standards, and reconfigure hardware for specific applications even after the product has been installed in the field—hence the name "field-programmable". Thus, it can be purchased off-the shelf and programmed by the user.

  An Application Specific Integrated Chip is an integrated chip designed for a particular use, rather than for a general purpose use. ASICs seem to be deemed as the best option for high-volume applications. The cost and performance advantages reaped out of ASIC gives it an upper hand. The fact that ASICs are built for specific applications allows them to have a very high density of useful logic gates on the chip and use the resources optimally. Thus greater gate count and lower power consumption gives ASIC a competitive edge over FPGA.

  System-on-Chip (SoC) is basically a microcontroller with small FPGA on the same chip. It is more geared towards complete flexibility and user interaction. The general idea with a system-on-chip is to allow provide circuitry with multiplexers and other routing facilities such that the signal can be routed through a number of circuits to produce many useful types of stimulus/response pattern without the processor intervention. The objective of designing a programmable device is to develop a system on a chip (SoC) that shall provide the cost, performance and power design that meets the end product requirement. And thus the SoC approach can be considered as a good compromise between FPGAs and ASICs. Integrating a programmable processor and an adaptive sensor interface into one system-on-chip (SoC) combines analog and digital

processing capability and rapid customization to different applications using the same integrated circuit. Single-chip integration of these components enhances performance while simultaneously reducing size, cost and power consumption.

- Among the hardware options, which is the best in all aspects, *i.e.*, cost, accuracy, speed, reliability and reproducibility?

  The FPGA, ASIC and PSoC options are available for hardware implementation of the digital control circuit, but at present only the FPGA option has been tried. The biggest advantage associated with FPGA is its dynamic re-programmable capability. The advantages associated with FPGA are listed below:

  i. Implementations can be updated in order to introduce new features even partially and during run-time
  ii. Rapid prototyping
  iii. Long product life cycle to mitigate obsolescence risk
  iv. Current FPGAs include high-speed multipliers and adders that can work at the highest supported frequency
  v. Reduction in area and energy consumption
  vi. Low cost and Low non-recurring expense (NRE)

  Although ASIC and PSoC also provide an upper-hand as compared to FPGA in terms of application, speed, handling higher frequencies, etc. the options are not yet tested for this project. But both the options are definitely on the radar.

- For the frequency bands of the Ground-based radiometer to be installed, what is the amount of the signal loss due to rain?

  For the four frequency bands proposed to be used in the ground-based radiometer, rain attenuation predictions have been carried out using the ITU-R 618.6 model. From the calculations it was inferred that the attenuation increases with both rain rate as well as with frequency. For the two earth stations under study (AES and DES), it was found that in the monsoon months of June-September, from 2010-2014, AES has higher attenuation with respect to the frequency, as compared to DES. However, the case

reverses when attenuation is calculated with respect to rain rate, where DES has greater values than AES.

6.2.RECOMMENDATIONS:

From the above results and their conclusions, the following recommendations are suggested:

- With only the FPGA being used in design implementation of the digital circuitry, other options such as ASIC and PSoC can be tried.
- So far in the digitizer selection only the single packaged ADS1278 has been used. Therefore other options like the inbuilt PSoC ADC and the individual digitizers ADC161S626 also need to be tested for in the hardware.
- Data transmission using ZigBee wireless module has been also achieved. The use of wireless module makes it efficient for outdoor activities as there is reduction in complexity due to removal of wire handling and there is reduction in weight also. However, only the ZigBee compatibility with the PSoC has been tested. Thus, it should also be checked for compatibility with other options also.
- The rain attenuation calculations are done using point data from automatic weather station (AWS) at the temporal resolution of 1-hour. This data has been converted to smaller integration time of 1-minute. However, for the future, satellite data (like TRMM) can be used with larger spatial coverage. This would help in determining the attenuation loss over the entire Indian subcontinent. Contour maps for rain rate and attenuations can also be generated from these, giving a better picture of the loss calculations.
- In the present study only the ITU-R 618.6 model has been implemented. But since ITU-R models are best suited for temperate climates, modifications in the model and specific attenuation coefficients can produce better results for tropical countries India.

REFERENCES:

[1] "Remote Sensing," *http://en.wikipedia.org/*. [Online]. Available: http://en.wikipedia.org/wiki/Remote_sensing. [Accessed: 16-Aug-2014].

[2] "Microwave Radiometer," *http://en.wikipedia.org/*. [Online]. Available: http://en.wikipedia.org/wiki/Microwave_radiometer. [Accessed: 16-Aug-2014].

[3] "FPGA Design Solutions for Military and Aerospace Applications," *http://www.synopsys.com*. [Online]. Available: http://www.synopsys.com/Solutions/IndustrySegmentSolutions/MilAero/Documents/mil-aero-brochure.pdf. [Accessed: 27-Sep-2014].

[4] F. Alimenti, D. Zito, A. Boni, M. Borgarino, A. Fonte, A. Carboni, S. Leone, M. Pifferi, L. Roselli, B. Neri, and others, "System-on-chip microwave radiometer for thermal remote sensing and its application to the forest fire detection," in *Electronics, Circuits and Systems, 2008. ICECS 2008. 15th IEEE International Conference on*, 2008, pp. 1265–1268.

[5] J. Xi, C. Yang, A. Mason, and P. Zhong, "Adaptive multi-sensor interface system-on-chip," in *Sensors, 2006. 5th IEEE Conference on*, 2006, pp. 50–53.

[6] R. Bhattacharya, R. Das, R. Guha, S. Deb Barman, and A. B. Bhattacharya, "Variablity of millimeterwave rain attenuation and rain rate prediction: A survey," *Indian J. RAdio Space Phys.*, vol. Volume 36, pp. 325–344, Aug. 2007.

[7] M. Sridhar, K. P. Raju, and C. S. Rao, "Estimation of rain attenuation based on ITU-R model in Guntur (AP), India," *ACEEE Int J Commun*, vol. 3, no. 03, pp. 6–8, 2012.

[8] P. A. Owolawi, S. J. Malinga, and T. J. O. Afullo, "Estimation of Terrestrial Rain Attenuation at Microwave and Millimeter Wave Signals in South Africa Using the ITU-R Model," *PIERS Proc. Kuala Lumpur Malays.*, 2012.

[9] M. R. Islam and A. R. Tharek, "Propagation study of microwave signals based on rain attenuation data at 26 GHz and 38 GHz measured in Malaysia," in *Microwave Conference, 1999 Asia Pacific*, 1999, vol. 3, pp. 602–605.

[10] R. A. Harris, *Radiowave propagation modelling for SatCom services and Ku-band and above: COST Action 255 ; final report*. Noordwijk: ESA Publ. Div., 2002.

[11] F. T. Ulaby, R. K. Moore, and A. K. Fung, *Microwave Remote Sensing: Active and Passive.*, vol. 1: Microwave remote sensing fundamentals and radiometry. Addison-Wesley Publishing Company, Advanced Book Program/World Science Division, 1981, 1986.

[12] N. Skou and D. M. Le Vine, *Microwave radiometer systems design and analysis*. Boston: Artech House, 2006.

[13] E07 Committee, "Test Method for Noise Equivalent Temperature Difference of Thermal Imaging Systems," ASTM International, 2011.

[14] W. Kester, Ed., *Analog-Digital Conversions*. Analog Devices, Incorporated, 2004.

[15] F. Reverter, "The Art of Directly Interfacing Sensors to Microcontrollers," *J. Low Power Electron. Appl.*, vol. 2, no. 4, pp. 265–281, Nov. 2012.

[16] "Microcontroller to Sensor Interfacing Techniques." BiPOM Electronics Inc., 03-Feb-2006.

[17] R. Ranjan, V. Karan, R. K. Chandel, V. Kumar, S. Kumar, and A. Kumar, "Review on Realization of Intelligence Monitoring System based on Remote Sensor Technology," *Undergrad. Acad. Res. J. UARJ*, vol. 1, no. 3,4, pp. 320–324, 2012.

[18] A. Hayek, B. Machmur, Y. Suna, and J. Borcsok, "FPGA-based wireless sensor network platform for safety systems," in *Telecommunications (ICT), 2012 19th International Conference on*, 2012, pp. 1–6.

[19] A. de la Piedra, A. Braeken, and A. Touhafi, "Sensor Systems Based on FPGAs and Their Applications: A Survey," *Sensors*, vol. 12, no. 12, pp. 12235–12264, Sep. 2012.

[20] "An FPGA Approach to Implementing Time-Critical Functions in Multi-Sensor Mobile Designs." Lattice Semiconductor.

[21] "Spartan-3AN FPGA Family Data Sheet." Xilinx, Inc., 12-Jun-2014.

[22] D. Tomanek, "What is PSoC," in *Applied Electronics (AE), 2010 International Conference on*, 2010, pp. 1–4.

[23] J. Jayapandian, "Embedded control and virtual instrument simplifies laboratory automation," *Curr. Sci.-BANGALORE-*, vol. 90, no. 6, p. 765, 2006.

[24] Q. M. Li, "A low-cost configurable PWM controller using programmable system-on-chip," in *Power Electronics Specialist Conference, 2003. PESC'03. 2003 IEEE 34th Annual*, 2003, vol. 3, pp. 1169–1174.

[25] R. Aragones, C. Ferrer, and J. Oliver, "Use of PSoC™ component in a frequency based acquisition method for smart sensors applications," in *Industrial Technology, 2004. IEEE ICIT'04. 2004 IEEE International Conference on*, 2004, vol. 3, pp. 1357–1362.

[26] A. Doboli, P. Kane, and D. Van Ess, "Dynamic reconfiguration in a PSoC device," in *Field-Programmable Technology, 2009. FPT 2009. International Conference on*, 2009, pp. 361–363.

[27] T. L. Propagation, "Navy Electricity And Electronics Training Series," 1998.

[28] K. Ahmed, "Satellite Communication RadioWave Propagation."

[29] "Millimeter-Wave (MMW) Radio Transmission: Atmospheric Propagation, Link Budget and System Availability," *http://www.lightpointe.com*. [Online]. Available: http://www.lightpointe.com/images/LightPointe_MM_Wave_Atmosheric_Propagation_and_Availability_White_Paper.pdf. [Accessed: 18-Oct-2014].

[30] S. P. Mason, "Atmospheric effects on radio frequency (RF) wave propagation in a humid, near-surface environment," DTIC Document, 2010.

[31] K. Sudhakar and M. V. Subramanyam, "Atmospheric Propagation and Measurable Effects in Microwave Range Transmission," *Res. J. Appl. Sci. Eng. Technol.*, vol. 3, no. 7, pp. 596–601, Jul. 2011.

[32] K. Sudhakar and M. V. Subramanyam, "Evaluation of atmospheric attenuation due to various parameters," in *Information Communication and Embedded Systems (ICICES), 2013 International Conference on*, 2013, pp. 609–612.

[33] T. Shiomi, *Wave Summit Course: Digital Broadcasting*. Ohmsha Ltd., Japan, 2000.

[34] T. Pratt, C. W. Bostian, and J. E. Allnut, *Satellite Communications*, 2nd ed. Wiley Publications, 2002.

[35] W. Zhang and N. Moayeri, "Project IEEE 802.16 Broadband Wireless Access Working Group," *Power*, vol. 1999, pp. 11–01, 1999.

[36] P. Series, "Specific Attenuation Model for Rain for use in Prediction Model," *Recomm. ITU-R P 8383*, 2005.

[37] P. Series, "Characteristics of precipitation for propagation modelling," *Recomm. ITU—R P837-6*, 2013.

[38] J. S. Mandeep and S. I. S. Hassan, "60- to 1-Min Rainfall-Rate Conversion: Comparison of Existing Prediction Methods with Data Obtained in the Southeast Asia Region," *J. Appl. Meteorol. Climatol.*, vol. 47, no. 3, pp. 925–930, Mar. 2008.

[39] "How to Analyse Rainfall data." DHV Consultants BV & DELFT HYDRAULICS.

[40] J. S. Mandeep and S. I. S. Hassan, "60- to 1-Min Rainfall-Rate Conversion: Comparison of Existing Prediction Methods with Data Obtained in the Southeast Asia Region," *J. Appl. Meteorol. Climatol.*, vol. 47, no. 3, pp. 925–930, Mar. 2008.

[41] J. H. Lee, Y.-S. Choi, J. K. Pack, and E. HA, "Conversion of rain rate distribution for various integration time," *IEEE Trans. Microw. Theory Tech.*, vol. 42, no. 11, pp. 2099–2106, 1994.

[42] J.-H. Lee, Y.-S. Kim, J.-H. Kim, and Y.-S. Choi, "Empirical conversion process of rain rate distribution for various integration time," in *Microwave Conference, 2000 Asia-Pacific*, 2000, pp. 1593–1597.

[43] A. P. Gallois, P. F. Hartigan, and A. M. Böck, "A comparison of slant path attenuation models applied to the selection of satellite beacon receiver sites," in *Antennas and Propagation, 1989. ICAP 89., Sixth International Conference on (Conf. Publ. No. 301)*, 1989, pp. 271–275.

[44] W. Myers and T. X. Richardson, "Project IEEE P802. 16 Broadband Wireless Access Working Group Title Comparison of Propagation Models," 1999.

[45] J. A. Garcia-Lopez, J. M. Hernando, and J. M. Selga, "Simple rain attenuation prediction method for satellite radio links," *Antennas Propag. IEEE Trans. On*, vol. 36, no. 3, pp. 444–448, 1988.

[46] Z. Qingling and J. Li, "Rain attenuation in millimeter wave ranges," in *Antennas, Propagation & EM Theory, 2006. ISAPE'06. 7th International Symposium on*, 2006, pp. 1–4.

[47] L. D. Emiliani, J. Agudelo, E. Gutierrez, J. Restrepo, and C. Fradique-Mendez, "Development of rain-attenuation and rain-rate maps for satellite system design in the Ku and Ka bands in Colombia," *Antennas Propag. Mag. IEEE*, vol. 46, no. 6, pp. 54–68, 2004.

[48] J. S. Ojo, M. O. Ajewole, and S. K. Sarkar, "Rain rate and rain attenuation prediction for satellite communication in Ku and Ka bands over Nigeria.," *Prog. Electromagn. Res. B*, vol. 5, pp. 207–223, 2008.

[49] A. I. Yussuff and N. H. Khamis, "Rain Attenuation Modelling and Mitigation in The Tropics: Brief Review," *Int. J. Electr. Comput. Eng. IJECE*, vol. 2, no. 6, pp. 748–757, 2012.

[50] R. M. Islam, Y. A. Abdulrahman, and T. A. Rahman, "An improved ITU-R rain attenuation prediction model over terrestrial microwave links in tropical region," *EURASIP J. Wirel. Commun. Netw.*, vol. 2012, no. 1, pp. 1–9, 2012.

[51] M. C. Kestwal, S. Joshi, and L. S. Garia, "Prediction of Rain Attenuation and Impact of Rain in Wave Propagation at Microwave Frequency for Tropical Region (Uttarakhand, India)," *Int. J. Microw. Sci. Technol.*, vol. 2014, pp. 1–6, 2014.

[52] N. Elfadil, Z. Nadir, M. A. Salam, and J. Rao, "Microwave attenuation studies due to rain for communication links operating in Malaysia," *Georgian Electron. Sci. J. Comput. Sci. Telecommun.*, no. 5, 2005.

[53] A. Maitra and K. Chakravarty, "Ku-band rain attenuation observations on an earth-space path in the Indian region," *28th URSI-GA*, pp. 23–29, 2005.

[54] U. Siddique, L. Ahmad, and G. Raja, "Microwave Attenuation and Prediction of Rain Outage for Wireless Networks in Pakistan's Tropical Region," *Int. J. Microw. Sci. Technol.*, vol. 2011, pp. 1–6, 2011.

[55] S. K. AR, C. S. Sum, J. Din, T. AR, M. Z. Abidin, and M. A. Awang, "Rain Attenuation Study over Terrestrial and Earth-Satellite Links in Malaysia."

[56] Maitra, "Rain attenuation modeling from measurements of rain drop size distribution in the Indian region," *IEEE Antennas Wirel. Propag. Lett.*, vol. 3, no. 1, pp. 180–181, Dec. 2004.

[57] S. Das, A. Maitra, and A. K. Shukla, "Rain attenuation modeling in the 10-100 GHz frequency using drop size distributions for different climatic zones in tropical India," *Prog. Electromagn. Res. B*, vol. 25, pp. 211–224, 2010.

[58] "Propagation data and prediction methods required for the design of Earth-space telecommunication systems ITU-R P.618-8." ITU Radiocommunication Assembly, 2003.

[59] M. Sridhar, K. P. Raju, C. S. Rao, and others, "Estimation of rain attenuation based on ITU-R model in Guntur (AP), India," *Aceee Int. J. Commun.*, vol. 3, no. 3, 2012.

[60] J. S. Ojo, M. O. Ajewole, and S. K. Sarkar, "Rain rate and rain attenuation prediction for satellite communication in Ku and Ka bands over Nigeria.," *Prog. Electromagn. Res. B*, vol. 5, pp. 207–223, 2008.

[61] R. A. Harris, *Radiowave propagation modelling for SatCom services and Ku-band and above: COST Action 255 ; final report*. Noordwijk: ESA Publ. Div., 2002.

APPENDIX:

The coefficients used in calculation of the specific attenuation for rain attenuations are given below:

Frequency (GHz)	k_H	k_V	a_H	a_V
1	0.0000387	0.0000352	0.912	0.880
2	0.000154	0.000138	0.963	0.923
4	0.000650	0.000591	1.121	1.075
6	0.00175	0.00155	1.308	1.265
7	0.00301	0.00265	1.332	1.312
8	0.00454	0.00395	1.327	1.310
10	0.0101	0.00887	1.276	1.264
12	0.0188	0.0168	1.217	1.200
15	0.0367	0.0335	1.154	1.128
20	0.0751	0.0691	1.099	1.065
25	0.124	0.113	1.061	1.030
30	0.187	0.167	1.021	1.000
35	0.263	0.233	0.979	0.963
40	0.350	0.310	0.939	0.929
45	0.442	0.393	0.903	0.897
50	0.536	0.479	0.873	0.868
60	0.707	0.642	0.826	0.824
70	0.851	0.784	0.793	0.793
80	0.975	0.906	0.769	0.769
90	1.06	0.999	0.753	0.754
100	1.12	1.06	0.743	0.744
120	1.18	1.13	0.731	0.732
150	1.31	1.27	0.710	0.711
200	1.45	1.42	0.689	0.690
300	1.36	1.35	0.688	0.689
400	1.32	1.31	0.683	0.684

MATLAB CODES:

A. FOR STATIC TEST-

```
numbit=16; % ADC Resolution %
file_name=input('Enter The File Name','s');
fid=fopen(file_name,'rt');
[v1_temp,count]=fscanf(fid,'%x');
fclose(fid);
Dc_voltage=input('Enter The DC Voltage in Volts:');
clc;
v1=v1_temp(1:8192);
disp('*-------------------------------+++++++++-----------------------
--------------*');
disp(' Number of Samples Read From  the File are:')
length(v1)
v1=v1;
code=v1(:,1);
code_count=zeros(1,2^numbit);
%dividing the full scale into 2^N number of bins%
for i=1:size(code),
code_count(code(i)+1)=code_count(code(i)+1) + 1;
end
scat1=max(code_count);
p_scat1=code_count/scat1;
p_scat2=find(p_scat1~=0);
p_scat3=find(p_scat1==1);
p_scat4=code_count;
disp(scat1)
disp(p_scat2)
disp(p_scat3)
disp('The Captured Code is:')
disp(p_scat3-1)
Step_Size=2.048/(2^numbit-1);
Ideal_Code=(Dc_voltage)/Step_Size;
disp('The Ideal Code is :')
disp(Ideal_Code)
if isempty(p_scat2)
disp('Percentage Scattering for unwanted codes is 0%')
else
disp('The Scattered Codes are:')
disp(p_scat2-1)
disp('The number of Occurences of Scattered Codes are:')
```

```
disp(p_scat4(p_scat2))
disp('The Percentage of Respective Scattered Codes are:')
disp(p_scat4(p_scat2)*100/length(v1));
end
figure;
plot([1:2^numbit],code_count,'-r',p_scat2-1,p_scat1(p_scat2));
title('CODE HISTOGRAM ');
xlabel('DIGITAL OUTPUT CODE');ylabel ('COUNTS'); grid on
```

B. DYNAMIC CODE:

```
date
file_name1 = input('Enter file name','s');
%Freq=input('Enter the frequency');
Fs=input('Enter the Sampling frequency');
disp('Running');
warning off
fp=fopen(file_name1,'rt');
CAPTURED_SIN1=fscanf(fp,'%x',4096);

fclose(fp);
No_of_Samples1=length(CAPTURED_SIN1);
i=0:1:No_of_Samples1-1;
No_of_Bits=12;
QUANTIZE_CAPTURE_SINE=CAPTURED_SIN1;

%....WEIGHTING OF SAMPLES IN TIME DOMAIN...%

WINDOW=hann(No_of_Samples1);
%wvtool(WINDOW)
Len_Samples=No_of_Samples1;

Coeff=[ 2.151527506679809e-001,   %  Coefficients of Cosine Sum Window
3.731348357785249e-001,           % Use this window for high
resolution measurments
 2.424243358446660e-001,
 1.166907592689211e-001,
 4.077422105878731e-002,
 1.000904500852923e-002,
 1.639806917362033e-003,
 1.651660820997142e-004,
 8.884663168541479e-006,
 1.938617116029048e-007,
```

```
 8.482485599330470e-010];

 Len_wind=Len_Samples;
 %disp('Length of window')
 %disp(Len_wind)

 W = zeros(1,Len_Samples);
 for I=0:1:Len_Samples-1
     W(I+1)=Coeff(1)-
Coeff(2)*cos(2*pi*I/Len_wind)+Coeff(3)*cos(4*pi*I/Len_wind)-
Coeff(4)*cos(6*pi*I/Len_wind)+Coeff(5)*cos(8*pi*I/Len_wind)-
Coeff(6)*cos(10*pi*I/Len_wind)+Coeff(7)*cos(12*pi*I/Len_wind)-
Coeff(8)*cos(14*pi*I/Len_wind)+Coeff(9)*cos(16*pi*I/Len_wind)-
Coeff(10)*cos(18*pi*I/Len_wind)+Coeff(11)*cos(20*pi*I/Len_wind);
 end

 WINDOW=W;

  WINDOW=hann(No_of_Samples1)';
FFT_Points=1*No_of_Samples1;
%FFT_Points=4096;
QUANTIZE_CAPTURE_SINE =    QUANTIZE_CAPTURE_SINE.*WINDOW';

QUANTIZE_CAPTURE_SPECTRUM = fft(QUANTIZE_CAPTURE_SINE,FFT_Points);
QUANTIZE_CAPTURE_SPECTRUM = abs(QUANTIZE_CAPTURE_SPECTRUM);
QUANTIZE_CAPTURE_SPECTRUM = fftshift(QUANTIZE_CAPTURE_SPECTRUM);
max1=max(QUANTIZE_CAPTURE_SPECTRUM);
max_index2=
find(QUANTIZE_CAPTURE_SPECTRUM==max(QUANTIZE_CAPTURE_SPECTRUM));
max_index21=
find(QUANTIZE_CAPTURE_SPECTRUM>=max(QUANTIZE_CAPTURE_SPECTRUM)/5);
if(No_of_Bits==8)
min_index21= min(max_index21)+1;
max_index22= max(max_index21)-1;
i=-2:1:2;
j=-2:1:2 ;
end
if(No_of_Bits==12)
min_index21= min(max_index21)+1;
max_index22= max(max_index21)-1;
i=-5:1:5;
j=-2:1:2 ;
```

```
end
signal_pow2=sum((QUANTIZE_CAPTURE_SPECTRUM(min_index21+i)).^2)+sum((QU
ANTIZE_CAPTURE_SPECTRUM(max_index22+i)).^2);
 disp('signal_pow2')
 disp(signal_pow2)
 noise_pow2=sum((QUANTIZE_CAPTURE_SPECTRUM).^2)-
sum(QUANTIZE_CAPTURE_SPECTRUM(round(No_of_Samples1/2)+i).^2)-
signal_pow2;
 disp('noise_pow2')
 disp(noise_pow2)
 %................ SINAD & ENOB CALCULATION...................%
 THEORETICAL_SNR=6.02*No_of_Bits+1.76;
disp('THEORETICAL_SNR')
disp(THEORETICAL_SNR)
SINAD_CAPTURE=10*log10(signal_pow2/noise_pow2);
disp('SINAD_CAPTURE');
disp(SINAD_CAPTURE);
ENOB_CALCULATED_FORMULAE = (SINAD_CAPTURE -
1.760912590556812420812890085306 2)/6.02;
disp('ENOB_CALCULATED_FORMULAE')
disp(ENOB_CALCULATED_FORMULAE)
%-----------------------------------------------------------%
i=-5:1:5;
MSE_Fundamental =
sum((QUANTIZE_CAPTURE_SPECTRUM(min_index21+i)).^2)+sum((QUANTIZE_CAPTU
RE_SPECTRUM(max_index22+i)).^2);
disp(MSE_Fundamental)
%-----------CALCULATION OF TOTAL HARMONICS POWER----------------%
MSE_Harmonics = 0;
QUANTIZE_CAPTURE_SPECTRUM1 =
QUANTIZE_CAPTURE_SPECTRUM(round(FFT_Points/2)+20:FFT_Points);
Funda = find(QUANTIZE_CAPTURE_SPECTRUM1 ==
max(QUANTIZE_CAPTURE_SPECTRUM1));
No1 = Funda-5:Funda+5;
QUANTIZE_CAPTURE_SPECTRUM1(No1) = 0;
Har1 = find (QUANTIZE_CAPTURE_SPECTRUM1 ==
max(QUANTIZE_CAPTURE_SPECTRUM1));
disp(Har1)
MSE_Harmonics =
MSE_Harmonics+2*sum((QUANTIZE_CAPTURE_SPECTRUM1(Har1+i)).^2);

QUANTIZE_CAPTURE_SPECTRUM1(Funda+i)=0;
Har2 = find (QUANTIZE_CAPTURE_SPECTRUM1 ==
max(QUANTIZE_CAPTURE_SPECTRUM1));
```

```
MSE_Harmonics =
MSE_Harmonics+2*sum((QUANTIZE_CAPTURE_SPECTRUM1(Har1+i)).^2);
QUANTIZE_CAPTURE_SPECTRUM1(Funda+i)=0;
Har3 = find (QUANTIZE_CAPTURE_SPECTRUM1 ==
max(QUANTIZE_CAPTURE_SPECTRUM1));
MSE_Harmonics =
MSE_Harmonics+2*sum((QUANTIZE_CAPTURE_SPECTRUM1(Har1+i)).^2);
QUANTIZE_CAPTURE_SPECTRUM1(Funda+i)=0;
disp(MSE_Harmonics)
Harmonics_Power=MSE_Harmonics;
disp('Harmonics_Power')
disp(Harmonics_Power)
%QUANTIZE_CAPTURE_SPECTRUM1(Har7+i)=0;
%-----------------------------------------------------------------------
--%
THD = 10*log10(MSE_Harmonics/MSE_Fundamental);
disp('THD')
disp(THD)
MSE_Noise = noise_pow2-MSE_Harmonics;
SINAD_CAPTURE;
SNR_CAPTURE = 10*log10(signal_pow2/abs(MSE_Noise));
disp('SNR_CAPTURE');
disp(SNR_CAPTURE)
QUANTIZE_CAPTURE_SPECTRUM =
QUANTIZE_CAPTURE_SPECTRUM/max(QUANTIZE_CAPTURE_SPECTRUM);
QUANTIZE_CAPTURE_SPECTRUM = 20*log10(QUANTIZE_CAPTURE_SPECTRUM);
%.............SFDR CALCULATION...............................%
QUANTIZE_CAPTURE_SPECTRUM1 = QUANTIZE_CAPTURE_SPECTRUM;
dc_index=(No_of_Samples1/2)-5:1:(No_of_Samples1/2)+5;
QUANTIZE_CAPTURE_SPECTRUM1(dc_index) = -100;
QUANTIZE_CAPTURE_SPECTRUM2 = QUANTIZE_CAPTURE_SPECTRUM1;
No1 = max_index2-5:max_index2+5;
QUANTIZE_CAPTURE_SPECTRUM1(No1) = -100;
No1 = [(min_index21-abs(i)): (min_index21+abs(i))];
QUANTIZE_CAPTURE_SPECTRUM1(No1)=-100;
No1 = [max_index22-abs(i) :max_index22+abs(i)];
QUANTIZE_CAPTURE_SPECTRUM1(max_index22-abs(i):max_index22+abs(i))=-
100;
QUANTIZE_CAPTURE_SPECTRUM1(No1)=-100;
QUANTIZE_CAPTURE_SPECTRUM(min_index21);
max(QUANTIZE_CAPTURE_SPECTRUM1);
SFDR =
QUANTIZE_CAPTURE_SPECTRUM(min(find(QUANTIZE_CAPTURE_SPECTRUM2==max(QUA
NTIZE_CAPTURE_SPECTRUM2)))) - max(QUANTIZE_CAPTURE_SPECTRUM1);
```

```
disp('SFDR in dB')
SFDR=-SFDR;
disp(SFDR)
...........DISPLAY OF POWER SPECTRUM..................
figure,plot(CAPTURED_SIN1),title('CAPTURED SINE WAVE');
axis([0 No_of_Samples1 min(CAPTURED_SIN1)
max(CAPTURED_SIN1)]),xlabel('NO OF SAMPLES '),ylabel('DATA RANGE');
i=-(No_of_Samples1/2):1:(No_of_Samples1/2)-1;
freq_index = (Fs/No_of_Samples1)*i;
freq_index=freq_index/(1e6);
figure; plot(freq_index,QUANTIZE_CAPTURE_SPECTRUM),title('FFT SPECTRUM
OF CAPTURED SINE WAVE');
xlabel('Frequency in MHz');
ylabel('Normalized Amplitude in dB');
figure,plot(QUANTIZE_CAPTURE_SPECTRUM),title('FFT SPECTRUM OF CAPTURED
SINE WAVE');
xlabel('Number  of Samples');
ylabel('Normalized Amplitude in dB');
```

C. CONTROLLER AND INTEGRATOR CODE:

```
#include <device.h>
#include <stdio.h>
#include <math.h>

/* Set the number of ADC samples used for calculations */
#define SAMPLES 512
/* Functions used in this project */
void Calculate(void);

/* Global variables used for storing calculated  parameters */
uint16 min,max;
uint32 ADC_Sample_Average;
uint16 ADC_Samples[SAMPLES];
uint16 ADC_Sample_Index = 0u;
uint8 ADC_Sample_Available = 0u;
void main()
{
/* Enable global interrupts */
CyGlobalIntEnable;
/* Start and initialize components */
isr_SW2_Start();
isr_SW1_Start();
```

```
UART_1_Start();
UART_1_PutString("Voltage Monitor:");
UART_1_PutCRLF(0x20);
ADC_DelSig_Start();
LCD_Char_Start();

/* Start of infinite loop */
for(;;)
{
/* Call the function that calculates AVERAGE*/
Calculate();
CyDelay(1000u);
}
}

void Calculate(void)
{
/* Local variables used by this function */
uint16 adc_sample;
uint16 i,j;
char res[2]; //char array
char res1[2];
/* Initialize variables */
adc_sample = 0;

/* Start ADC conversion */
ADC_DelSig_StartConvert();
//
for (j = 0u; j < SAMPLES; j++)
{
ADC_DelSig_IsEndConversion(ADC_DelSig_WAIT_FOR_RESULT);
adc_sample = ADC_DelSig_GetResult16();
if(adc_sample >0xFFFF)
{
adc_sample =0xFFFF;
}
else if(adc_sample < 0)
{
adc_sample =0;
}
else
{
}
ADC_Samples[ADC_Sample_Index++] =adc_sample;
```

```
sprintf(res1,"%x",adc_sample );
UART_1_PutString(res1);
UART_1_PutCRLF(0x20);
}

if (ADC_Sample_Index == SAMPLES)
{
ADC_Sample_Average = 0u;
for (i = 0u; i < SAMPLES; i++)
{
ADC_Sample_Average += ADC_Samples[i];
}
ADC_Sample_Average /= SAMPLES;
ADC_Sample_Index = 0u;
sprintf(res,"%x",ADC_Sample_Average );
UART_1_PutString(res);
UART_1_PutCRLF(0x20);
}
}
/* [] END OF FILE */
```